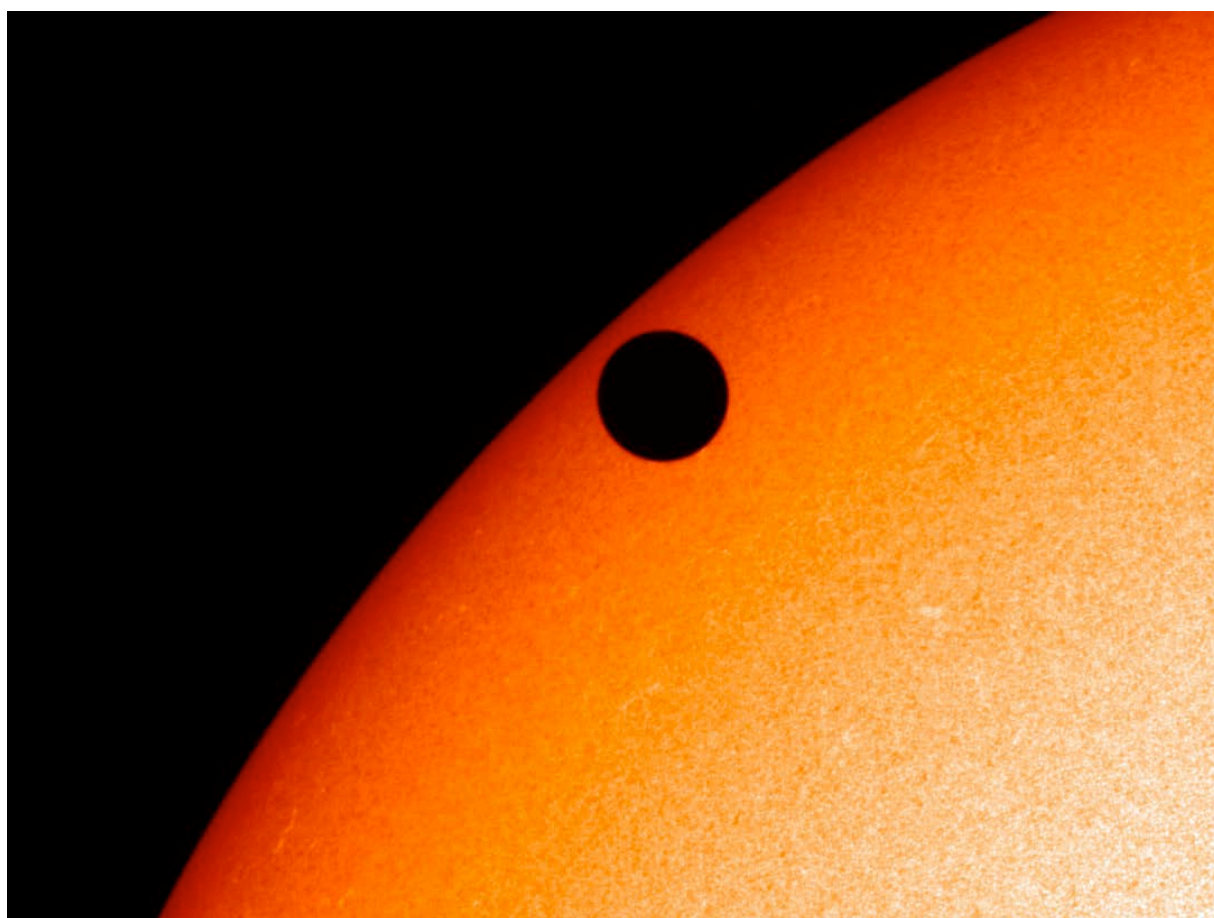


CHEOPS

CHaracterising ExOPlanet Satellite



Definition Study Report

The front page shows a real image of an Earth-size planet transiting a bright star: the June 2012 transit of Venus observed in the visible by the Helioseismic and Magnetic Imager on-board the *Solar Dynamics Observatory*. CHEOPS will use ultraprecise photometry to observe transits of larger versions of Venus or the Earth around other stars – the “super-Earths”. CHEOPS aims at using the information uniquely obtained during transits to characterise the natures of these exoplanets.

CHEOPS Definition Study – Mission Summary	
Cosmic Vision Theme	What are the conditions for planet formation and the emergence of life?
Key scientific goals	Measure the bulk density of super-Earths and Neptunes orbiting bright stars and provide golden targets for future in-depth characterisation studies of exoplanets in these mass and size ranges.
Observational Concept	Observations of planetary transits through precision photometry of at least 20 ppm (goal: 10 ppm) in 6 hours of integration time.
Targets	Known exoplanet host stars brighter than the 12 th magnitude in the V band
Primary products	Very accurate transit light curves and calibrated images
Payload	<p>Photometer with single, frame-transfer, back-illuminated CCD detector, operating in the visible range</p> <p>On-axis Ritchey-Chrétien telescope of 33 cm diameter</p> <p>FOV: 19 arcmin × 19 arcmin (need to acquire target + background sampling)</p>
Description of Spacecraft	<p>3-axis stabilised</p> <p>Pointing accuracy: 8 arcsec rms over a 48 hour observation</p> <p>Mass: ~ 250 kg</p> <p>Dimensions: ~ 1.5 m × 1.4 m × 1.5 m</p> <p>AOCS: Instrument measurements in the attitude control loop, two autonomous Star Trackers</p> <p>Attitude: Roll around inertially fixed line-of-sight direction</p> <p>Telemetry rate: 1 Gbit/day downlink</p>
Mission Profile	<p>Baseline orbit: Circular Sun-synchronous with an altitude in the range between 620 and 800 km – Local time of the ascending node 6 am (nominal option, with 6 pm as back-up)</p> <p>Launch: end 2017</p> <p>Launcher: As auxiliary payload or co-passenger in Vega (VESPA adapter) or Soyuz (under ASAP-S) - baseline scenarios - or in other small launch vehicles (e.g. PSLV)</p> <p>Nominal mission duration: 3.5 years</p>

Foreword

The CHaracterising ExOPlanet Satellite (CHEOPS) mission was proposed in response to the “2012 Call for a Small mission opportunity in ESA's Science Programme for a launch in 2017”, issued on 9 March 2012. The proposal was led by Prof. Willy Benz from the University of Bern. Following the review and positive recommendation by the Advisory structure, CHEOPS was selected on 19 October 2012 by the Science Programme Committee (SPC) for a definition phase study as the first Small mission in Cosmic Vision 2015-2025. CHEOPS is an ESA mission to be implemented in partnership with Switzerland, with a number of member states delivering significant contributions. These member states are Austria, Belgium, France, Germany, Hungary, Italy, Portugal, Sweden, and UK, and will cooperate under a Swiss-led CHEOPS Mission Consortium.

The call defined strict boundary conditions for the Small Mission, in particular i) a development time not exceeding 3.5-4 years, leading to a launch in 2017, and ii) a total cost to be covered by the ESA Science Programme limited to 50 M€ at 2012 economic conditions. In addition, the call indicated a limit to the total mission cost of approximately 150 M€. These conditions impose strong constraints to the schedule and to the approach adopted for the current study and future implementation activities.

Immediately after the selection, ESA carried out an internal study, which set the basis for the definition of the mission science requirements, the system requirements for satellite and payload, and the preparation of the Invitation to Tender (ITT) for the ESA industrial activities. The ITT was issued at the end of March 2013, covering two distinct phases, namely a competitive definition study, phase A/B1, and the actual mission implementation, the latter being subordinated to mission adoption by SPC in February 2014. In June 2013 two industrial contractors were selected for the competitive definition phase. The work started at the beginning of July 2013, and will be completed with the mission level Preliminary Requirements Review in December 2013 and the System Requirements Review in March 2014. Subsequently, one of the two contractors will be selected for carrying out the implementation phase.

In parallel, the CHEOPS Mission Consortium has performed the definition study for the payload. The instrument PRR was successfully completed in June 2013, with the baseline payload design judged to be feasible and compatible with the allocated resources. The definition study for the Ground Segment was kicked off in April 2013, focusing on the definition of requirements and plans for the Mission Operations Centre and the Science Operations Centre, both provided by the consortium. The instrument System Requirements Review and the Ground Segment Requirements Review are on-going at the time of writing this report.

Of particular relevance for a small mission is the large flight heritage of the spacecraft solutions offered by the Industrial contractors, which are based on existing platform designs. This is also applicable to the payload components, for which the consortium can exploit significant heritage from the *CoRoT* mission and benefit from the expertise acquired during its scientific operation.

This report presents the outcome of the CHEOPS Definition study. It describes the resulting mission concept that will fulfil the mission science requirements, and therefore allow us to achieve the science objectives presented in the original proposal, and further detailed and elaborated in this document.

The CHEOPS Study Team

Authorship, acknowledgements

This report has been prepared by members of the CHEOPS Team listed below.

CHEOPS Mission Consortium (CMC)		
<i>Name</i>	<i>Affiliation</i>	<i>City, Country</i>
Willy Benz (Principal Investigator)	University of Bern	Bern, Switzerland
David Ehrenreich	Université de Genève	Geneva, Switzerland
Christopher Broeg	Universität Bern	Bern, Switzerland
Didier Queloz	Université de Genève	Geneva, Switzerland
Mathias Beck	Université de Genève	Geneva, Switzerland
Yann Alibert	Universität Bern	Bern, Switzerland
François Bouchy	LAM	Marseille, France
Michaël Gillon	Université de Liège	Liege, Belgium
Manuel Güdel	Universität Wien	Vienna, Austria
Kevin Heng	Universität Bern	Bern, Switzerland
László Kiss	Konkoly Observatory	Budapest, Hungary
Helmut Lammer	IWF	Graz, Austria
Christophe Lovis	Université de Genève	Geneva, Switzerland
Michael Meyer	ETH Zürich	Zürich, Switzerland
Giampaolo Piotto	Università degli Studi di Padova	Padova, Italy
Don Pollacco	University of Warwick	Warwick, UK
Nuno C. Santos	CAUP	Porto, Portugal
Valérie Van Grootel	Université de Liège	Liege, Belgium

The ESA Team supporting the activities is composed by:

ESA study team		
Nicola Rando (Study Manager)	ESA/ESTEC	Noordwijk, The Netherlands
Ana M. Heras (Study Scientist)	ESA/ESTEC	Noordwijk, The Netherlands
Carlos Corral van Damme (System Engineer)	ESA/ESTEC	Noordwijk, The Netherlands
Francesco Ratti (Principal Payload Engineer)	ESA/ESTEC	Noordwijk, The Netherlands
Joel Asquier (Platform Engineer)	ESA/ESTEC	Noordwijk, The Netherlands
Rainer Timm (Operations support)	ESA/ESOC	Darmstadt, Germany
ESA Coordinator		
Arvind Parmar	ESA/ESTEC	Noordwijk, The Netherlands

We also acknowledge the contribution of (by alphabetical order): Luca Borsato (Università degli Studi di Padova, IT), Giordano Bruno (Universität Bern, CH), Robert Buxton (Universität Bern, CH), Bruno Chazelas (Université de Genève, CH), Magali Deleuil (Laboratoire d'Astrophysique de Marseille, FR), Brice-Olivier Demory (University of Cambridge, UK), Andrea Fortier (Universität Bern, CH), Corentin Guillo (SACC, UK), Antonio Gutiérrez Peña (DEIMOS Engenharia, Lisbon, PT), Johann Hasiba (IWF, AT), Demetrio Magrin (INAF, IT), Matteo Munari (INAF, IT), Valerio Nascimbeni (Università degli Studi di Padova, IT), Göran Olofsson (Stockholm University, SE), Harald Ottacher (IWF, AT), Isabella Pagano (Osservatorio Astrofisico di Catania-INAF, IT), Gisbert Peter (DLR, GE), Daniele Piazza (Universität Bern, CH), Jean-Yves Plesseria (CSL, BE), Roberto Ragazzoni (INAF-OAPD, IT), Reiner Rohlfs (Université de Genève, CH), Manfred Steller (IWF, AT), Gyula Szabó (Konkoly Observatory/ELTE Gothard Asztrofizikai Observatórium, HU), Janos Szoke (ADM, HU), Matthias Tschentscher (DLR, GE), Holger Venus (DLR, GE), Ingo Walter (DLR, GE), Udo Wehmeier (Universität Bern, CH), François Wildi (Université de Genève, CH)

Table of contents

1	EXECUTIVE SUMMARY	8
2	SCIENTIFIC OBJECTIVES	11
2.1	Exoplanets today	11
2.1.1	From the census of exoplanets to their detailed characterisation.....	11
2.1.1.1	The educated transit searches and the discovery of “Rosetta stone” planets	14
2.1.1.2	The transit surveys and the rise of super-Earths and Earth-size planets	15
2.1.2	Key science questions.....	17
2.1.3	Mission goals.....	18
2.2	Structures of exoplanets and planetary systems.....	18
2.2.1	Interiors of exoplanets	18
2.2.1.1	Constraints on planetary interiors from measured radius and mass: what is possible?.....	19
2.2.1.2	Relations between planetary structures and planetary formation.....	21
2.2.1.2.1	Constraints on the critical core mass for the core accretion formation scenario	21
2.2.1.2.2	Constraints on migration paths	21
2.2.1.3	Precision on planetary radius measurements with CHEOPS	22
2.2.2	Atmospheres & envelopes	24
2.2.2.1	Identification of planets with atmospheres or fluid envelopes.....	24
2.2.2.2	Constraints on atmospheric properties from visible broadband photometry	24
2.2.2.2.1	Constraints from the transit light curve	25
2.2.2.2.2	Constraints from the phase curve.....	25
2.2.2.2.3	Constraints from the occultation event	26
2.2.2.3	Atmospheric evolution of close-in exoplanets.....	27
2.2.3	Orbital dynamics of planetary systems.....	29
2.2.3.1	Detection of additional planets through transit time variations	29
2.2.3.2	Optimisation of the extraction of dynamical information from the light curve	30
2.2.3.3	Detection of exomoons	33
2.3	CHEOPS targets and expected transit yield.....	34
2.3.1	Planetary systems from ground-based Doppler surveys.....	35
2.3.1.1.1	On-going velocimetric surveys.....	36
2.3.1.1.2	Upcoming velocimetric surveys	36
2.3.2	Planets from ground-based transit surveys	37
2.3.2.1.1	Current Planet Yield	37
2.3.2.1.2	Expected planet yield in 2014–2017.....	38
2.3.3	M dwarfs in CHEOPS target list.....	38
2.3.4	CHEOPS target stellar properties	39
2.3.4.1	Stellar spectroscopic analysis for CHEOPS targets	39
2.3.4.1.1	Main sequence stars with F, G, and K spectral types	40
2.3.4.1.2	The peculiar case(s) of M dwarfs	41
2.3.4.2	Characterisation of the masses, radii, and ages of the host stars.....	41
2.3.4.2.1	Classical method from stellar physics.....	41
2.3.4.2.2	Asteroseismology for CHEOPS targets.....	42
2.3.4.3	Energetic (XUV) radiation environment of CHEOPS planetary systems.....	43
2.4	Synergies with other missions.....	44
2.4.1	Golden targets for atmospheric characterisation with <i>JWST</i>	44
2.4.2	Synergies between CHEOPS and TESS.....	46
3	SCIENTIFIC REQUIREMENTS	48
3.1	Photometric accuracy	48
3.2	Sky coverage	49
3.3	Target observability	50
3.4	Magnitude range of targets and exposure times.....	51
3.5	Time sampling & precision of the light curves.....	52

3.6	Lifetime.....	52
4	PAYLOAD AND PERFORMANCE.....	53
4.1	Instrument Description.....	53
4.1.1	Optical Telescope Assembly (OTA).....	53
4.1.2	Baffle and Cover Assembly (BCA).....	53
4.1.3	Back-End Electronics Box (BEE) and Sensor Electronics Module (SEM).....	54
4.2	Design Challenges.....	54
4.3	Instrument Decomposition.....	55
4.4	CIS Design.....	56
4.4.1	Telescope optical design.....	56
4.4.2	Back-End Optics design.....	57
4.4.2.1	Glasses selection.....	57
4.4.2.2	Optical design.....	58
4.4.3	Defocused PSFs performance.....	59
4.4.4	Baffle and Cover Assembly.....	60
4.4.5	Telescope Stray light analysis.....	61
4.4.6	CCD Detector.....	61
4.4.7	Focal Plane Module and Sensor Electronics Module.....	62
4.4.7.1	FPM mechanical and thermal design.....	62
4.4.7.2	FEE and FPA Electrical Design.....	64
4.4.7.3	SEM electrical design.....	64
4.4.7.4	Data transfer to DPU.....	65
4.4.8	CIS Computer (DPU) and Power distribution (DCDC).....	65
4.5	Interfaces and resource requirements.....	66
4.5.1	Mass.....	66
4.5.2	Power Budget.....	66
4.6	Instrument Performance and Noise Budget.....	68
4.6.1	Noise Model.....	68
4.6.2	Noise Budget.....	69
5	MISSION DESIGN.....	71
5.1	Operational orbit and mission profile.....	71
5.2	Environment.....	72
5.3	Spacecraft design.....	74
5.3.1	Spacecraft resource budgets.....	77
5.3.2	Modifications to Standard Platforms.....	78
5.4	Definition phase activities.....	79
5.4.1	Industrial studies.....	79
5.4.2	Compatibility with different launcher vehicles.....	81
5.5	Programmatic aspects.....	81
5.5.1	Contributions from consortium.....	81
5.5.2	Provision of AIV services.....	82
5.5.3	Interface to MOC.....	82
5.5.4	AIV approach and model philosophy.....	83
5.5.5	Project schedule and equipment qualification status.....	83
5.5.6	Approach to LV selection.....	83
5.5.7	Risk assessment summary.....	84
5.5.7.1	Payload Risks.....	85
5.5.7.2	Platform Risks.....	85
6	GROUND SEGMENT.....	86
6.1	Overview.....	86
6.1.1	Ground Stations.....	86
6.1.2	Mission Operations Centre.....	86
6.1.3	Science Operations Centre.....	86

6.1.4	Orbit and ground contacts.....	87
6.2	Mission Operations	87
6.2.1	Staffing and operations automation	87
6.2.2	Mission planning	87
6.2.3	Health and safety critical monitoring.....	88
6.2.4	Auxiliary data	88
6.2.5	Subsystem provision, integration and validation.....	88
6.3	Science operations and data handling/archiving	88
6.3.1	Staffing and operations automation	88
6.3.2	Science target definition	88
6.3.2.1	Core science programme.....	88
6.3.2.2	Open-time science programmes	88
6.3.3	Payload planning	89
6.3.4	Data processing.....	89
6.3.4.1	Quick Look	89
6.3.4.2	Data Reduction.....	89
6.3.5	Data archiving and distribution.....	89
	Archive mirror	89
6.3.6	Data analysis.....	90
6.3.7	In-flight calibrations	90
6.3.8	Instrument monitoring	90
6.4	Data Products	90
7	MANAGEMENT	91
7.1	Project management	91
7.1.1	Organisational structure.....	92
7.1.1.1	Overview.....	92
7.1.1.2	Joint Management Team.....	92
7.1.1.3	Joint Project Office	92
7.1.1.4	Steering Committee.....	93
7.1.2	CHEOPS Mission Consortium Board.....	93
7.2	Schedule.....	93
7.3	Science Management	94
7.3.1	CHEOPS Science Team.....	94
7.3.2	Guest observers.....	95
7.3.3	Data rights.....	95
8	COMMUNICATION AND OUTREACH.....	96
9	REFERENCES.....	97
10	LIST OF ACRONYMS	102

1 Executive summary

The discovery of planets around other stars (exoplanets) has opened one of the most exciting fields in modern astronomy. After nearly two decades mainly dedicated to a census of these exoplanets, we are entering the era of exoplanetology; the physical and chemical characterisation of exoplanets and their systems. As seen from Earth, a fraction of planetary systems are inclined in a way that it is possible to see planets transiting across the surfaces of their host stars. ***Exoplanets transiting bright stars are the key to exoplanetology.***

The *Characterising Exoplanet Satellite (CHEOPS)* will be the first mission dedicated to search for transits of exoplanets by means of ultrahigh precision photometry on bright stars already known to host planets. It will provide the unique capability of determining accurate radii for a subset of those planets for which the mass has already been estimated from ground-based spectroscopic surveys, providing on-the-fly characterisation for exoplanets located almost everywhere in the sky. It will also provide accurate radii for new planets discovered by the next generation of ground-based transits surveys (from super-Earth to Neptune-size). By unveiling transiting exoplanets with high potential for in-depth characterisation, CHEOPS will provide “golden targets” for future instruments suited to the spectroscopic characterisation of exoplanetary atmospheres.

Large and high-precision spectroscopic (or “Doppler”) surveys carried out from the ground during the last years have identified hundreds of stars hosting planets with masses below Saturn’s. The natures of these exoplanets are largely unknown because the planets in our Solar System poorly sample the range of masses extending from telluric planets such as Venus or the Earth ($1 M_{\oplus}$) to ice giants such as Uranus ($14 M_{\oplus}$) or Neptune ($17 M_{\oplus}$), and from ice giants to gas giants like Saturn ($95 M_{\oplus}$). On the other hand, there is an apparent continuum of exoplanets detected with masses ranging from 1 to $10 M_{\oplus}$ (the so-called “super-Earths”), from 10 to $30 M_{\oplus}$ (the “Neptunes”), and up to the mass of Saturn. Determining the physical properties of these objects – most of them with no equivalent in the Solar System – is a critical step towards the understanding of the origins and evolutions of planets.

The Doppler surveys will continue to operate and detect more of these intriguing exoplanets in the foreseeable future. The characteristics of the host stars (bright magnitudes, low activity levels, etc.) and the knowledge of the planet ephemerids make them ideal targets for precision photometric measurements from space. CHEOPS will be the only facility dedicated to follow-up all these targets for a first-step characterisation via precise radius measurements.

The new generation of ground-based transit surveys (e.g., NGTS), capable of reaching photometric precisions of one millimagnitude on stars of the 13th magnitude and brighter, provide another source of targets for CHEOPS. By the end of 2017, NGTS alone will provide about 50 targets with radii $< 6 R_{\oplus}$, which CHEOPS will measure to a precision of 10%. These stars are also bright enough to make precise mass determination via radial velocity follow-up measurements possible, in contrast with previous missions aiming at faint stars such as *CoRoT* and *Kepler*. While ground-based searches are well-suited to *detect* the transits and fix the ephemerids, CHEOPS precision is crucial to obtain accurate measurements of planet radii.

Knowing where to look and at what time to observe makes CHEOPS the most efficient instrument to search for shallow transits and to determine accurate radii for planets in the super-Earth to Neptune mass range.

The main science goals of the CHEOPS mission will be to measure the bulk density of super-Earths and Neptunes orbiting bright stars and provide golden targets for future in-depth characterisation studies of exoplanets in these mass and size ranges. With an accurate knowledge of masses and radii, hence on the bulk densities, CHEOPS will set new constraints on the structure and hence on the formation and evolution of planets in this mass range. In particular, CHEOPS will:

- Perform first-step characterisations of super-Earths, by measuring the radii and densities in a planetary mass range for which only a handful of data exist and to a precision never achieved before, and by

identifying planets with significant atmospheres as a function of their mass, distance to the star, and stellar parameters. The presence (or absence) of large gaseous envelopes bears directly on fundamental issues such as runaway gas accretion in the core accretion scenario or the loss of primordial H/He atmospheres.

- Obtain new insights into the physics and formation processes of Neptunes, by measuring accurate radii and densities for Neptunes, deriving minimum values of their gas mass fractions, and inferring possible evolution paths.
- Provide golden targets for future ground- (e.g., E-ELT) and space-based (e.g., *JWST*) facilities with spectroscopic capabilities. With well-determined radii and masses, the CHEOPS planets will constitute the best sample of targets within the solar neighbourhood and spread over the whole sky for such future studies.
- Probe the atmosphere of known hot Jupiters in order to study the physical mechanisms and efficiency of the energy transport from the dayside to the night side of the planet.

CHEOPS will also offer 20% of open time to the community, which will be allocated through competitive scientific review.

To reach its goals, CHEOPS will measure photometric signals with a precision limited by stellar photon noise of 150 ppm in one minute for a 9th-magnitude star in the *V* band. This precision allows the detection of an Earth-size planet transiting a star slightly smaller than the Sun ($0.9 R_{\odot}$) with a 50 day period, detected with a signal-to-noise ratio > 5 (100-ppm transit depth). This precision will be achieved by using a single frame-transfer back-side illuminated CCD detector located in the focal plane assembly of a 33-cm diameter on-axis telescope. The optical design is based on a Ritchey-Chrétien telescope and a defocused image of the target star. The optical design of the CHEOPS telescope will minimise the stray light contamination onto the detector with a dedicated field stop and a baffling system. This design meets the requirement of < 10 ppm (70 ppm) noise from stray light for 9th-magnitude stars (12th-magnitude stars, respectively) in the *V* band for more than 50% of the sky over 50 days per year. Thermal control of the detector will be obtained by coupling the detector to a radiator always exposed to deep space.

The telescope will reside on a spacecraft platform providing pointing stability of < 8 arcsec (rms) over a 48-h observing period. The spacecraft will be 3-axis stabilised but nadir locked with the thermal interface between the spacecraft bus and instrument payload remaining stable to within one degree. The spacecraft will provide 60 W continuous power for instrument operations and allow for at least 1.2 Gbit day⁻¹ downlink.

The baseline orbit satisfying the science requirements is a Sun-synchronous orbit (SSO) with an altitude in the range 620–800 km and a mean local time of the ascending node of 6 am. This choice optimises uninterrupted observations and keeps thermal variations of the spacecraft, and stray light on the satellite to a minimum, as the orbital plane follows as close as possible the day/night terminator. A shared launch is envisioned which, given the mass of the spacecraft (< 250 kg), will be possible using a number of existing launchers (Vega, Dnepr, Rocket).

The CHEOPS mission baseline relies completely on components with flight heritage. This is valid for the platform as well as for the payload components. For the latter, the team can exploit significant heritage from the *CoRoT* mission, minimising both cost and risk.

The CHEOPS Ground Segment consists of the ground station(s), the Mission Operations Centre and the Science Operations Centre. The ground station(s) will support the telemetry and telecommand communications with the spacecraft. The Mission Operations Centre will be responsible for the operation and health monitoring of the spacecraft. The Mission Operations Centre will receive the satellite telemetry and transfer it to the Science Operations Centre, where it will be processed to generate the mission data products that will be archived and made available to the mission users. The Science Operations Centre is also responsible for the scientific mission planning and the quality control of the observations.

CHEOPS is an ESA mission to be implemented in partnership with Switzerland, with a number of member states delivering significant contributions. These member states are Austria, Belgium, France, Germany, Hungary, Italy, Portugal, Sweden, and UK, and will cooperate under a Swiss-led CHEOPS Mission

Consortium (CMC). ESA will be in charge of the overall mission architecture with the support of the CMC. As such, ESA will manage the overall CHEOPS spacecraft development, integration and validation, up to the completion of the in-orbit Commissioning phase. The CMC will provide the payload, which consists of the telescope and the instrument, the ground segment, mission and science operations, and contributions to the integration and validation activities. The CMC will be led Prof. Willy Benz as Principal Investigator (PI).

The CMC will establish a core science programme, which will define the distribution of observing time among the science objectives, and which will cover up to 80% of the nominal duration of the mission. The remaining 20% of observing time will be open to guest observers to conduct scientific investigations. Proposals will be requested yearly through an open ESA AO to the general scientific community and will be selected on scientific merit by a Time Allocation Committee (TAC). In order to allow important new targets to be included in the open time programme at any time during the mission, up to 25% of the open time will be allocated to a discretionary programme, overseen by ESA in consultation with the chair of the TAC and the PI.

A CHEOPS Science Team (CST) will be constituted to advise the PI on all mission scientific matters. The members of the CST will have access to all data of the core science programme as soon as they are available. The data from a particular target of the core observing programme and the open time programme will have associated a 1-year proprietary period, after which all data products will be publicly available through the CHEOPS science archive. The 1-year proprietary time will begin just after the last measurement on that particular target has been received, and the observation declared complete by the CST after the corresponding quality-check. In order to ensure a timely publication of scientific results, the proprietary time will not exceed 1.5 years counting from the first measurement of the corresponding target.

To ensure a commensurate involvement of scientists from ESA Member States in the CHEOPS mission, five CST members, corresponding to a fraction of 20% of the non-ex-officio CST members, will be appointed by ESA through an AO.

The CHEOPS mission fits within both the technical readiness requirements and the cost envelope defined by the ESA call for S-missions, yet represents a breakthrough opportunity in furthering our understanding of the formation and evolution of planetary systems.

2 Scientific objectives

2.1 Exoplanets today

The discovery in 1995 of the first giant planet outside of the Solar System sparked a real revolution in astronomy (Mayor & Queloz 1995). The completely unexpected characteristics of this first planet captured the imagination and interest of the scientific community and the general public alike. Ten years later, ESA defined the conditions for planet formation and the emergence of life as one of its top scientific priorities for the period 2015–2025 (*Cosmic Vision 2015–2025*, 2005). Today, one thousand exoplanets have been found (or confirmed) with the “radial velocity” technique. This method measures the perturbation in the motion of a star caused by the presence of an orbiting exoplanet: the star moves around the centre of mass of the system, producing a Doppler shift detectable in spectroscopy. The amplitude and period of this shift provides a measure of the minimum mass¹ and of the revolution period of the planet around the star. Through ground-based radial velocity surveys, we have learned that planets are common in the Solar neighbourhood (~100 pc), and that the properties of planets and planetary systems are much more diverse than originally predicted (Udry & Santos 2007). In recent years, the young field of exoplanets has been experiencing a fantastic acceleration in terms of instrumental developments, observational discoveries, and theoretical advances. The rise of space-borne experiments capable to photometrically detect thousands of exoplanet candidates when they transit across the surface of their host stars (*CoRoT*, 2006; *Kepler*, 2009), has confirmed that exoplanets and exoplanetary systems are ubiquitous and that their diversity goes far beyond what we know in the Solar System. Breakthrough measurements have furthermore allowed to access the properties of exoplanets previously restricted to planets within our Solar System: the first direct detections of a handful of giant exoplanets with high-contrast imaging (Marois et al. 2008; Kalas et al. 2008; Lagrange et al. 2009) and the first analyses of exoplanetary atmospheres with transmission spectroscopy during transits, from the ultraviolet to the near-infrared (Charbonneau et al. 2002; Vidal-Madjar et al. 2003; Deming et al. 2013) and emission spectroscopy during planetary occultations (Grillmair et al. 2007) are opening the path towards the detailed physical and chemical characterisation of exoplanets, yielding unmatched constraints about their origins, evolutions, and habitability.

2.1.1 From the census of exoplanets to their detailed characterisation

In our Solar System, the giant planets (Jupiter, Saturn, Uranus, Neptune) are located relatively far from the Sun. This has been explained by the fact that, in order to grow massive fast enough, these bodies require volatile species in condensed form (ices), which are only available in cold and hence distant regions of the protoplanetary disc. In contrast, the first detected giant exoplanets are unexpectedly located very close to their host stars ($\lesssim 0.1$ au), in much-too-hot and poor-in-mass regions to make in-situ formation possible. The concept of planetary migration (Lin et al. 1996; Ward 1997), involving a formation beyond the “snow line” and the decrease of the star-planet distance via gravitational interactions with the circumstellar gas disc, has been proposed to explain the existence of these “hot Jupiters”. While such interactions lead to changes in the semi-major axis of the orbits, they also damp both inclinations and eccentricities. Hence, one normally would expect relatively circular planetary orbits lying within the plane of the circumstellar disc. Surprisingly measurements of the angle between the orbits of the planets and the equatorial plane of their host stars have shown that hot Jupiters on non-coplanar orbits, or even on retrograde orbits are more common than previously thought (Queloz et al. 2000; Hébrard et al. 2008; Triaud 2011 and references therein). These misaligned orbits have been interpreted as possibly resulting from dynamical interactions occurring in multi-planet systems after the gaseous disc has dissipated. Furthermore, most giant planets with intermediate revolution periods have eccentric orbits, which also suggests that violent, multi-body dynamical interactions play a preponderant role in addition to progressive disc-driven migration in determining the final planetary orbits (Juric & Tremaine 2008; Chatterjee et al. 2008). In summary, it is indeed striking that the bulk of the

¹ Because the inclination of the planetary system is unknown, the quantity measured with the radial velocity technique is the minimum mass of the planet $M_p \sin i$, where M_p is the true mass of the planet and i the inclination of the system with respect to the plan of the sky.

exoplanets discovered so far have distinctly different characteristics than those expected from Solar System studies.

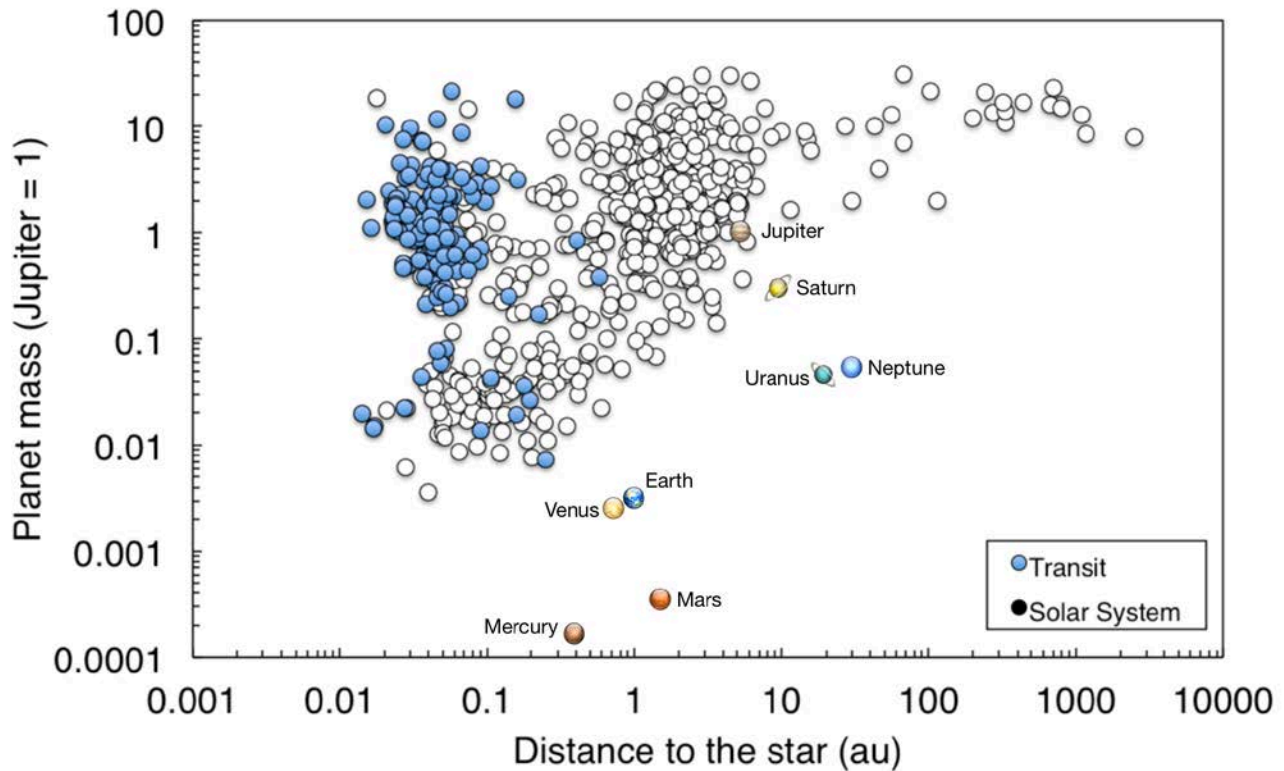


Figure 1 | Mass-distance diagram for exoplanets (white) and Solar System planets. Confirmed transiting exoplanets are shown in blue.

Despite these discoveries, we are only at the beginning of a revolution that will place the Solar System, its planets, and by extension the Earth, in a global perspective. Beyond the architecture of planetary systems, the study of the physical and chemical characteristics of exoplanets themselves will yield critical new insights into their origins and the main processes driving their evolution (among which, the emergence of life). A handful of key quantities are required to start characterising an exoplanet.

The first and most fundamental key quantity is, as for all astrophysical objects, the mass. Radial velocity measurements only provide a minimum mass, which, based on statistical arguments, is however considered representative of the true mass of the planet. The true mass is really revealed when the inclination of the planetary system is known, which is the case for transiting planets.

A significant fraction (over 30%) of known exoplanets is found transiting their host star. This event causes a characteristic dimming of the light received from the star that is proportional to the fractional area covered by the planet. The photometric monitoring of such an event is called a transit light curve and is represented in Figure 2.

The depth of the transit light curve reveals the second key quantity: the size of the planet, obtained relatively to the size of the star. Together, the mass and the size yield the first simple characterisation of the nature of the planet: its mean density. (As we will see in the next sections, the mass is also essential to derive the atmospheric properties of a planet.) The first transit was detected on the solar-type star HD 209458, known by velocimetry to host a hot Jupiter. The photometric follow-up of this bright star ($V = 7.8$ mag) revealed a planet larger than Jupiter and with a mean density lower than Saturn, hence made of gas, most likely hydrogen and helium (Charbonneau et al. 2000; Henry et al. 2000).

Today, there are two complementary approaches to detect transiting planets. The first approach can be called “educated” transit search: it consists of following up known planetary systems discovered by velocimetry

(see 2.1.1.1 below). The second approach is called transit survey and consists of searching for transit events by monitoring large numbers of stars (see 2.1.1.2 below).

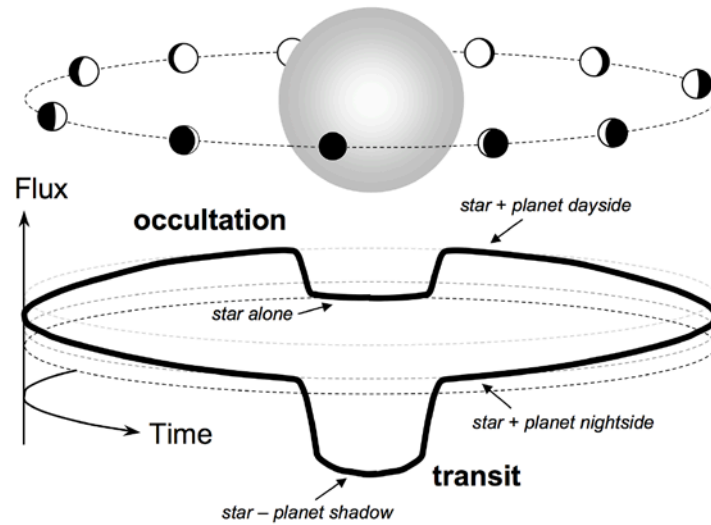


Figure 2 | Sketch of a transit and occultation. From Winn (2010).

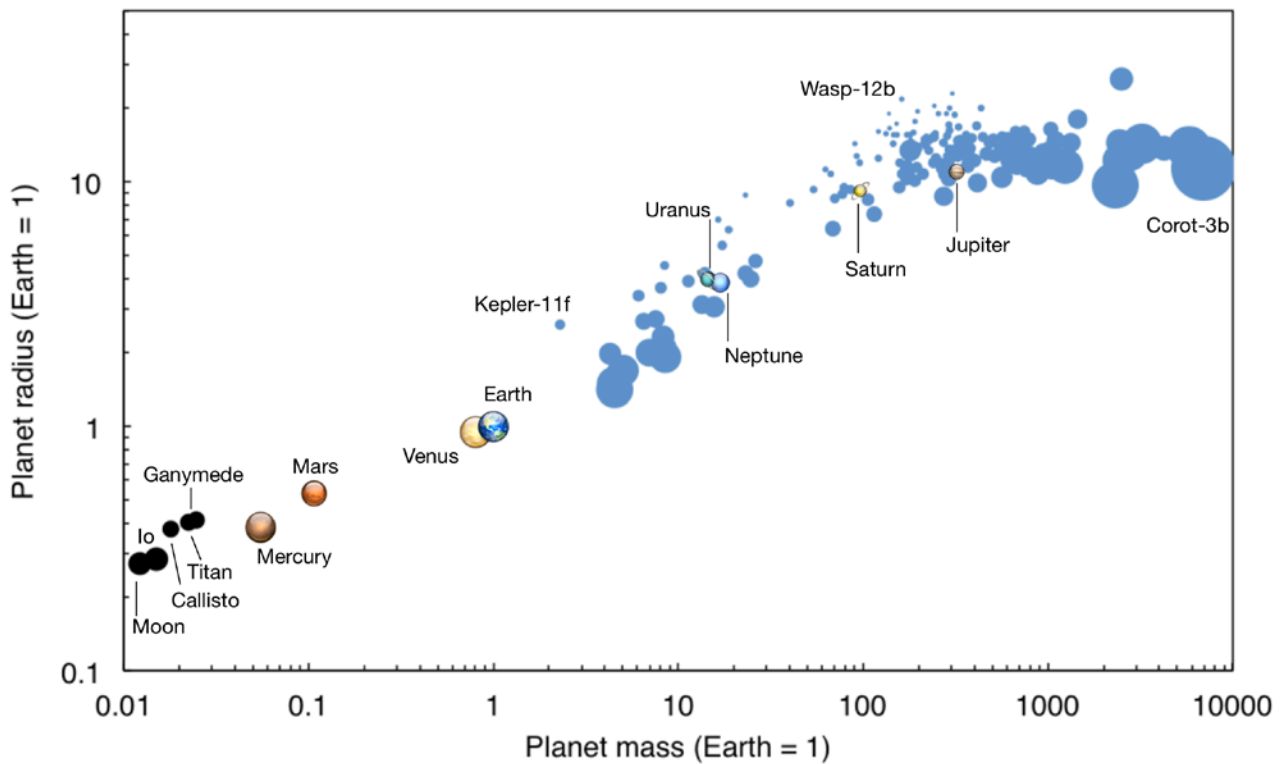


Figure 3 | Mass-radius diagram for exoplanets (blue) and for the planets and the largest moons in the Solar System. For exoplanets, the radius is measured from the transit light curve and the mass from velocimetry. The mean density is represented by the size of the points; The larger the symbol, the denser the planet.

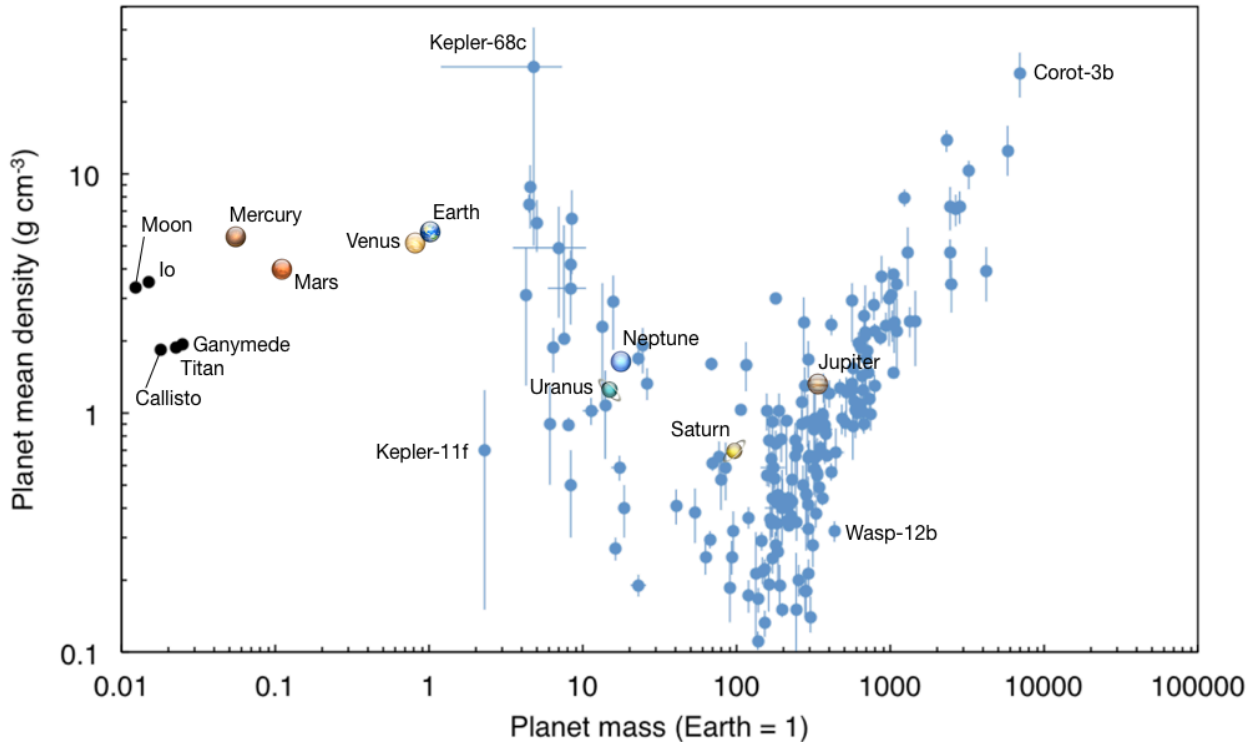


Figure 4 | Mean density of Solar System planets, largest moons (black), and transiting exoplanets (blue) with measured masses and radii.

2.1.1.1 The educated transit searches and the discovery of “Rosetta stone” planets

For educated transit searches, the ephemeris of the inferior conjunction (the time when the transit could occur) is known to a precision depending upon how accurately the orbit is known. Therefore, the transit can be searched for in photometry at specific times without having to stare at the star for days, weeks, or months, making this approach very efficient provided a large-enough amount of potential targets are known.

In fact, the improvements and intensive efforts made during the last decade by teams carrying out Doppler surveys have led to the identification of numerous planetary systems hosting Neptune-mass planets of ~ 10 – $30 M_{\oplus}$, that we will hereafter call “Neptunes”, and exoplanets with masses between 1 and $10 M_{\oplus}$, unknown in the Solar System and dubbed “super-Earths” (see Figure 5 for the naming convention). This clearly indicates that low-mass planets orbiting solar-type stars must be very common (Mayor et al. 2011), a fact that can also be extended to later-type stars (Bonfils et al. 2012). The nature of these exoplanets, much smaller than the gas giants, represents one of the great challenges offered by the study of exoplanets, especially as they are often found very close to their stars, in extreme conditions of irradiation, unlike anything known in the Solar System. Addressing this challenge requires a systematic educated transit search of all super-Earths and Neptunes detected via Doppler surveys. In practise, this is difficult because the photometric transit search from the ground is limited to giant planets (or ice giants around red dwarf stars), and the observing time needed to follow-up these systems from space, with the high precisions offered by *Spitzer* or the *Hubble Space Telescope (HST)*, is sparse and expensive.

Because radial velocity surveys target bright stars, the discovered planets successfully followed-up and detected in transit represent additional high-value science objects for which both mass and radius will be accurately known. At present only a handful of such objects have been discovered, hence the potential for progress is enormous. The stellar brightness is also critical to perform studies of the planetary atmosphere via transmission spectroscopy during the transit. The exoplanets found with educated transit searches, such as the hot Jupiters HD 209458b and HD 189733b, and the warm Neptune GJ 436b, act as “Rosetta stones” for the field of exoplanetology. The many studies dedicated to these planets have allowed astronomers to gain exceptional knowledge about the physics, chemistry, and origins of these objects.

CHEOPS will provide a unique way to extend this approach, by a systematic photometric follow-up of exoplanets detected by large surveys. By knowing where and when to look, and benefiting from excellent knowledge of the targeted stars and ultra-high photometric precision, CHEOPS will be able to unveil the golden targets of tomorrow’s exoplanetology: the super-Earths and Neptunes most prone to characterisation, each of which likely to become a Rosetta stone to decipher the nature of these mysterious objects.

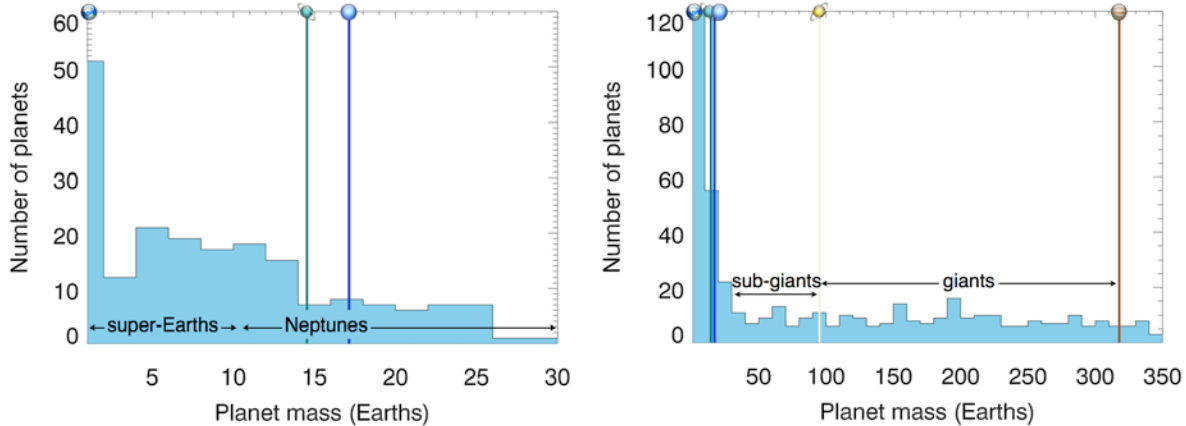


Figure 5 | Histograms showing the mass distribution of all known exoplanets (source: www.exoplanet.eu, July 2013) and the naming conventions adopted throughout this document: super-Earths ($1\text{--}10 M_{\oplus}$), Neptunes ($10\text{--}30 M_{\oplus}$), sub-giants ($30\text{--}100 M_{\oplus}$), and giants (above $100 M_{\oplus}$). **Left panel**— Distribution of planetary masses from 1 to $30 M_{\oplus}$ (bin size of $2 M_{\oplus}$). **Right panel**— Distribution of planetary masses from 1 to $350 M_{\oplus}$ (bin size of $10 M_{\oplus}$). The masses of Solar System planets are shown by vertical lines.

2.1.1.2 The transit surveys and the rise of super-Earths and Earth-size planets

The second approach to detect transits – the transit survey – has already provided clear evidence that small exoplanets are ubiquitous. From the ground, bright to moderately-bright stars can be monitored over the whole sky in photometry to search for transits of previously unknown exoplanets. This approach has proven to be extremely fruitful in terms of detection numbers. The WASP and HATNet surveys have been particularly prolific, with an average rate of 1 planet discovered every 3 weeks. These are mostly giant planets around moderately bright stars ($V > 10$ mag). Because of several sources of false-positive (e.g., background eclipsing binaries blended with the target), follow-up velocimetry is essential to validate the transits and provide the necessary mass measurement. For the range of magnitude considered and for the size of the planets discoverable by transit from the ground, this approach has worked very well and has increased the number of transiting objects to represent about a third of the total population of exoplanets known. However, accessing exoplanets smaller than Neptune, typically 3–4 Earth radii (R_{\oplus}), orbiting solar-type stars is nearly impossible from the ground, where the photometric precision is limited by correlated noise induced by the terrestrial atmosphere.

The revolution came from space-borne telescopes, with the launches of the CNES-led mission *CoRoT* and NASA’s mission *Kepler*. *CoRoT* was the first space mission dedicated to detecting transiting planets, successfully launched in December 2006. It was a pioneer in its use of ultra-precision photometry with high sampling rate. The satellite primarily observed two fields of view, each 4 square degrees, once per year. Each field counted typically 5 000–6 000 dwarf stars with magnitudes ranging from ~ 11 to 16. After 5 years of operations, *CoRoT* has discovered dozens of exoplanets, among which the first rocky planet Corot-7-b (Léger et al. 2009). Two years after *CoRoT*, the launch of the *Kepler* mission has turned out to be a landmark in transiting planet searches. *Kepler* has been measuring continuously brightness variations of about 100 000 solar-like stars to an accuracy of ~ 20 ppm (Gilliland et al. 2011) in a single field of view of approximately $100 \times 100 \text{ deg}^2$. *Kepler* found several thousands of transiting planet candidates, some of them with radii smaller than Earth (e.g., Fressin et al. 2011) and many multiple (often packed) transiting systems. With these discoveries, *Kepler* has provided the community with a large uniform database of potential planetary systems, enabling the derivation of distribution functions for planetary orbits, radii, and hierarchical structure of systems (Borucki et al. 2011; Batalha et al. 2013).

Both *CoRoT* and *Kepler* have been successful in reaching their design goals. However, it is revealing that despite this, only two rocky planets have been identified for certain (Corot-7b and Kepler-10b). This paucity of the most interesting targets is related to the faintness of the target stars. The need to stare at a given field for a long time (in order not to miss a transit) as well as to have large numbers of targets in a given field of view (to maximise the chance of detection) dictated that both *CoRoT* and *Kepler* would search for transits on stars with typical magnitudes in the range $V \sim 13\text{--}16$ mag. Measuring sufficiently-precise radial velocities for stars this faint, in order to obtain a reliable mass of an Earth-like or super-Earth planet, is virtually impossible. The example of Corot-7b shows that with the currently most precise planet hunting instrument, the HARPS spectrograph at ESO's 3.6-m telescope in La Silla, it is possible to measure the mass of small planets in the super-Earth domain, located on short period orbit for stars brighter than $V \sim 11$ mag. Similar measurements for planets with longer orbital periods on fainter stars, typical of *Kepler* candidates, would however, require a prohibitive amount of telescope time. In total, *Kepler* has found a dozen of the smallest transiting planetary candidates orbiting stars brighter than the 11th magnitude. Only a fraction of them offers hope for the accurate determination of the planet candidate masses with the recently installed HARPS-North facility. Hence, *CoRoT* and *Kepler* while demonstrating the existence of small rocky planets and providing reliable statistics as to their numbers, allow the characterisation of only a handful of exoplanets and do not provide the key targets for future spectroscopic facilities on the ground or in space.

The exact nature of super-Earth planets remains a matter of fierce debate: are they scaled-up versions of our telluric planets? Small Neptunes? Other kind of objects, such as ocean planets (Léger et al. 2004; Kuchner et al. 2003)? Are they surrounded by thin transparent atmospheres or by thick steam envelopes? Are they enshrouded in clouds? From the handful of small planets with both mass and size estimates, the structure and properties of these objects remains elusive. By obtaining precise radii for super-Earths and Neptunes with precise masses, CHEOPS will provide key elements to answer these questions.

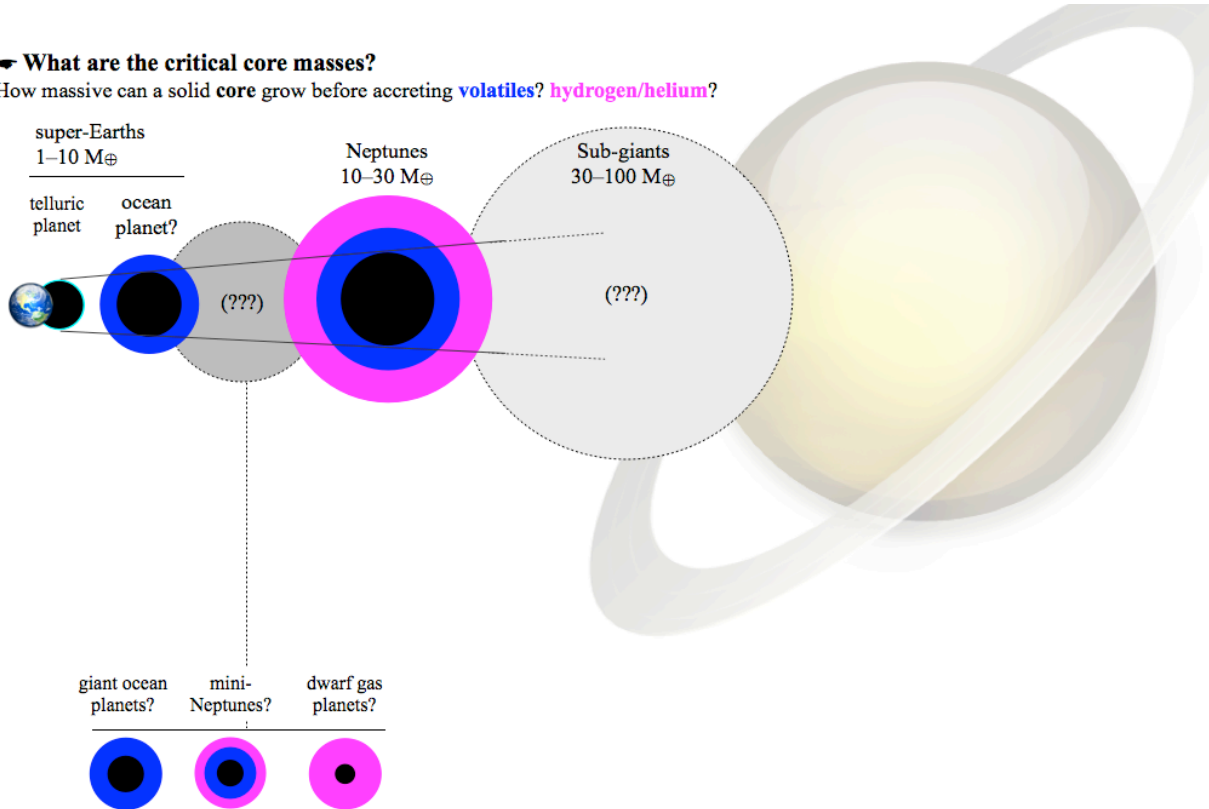
Finally, exoplanets transiting bright stars offer the opportunity to learn essential information about their atmospheres. During the transit, a small fraction of the stellar light is filtered by the atmospheric limb of the exoplanet, and the spectroscopic analysis of this light can reveal the structure, composition, and dynamics of the atmosphere. Because they both transit nearby stars with similarly-bright magnitudes ($V = 7.8$ mag), the exotic atmospheres of the prototypical hot Jupiters HD 189733b and HD 209458b have been scrutinised with the *Hubble Space Telescope* from the ultraviolet to the near-infrared, enabling enormous progresses in our understanding of these giant worlds. In the coming years, the idea is to extend such studies to Neptunes and super-Earths. The case of the small planet GJ 1214b ($\sim 6 M_{\oplus}$) shows how difficult a characterisation of a low-mass object is compared to giant planets. After many dedicated campaigns, the true nature of this planet – Neptune or ocean planet? – remains elusive (e.g., Berta et al. 2012). The study of these objects will clearly take advantage of the rise of such powerful telescopes as the *James Webb Space Telescope* and the European Extremely Large Telescope. CHEOPS will allow the discovery of the golden targets these facilities will be awaiting, and will do so with a level of characterisation that will enable a focus on the most exciting exoplanets.

2.1.2 Key science questions

The science questions that will be addressed by CHEOPS closely match the interests of the community about the possible natures of super-Earths and Neptunes planets. More specifically, the sections of this Science Objective chapter will detail how CHEOPS will shed light on the key points illustrated on this page.

What are the critical core masses?

How massive can a solid core grow before accreting volatiles? hydrogen/helium?

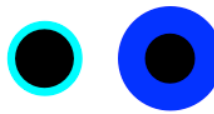


Are there new family of planets?

What are planets 10× less dense than Saturn made of? (⇒Kepler-11f)
 What are the natures of exoplanets between super-Earths and Neptunes? (⇒GJ 3470b)
 What is the diversity of sub-giant planets up to 100 Earth masses?

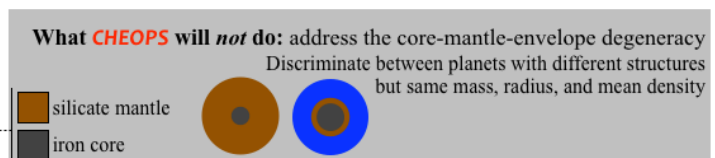
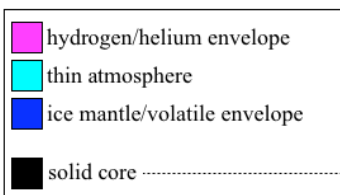
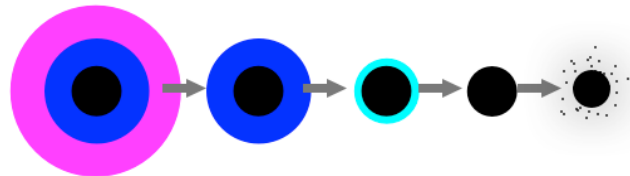
Which super-Earths have volatile envelopes?

Which ones are amenable to atmospheric characterisation?
 bear habitable conditions?



What is the fate of highly-irradiated exoplanets?

Do all irradiated exoplanet lose their atmospheres?
 Are hot super-Earths evaporation remnants? (⇒Corot-7b)
 Can rocky planets disintegrate? (⇒KIC 12557548b)



2.1.3 Mission goals

The goal of the CHEOPS mission is to measure the bulk density of super-Earths and Neptunes orbiting bright stars and provide golden targets for subsequent, in-depth characterisation studies of exoplanets in these mass and size ranges. The bulk density is a key parameter allowing us to gain insight in the physical nature of these exoplanets. This will be achieved by measuring high-precision photometric sequences to detect the variation in the stellar brightness induced by a transiting planet.

CHEOPS is built to achieve a photometric precision similar to *Kepler* while observing much brighter stars located almost anywhere on the sky. The CHEOPS target list will mainly consist of stars with small exoplanets previously detected by accurate Doppler surveys and known transiting Neptune-size planets detected by ground-based photometric surveys. CHEOPS is also currently envisioned following-up a significant number of targets from the *TESS* survey (see 2.4.2).

In comparison with random searches such as those carried out by *CoRoT* and *Kepler*, CHEOPS will be incredibly more efficient. Knowing *where to look* and at *what time to observe* is priceless information particularly to detect (and characterise) long-period transiting systems (up to 50 days of revolution period).

The prime mission goals are:

1. **Performing first-step characterisations of super-Earths:** Measuring the radius, density, and inferring the presence or absence of a significant atmospheric envelope for super-Earths in a wide range of environmental conditions. This will be achieved by searching for shallow transits on bright stars ($6 < V < 9$ mag) already known to host planets in this mass range with revolution periods up to 50 days.
2. **Obtaining new insights into the physics and formation processes of Neptunes:** Measuring accurate radii for Neptunes, determining precise densities, deriving minimum values of their gas mass fractions, and inferring possible evolution paths. This will be achieved by characterising the transit light curves of tens of Neptunes with revolution periods up to 13 days, previously detected in transit across stars brighter than the 12th magnitude in the *V* band.
3. **Building a collection of “golden targets” for exoplanetology:** The small mass exoplanets transiting bright stars observed by CHEOPS will be the best suited targets for in-depth atmospheric characterisation by spectroscopic facilities contemporaneous or subsequent to the mission (e.g., the *James Webb Space Telescope*).

Secondary objectives directly deriving from the capacity of CHEOPS to achieve its prime goals are:

4. **Estimating the albedo and cloud coverage of hot Jupiters:** Measuring the phase modulation of a handful of short-period giant planets along their orbits at optical wavelengths will show how these exoplanets reflect the stellar light, allowing to map the reflectivity of the planetary surface and gain knowledge of the cloud coverage homogeneity. This will be achieved by monitoring complete revolution periods of hot giant planets to obtain their phase curves and, in some cases, their secondary eclipses.
5. **Searching for co-aligned, inner and smaller planets in systems with transiting Neptunes:** Searching in these systems a shallower transit from a smaller planet otherwise undetectable by transit surveys has a good chance of success. As shown by *Kepler*, about 1/3 of the transiting Neptune-size planet candidates harbour additional smaller transiting companions. CHEOPS will be ideally suited to detect them. Observations of transit time variations can also be used to detect additional planets.

2.2 Structures of exoplanets and planetary systems

2.2.1 Interiors of exoplanets

As illustrated by Figure 3, Solar System planets very loosely sample the diversity of possible masses and radii below Saturn. Current exoplanet search programmes have discovered a continuum of mass or size

objects, ranging between telluric planets and ice giants on the one hand, and between ice giants and gas giants on the other hand. Almost no constraints exist so far on the possible structures, compositions, and origins of these exoplanets.

The knowledge of the planetary radius by transit measurements combined with the determination of its mass through radial velocimetry allows the determination of the mean bulk density of the planet. It represents our most direct way to constrain the planetary structure and hence its bulk composition. The mass and radius measurements available today for super-Earths are shown in Figure 6. Although the uncertainties on the mass, radius, or both, are large in most cases, the current measurements suggest that several of these known super-Earths are not Earth-like in terms of composition. A telluric planet like the Earth is literally dry, as it bears only 0.01 to 0.1%wt² of water. In contrast, much larger fraction of water (or other volatile species) are needed in order to explain the large radii of several known transiting super-Earths. In fact, as can be seen in Figure 6, a 5-M_⊕ “ocean planet” composed by 50%wt of solid refractory material (rocks and metals) and by 50%wt of volatile material (water) has a radius roughly 30% as large as a 5-M_⊕ Earth-like planet (mainly composed by rocks and metals).

Recent studies explore the possibility that low-density super-Earths could be composed of large rocky cores surrounded by hydrogen-rich envelopes (e.g., Elkins-Tanton & Seager 2008). Such envelopes would have an even more dramatic effect on the planetary radius than a steam envelope, due to the reduced molecular weight of hydrogen compared to water. Therefore, 1 to 2%wt percents of hydrogen could have the same impact on the radius of a super-Earth than ~20%wt of water or more.

2.2.1.1 Constraints on planetary interiors from measured radius and mass: what is possible?

As mentioned above and extensively discussed in the literature (e.g., Valencia et al. 2007; Sotin et al. 2007), the mean density alone does not allow deriving a unique internal structure. Rather, the mean density allows us to determine an ensemble of compositions and structures that match the observed mass and radius.

Interestingly, this uniqueness problem is also affecting our knowledge of the interior of Solar System planets. In this case, additional quantities constraining the models can be determined either by laboratory measurements (e.g. meteoritic samples), remote sensing (e.g. spectroscopy), or in-situ measurements (e.g. gravitational moments or chemical composition measurements). However, even with these additional quantities helping narrowing down the possibilities, additional assumptions are needed (e.g., bulk composition, degree of differentiation, internal degree of rotation, etc.) to be able to determine an internal structure. One key assumption is to consider that the stellar abundances are representative of the bulk composition of inner planets.³ Using this assumption for the Solar System, Sotin et al. (2007) modelled the structure of the telluric planets. They were able to reproduce the main features of the internal structures of the Earth, Venus, and Mars.

In the case of exoplanets, the situation is even more difficult as essentially no additional information is directly measurable. However, using the Solar System as a guide, the photospheric abundances of the host stars could be used as a first proxy for the bulk composition of the planets (doing this would provide good internal structures for Earth, Venus and Mars). Given that the CHEOPS targets are bright stars, this information will be readily available. Furthermore, as illustrated by the “ocean planet” model (Léger et al. 2004; Ehrenreich et al. 2006), Solar System objects (e.g. icy moons) can inspire internal structures of exoplanets (one of the science motivation of ESA’s *JUICE* mission). In any case, setting constraints on the possible internal structures of different types of exoplanets from their mean density is an important step towards comparative planetology. In this approach, detail knowledge is replaced over time by sample size from which new insights can be derived. This has been compellingly illustrated by the paradigm shift in planet formation theory that followed the discovery of exoplanets.

² Weight percentage (%wt).

³ In the case of the Solar System, stellar (solar) and meteoritic abundances agree in most cases to within 10%. Consistent abundances between the star and planets is also a prediction of recent formation-composition models for other planetary systems (Thiabaud et al., submitted; Marbœuf et al., submitted). For the CHEOPS systems, relative stellar abundances (e.g., iron-to-silicon [Fe/Si] and magnesium-to-silicon [Mg/Si] abundances) could be determined to better than 0.1 dex (§2.3.4).

For super-Earths, the degeneracy of possible structures lies in the difficulty to estimate the respective amounts of metals in the core (mainly iron), rocks (silicates in the mantle), volatile species (mainly water), and even gas (H/He). For instance, two planets, one made of silicates, and one made of iron and water, can have the same mass and radius. However, it is possible, based on the determination of both the mass and radius, to determine unambiguously a *minimum* mass of gas in planets. Indeed, all planets located above the solid blue curve in Figure 6 should have a sizeable H/He-gas atmosphere (see, e.g., Kipping et al. 2013): for a given mass, the radius of a pure water planet represents an upper limit for the radius of a planet devoid of H/He. Therefore, a lower limit to the envelope mass can be derived by matching the observed radius and mass, assuming a pure-water ice core, a composition of the envelope, and a temperature (corresponding to the equilibrium temperature with the stellar flux, an adequate assumption if the planet is not located too close to its star).

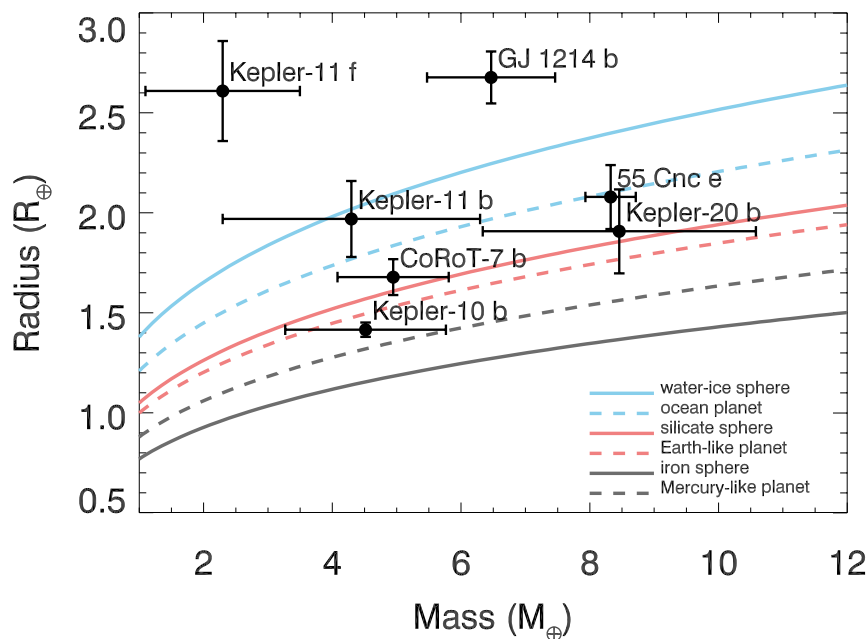


Figure 6 | Mass-radius relationship for different bulk composition of the planet (adapted from Wagner et al. 2011) with superimposed known transiting super-Earths where both the mass and the radius of the planet have been measured (with the $1\text{-}\sigma$ errors on these parameters). So far, in most cases the error bars are too large to obtain an unambiguous measurement of the bulk structure of the planets.

For those planets located below the 100%-water model in Figure 6 (solid blue curve), it is in general not possible to disentangle the fraction of volatile species from the fraction of H/He gas. The class of exoplanets that are so close to their parent star that they have lost their H/He envelope as a result of erosion by stellar irradiation (see §2.2.2.3) represents a notable exception to this problem. This may have happened to super-Earths such as Corot-7b, Kepler-10b, Kepler-78b or 55 Cancri e (Lecavelier des Etangs 2007; Valencia et al. 2010; Ehrenreich & Désert 2011; Gillon et al. 2012; Pepe et al. 2013). In such cases, it could be possible to derive the planetary radius as a function of planetary mass, given the (measured) stellar abundances and assuming a mass fraction of volatile species.

The comparison between the observed and the theoretical radii could therefore be used to yield first-order constraints on the amount of volatiles in the class of highly irradiated planets. This volatile fraction is in fact the dominant parameter influencing the radius of a super-Earth in the absence of H/He (Grasset et al. 2009). The CHEOPS precision on the radius measurements ($< 10\%$; see §2.2.1.3) will allow us to determine the fraction of volatiles on a hot super-Earth devoid of a H/He gas envelope with an uncertainty $\approx 33\%$ (Grasset et al. 2009).

For super-Earths at larger separations from their host stars and thus in milder conditions in terms of stellar irradiation, an important consequence of the presence of a massive envelope of volatile species is the formation of a high-pressure ice mantle enshrouding the rocky core. In fact, according to the phase diagram of water, high-pressure ices can exist at temperatures up to $\sim 1\,000$ K for pressures of ~ 100 GPa. These

conditions are typically expected in the depths of ocean planets. Alibert (2013) formulates a criterion yielding, as a function of the super-Earth mass, the critical planetary radius above which an icy mantle is a natural outcome of internal structure models. This criterion could be applied to the long-period (< 50 days) super-Earths detected in transit by CHEOPS.

2.2.1.2 Relations between planetary structures and planetary formation

2.2.1.2.1 Constraints on the critical core mass for the core accretion formation scenario

In the core accretion model, the most widely accepted scenario to explain the formation of low-mass and close-in planets, the growth of a planet occurs in two phases (Pollack et al. 1996). In the first phase, a planetary core forms by accretion of planetesimals. Already during this phase, the core can gravitationally accrete some gas originating from the protoplanetary disc. When the mass of the core is larger than a so-called critical mass, the accretion rate of gas increases in a runaway mode, leading to the rapid formation of a massive gaseous envelope. In this respect, in our Solar System it is not clear why Uranus and Neptune did not accrete larger gaseous envelopes as their core masses are thought to be similar to those of Jupiter or Saturn.

The value of this critical core mass represents the transition between low-mass core-dominated planets (somehow similar to scaled-up version of the telluric planets) and envelope-dominated planets. Measuring the critical core mass, and its dependence on semi-major axis and stellar properties, such as the metallicity, would be of primordial importance for planetary science. Such a measurement would definitely establish the core accretion theory as the physical process of planetary formation, provide a physical explanation for the origin of different types of planets, and allow constraining some of the properties of the building blocks of planets (see, e.g., Fortier et al. 2013).

In fact, the critical core mass mainly depends on the properties of planetesimals and the typical opacity of gas and dust in the circumstellar disc: the critical core mass is larger for higher opacity, hence for higher metallicity. Observationally, the critical core mass can be determined by measuring the mean density of a sample of planets with similar semi-major axis and metallicity (known for all CHEOPS targets). Below the mass of Saturn, it is expected that planets with sub-critical cores have densities higher than planets with super-critical cores, which should have accreted massive envelopes. The transition mass between high-density and low-density planets should therefore give an estimation of the mass of planets with cores at the critical mass, which can be related, using internal structure models, to the mass of the critical core itself.

2.2.1.2.2 Constraints on migration paths

There is ample evidence that planets are not born where they are observed today but that they have migrated during their formation possibly over large orbital distances. The present-day observed location could therefore have been reached following different paths depending upon the growth history of the planet and the interactions with the gaseous disc and/or other planets. Each of these paths samples different regions of the proto-nebula in varying proportions leading to unique combinations corresponding to the growth history and chemistry, appropriate to the amount of time spent at a given orbital radius. As a result, the bulk composition, and hence the mean density, will depend upon which track was followed.

Simulations have been performed to illustrate this aspect. Figure 7 sketches three possible resulting formation tracks for three test-planets in different disc models. The simulation is based on the Bern planetary system formation model (see Alibert et al. 2013). The three planets end their evolution close to the star (~ 0.05 au), with similar masses ($\sim 9 M_{\oplus}$), but with significantly different amount of accreted gas. The differences in composition translate into differences in radius. The more gas-rich planet (starting at 2 au) grows to a final radius of $5.5 R_{\oplus}$, hence has a bulk density of 0.3 g cm^{-3} , while the less gas-rich planet (starting at 1.4 au) has a radius of $4.4 R_{\oplus}$, and a bulk density of 0.6 g cm^{-3} , and the intermediate one (starting at 2.5 au) a radius of $3.9 R_{\oplus}$ and a bulk density of 0.8 g cm^{-3} . By measuring the planetary radii and bulk densities, CHEOPS will place constraints on the migration tracks of exoplanets. CHEOPS will achieve a precision of 30% on the bulk density (see §2.2.1.3 below), which will allow the discrimination of the cases described above.

Concerning volatile species, the presence of sizeable amounts of water in the planet, which could be constrained for close-in super-Earths as described in §2.2.1.1, is also only possible if a transport of matter

has occurred during the formation epoch of these planetary systems. Possible transport mechanisms include planetary migration, radial drift of planetesimals, or a combination of both effects. CHEOPS observations of volatile-rich super-Earths will therefore be useful to set constraints on transport mechanisms in the protoplanetary discs.

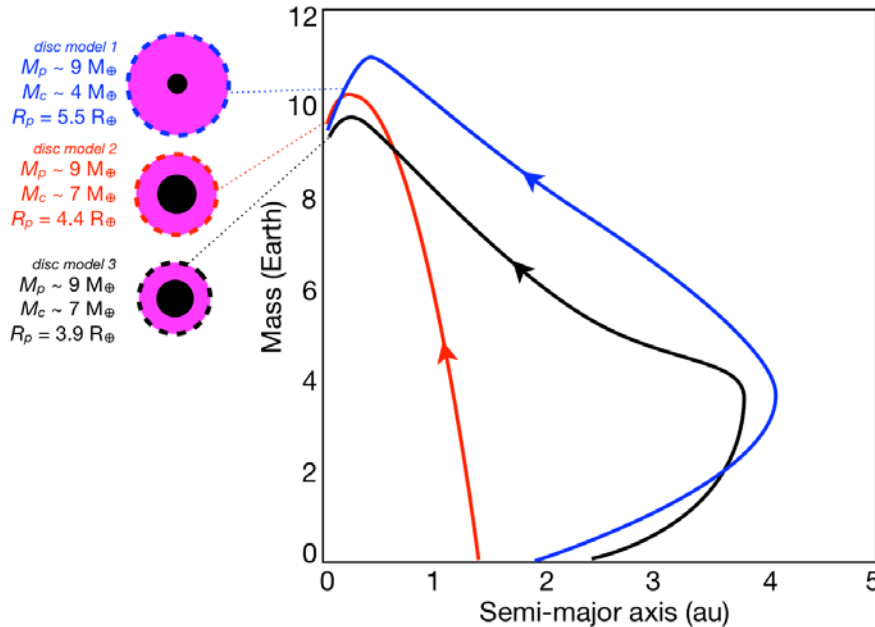


Figure 7 | Sketch of possible migration tracks for three exoplanets with different formation and migration history, based on Bern planetary system formation models. The tracks show the evolution (from mass 0) of the planetary masses along with the evolution of the separations (starting at 1.4, 2, and 2.4 au from the star). The three colours correspond to three different initial conditions (starting location of the planets, properties of the protoplanetary disc). All planets end up at ~ 0.05 au with similar masses ($\sim 9 M_{\oplus}$) but different core masses (black) and radii, as illustrated on the left-hand side of the figure.

2.2.1.3 Precision on planetary radius measurements with CHEOPS

The large population of short-period ($P < 100$ days) low-mass ($M_p < 30 M_{\oplus}$) planets discovered by HARPS and *Kepler* around solar-type stars shows an impressively large spread in masses and radii that probably reflects a significant inhomogeneity in composition and orbital origin (Mayor et al. 2011; Batalha et al. 2013; Chiang & Laughlin 2013, and the above example). Some of these planets could be silicate-rich planets formed in-situ, some could be terrestrial planets having accreted a hydrogen envelope or having outgassed a dense metal-rich atmosphere, some could be remnants of migrating giant planets having lost a fraction of their primordial atmosphere, etc.

The precise measurement of the mean density of exoplanets is necessary to constrain the bulk compositions and discriminate between families of planets: telluric (rocky) super-Earths, volatile-rich super-Earths, and Neptunes. Useful compositional constraints require a precision of $\sim 20\text{--}30\%$ on the density. This precision requirement on the density measurement translates into the need for CHEOPS to measure the mass and radius of the planet to better than 10%. Such precision will be achievable for all the telluric planets that will be probed by CHEOPS orbiting stars brighter than $V = 9$ mag. In this magnitude range, the 10%-precision mass measurements will be possible with precision Doppler measurements obtained by instruments like HARPS, HARPS-North, Espresso, etc. (see §2.3.1), while CHEOPS will provide the needed 10%-precision on the radii. This key specification defines the photometric precision required by the mission.

In order to quantitatively assess the photometric performances that CHEOPS will have to reach, extensive simulations have been performed, considering the smallest planet that CHEOPS could study, an Earth-sized planet transiting a nearby solar-type star. More specifically, the assumptions of the simulations are given in Table 1.

Table 1 | Summary of the parameters used in the simulation to assess the photometric precision needed by CHEOPS.

Parameter	Value
Radius of the planet, R_p (R_\oplus)	1
Revolution period of the planet, P (days)	30
Stellar magnitude, V (mag)	8.5
Stellar mass, M_* (M_\odot)	0.92 ± 0.045
Stellar radius, R_* (R_\odot)	0.94 ± 0.08
Stellar effective temperature, T_{eff} (K)	$5\,500 \pm 50$
Transit impact parameter, b	0.25

The transit depth corresponding to these parameters is $(R_p/R_*)^2 = 95$ parts-per-million (ppm). The magnitude of the star corresponds to the faint end of the samples typically targeted by the *highest-precision* Doppler surveys. The impact parameter of the transit is assumed to be $b = 0.25$, corresponding to a transit duration of ~ 5.5 h. CHEOPS observation is assumed continuous over a (up to) 48-h period centred on the transit, with exposure times of 1 min. Some prior knowledge of the stellar parameters is assumed to come from independent measurements with realistic precisions for a bright nearby star (§2.3.4), yielding the uncertainties associated with the stellar parameters. The temperature measurement is assumed to come from high-resolution spectroscopy (as described in §2.3.4), the stellar radius can come from long-basis interferometry or precise parallax and apparent magnitude measurements (as will be provided by the *Gaia* mission), and the stellar mass uncertainty is estimated from stellar evolution modelling using the measured spectroscopic parameters as inputs. The normal distributions corresponding to these measurements were used as prior distributions in the Bayesian model described below.

The white noise in CHEOPS measurements is estimated to be 111 ppm, taking photon, read-out, dark current, and background noises into account. This theoretical white noise is then used to simulate transit light curves, assuming a smooth trend to represent the low-frequency variability of the star, and assuming the presence (or absence) of a systematic effect leading to correlation of the noise with time. This correlated noise (also known as “red noise”) is modelled as a sine function, tuned to test different frequencies and amplitudes. The goal of these simulations is to assess, for different frequencies, the highest amplitude of the correlated noise that could be acceptable for CHEOPS, with respect to its scientific objectives.

The resulting light curves (one example is shown in Figure 8, *right*) were analysed with a Markov chain Monte-Carlo (MCMC) code (Gillon et al. 2012), taking into account the prior distributions on the stellar parameters and also the correlation of the noise, to derive realistic posterior distributions on the transit and physical parameters of the system. For each period of the assumed sinusoidal systematic effect, several phases were tested and the results were averaged. The trend representing stellar variability was modelled in the MCMC as a second-order time polynomial.

Figure 8 (*left*) shows the resulting relative error on the planetary radius as a function of the correlated noise amplitude, for 3 different periods for the systematic effects corresponding to half, one, and two orbital period(s) of CHEOPS around the Earth (50, 100, and 200 min, respectively). Indeed, variations along the spacecraft orbit, in particular variations in the thermal environment of the satellite, are expected to be the prime source of systematic effects on the photometry. Figure 8 (*left*) shows that for red noise amplitude > 30 ppm, the 10% precision on the planetary radius is not achieved, especially for the longer periods of the correlated noise. *The conclusion of these simulations is that in order to measure planetary radii with the precision required to fulfil the scientific objectives, the maximum tolerated level of correlated noise in CHEOPS photometry should be < 20 ppm.*

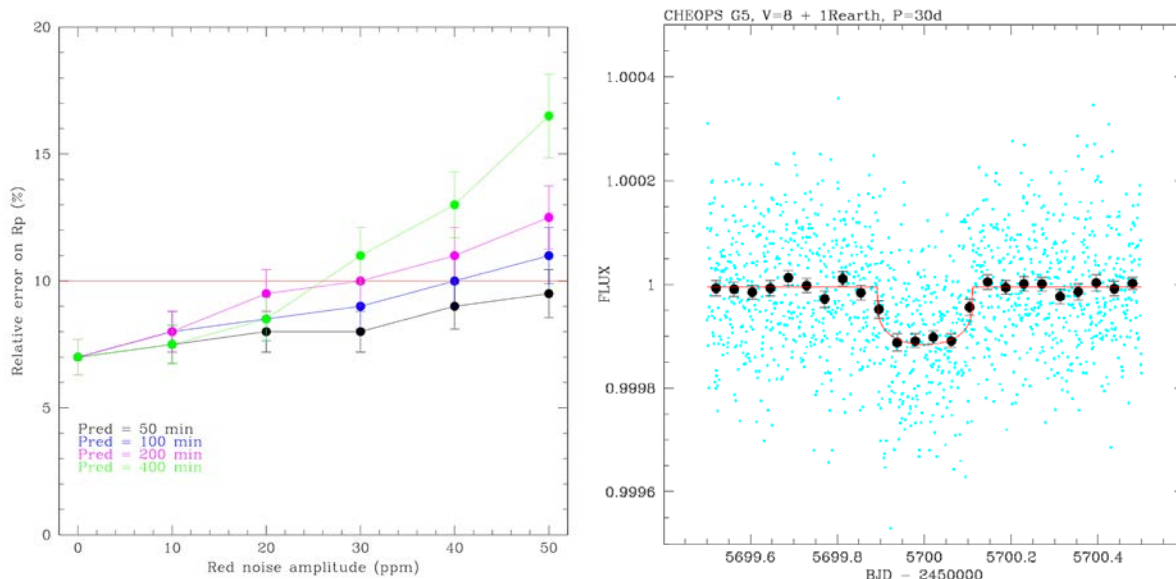


Figure 8 / **Left panel**— Relative precision on the transiting planet radius as a function of the amplitude of the red noise injected in the data, for three different frequencies of the red noise. **Right panel**— Simulated CHEOPS light curve assuming a red noise amplitude of 20 ppm and a period of 100 min, unbinned (cyan dots) and binned per hour (black dots), with the best-fit transit model superimposed (red curve).

2.2.2 Atmospheres & envelopes

2.2.2.1 Identification of planets with atmospheres or fluid envelopes

As the scientific community prepares for the rise of powerful telescopes with large collecting surfaces such as the *James Webb Space Telescope (JWST)* in space or the European Extremely Large Telescope (E-ELT) on the ground, a central question to ask is: what are the best targets for follow-up, atmospheric spectroscopy of small exoplanets? Super-Earths with sizes of about $2 R_{\oplus}$ are believed to be either composed predominantly of rock or scaled-down versions of Neptune with thick gaseous envelopes. If the bulk composition of an exoplanet cannot be made from a material lighter than water, then one can calculate the thickness of the atmosphere, relative to the measured radius, by utilising the mass-radius relation of pure water (Kipping et al. 2013). Negative values of this metric imply a mostly rocky composition (e.g., Earth, Kepler-36b; Kipping et al. 2013). By quantifying this metric for the entire CHEOPS catalogue of small exoplanets, one can construct a valuable database of optimal follow-up targets. Knowledge of the fraction of small exoplanets with and without thick atmospheres, as a function of their other properties, provides a direct constraint on planet formation theories (§2.2.1.2).

2.2.2.2 Constraints on atmospheric properties from visible broadband photometry

In the past decade, numerous studies have been published on the use of wavelength-dependent primary transits and secondary eclipses to characterise the atmospheres of exoplanets, including the super-Earths GJ 1214b (e.g., Charbonneau et al. 2009; Bean et al. 2010; Berta et al. 2012; de Mooij et al. 2012), 55 Cancri e (e.g., Demory et al. 2012; Ehrenreich et al. 2012; Crossfield et al. 2012), and GJ 3470b (e.g., Nascimbeni et al. 2013). Highlights include the claimed detections of molecular features (in the infrared; e.g., Knutson et al. 2011) to the inferred presence of clouds or hazes (in the visible; e.g., Pont et al. 2013) in the atmospheres of hot Jupiters, and even the detection of the exospheres of hot Jupiters (e.g., Vidal-Madjar et al. 2003; Lecavelier des Etangs et al. 2012). While future missions like *JWST* are poised to obtain infrared spectra of exoplanetary atmospheres, visible data provide crucial and complementary information on the properties of these atmospheres. Specifically, visible data determine the albedo (Evans et al. 2013), the presence of scattering (which is caused by the dominant atmospheric gas or by haze particles), and the relative abundance of clouds or hazes in the atmosphere. Clouds have long been an obstacle in our understanding of the atmospheres of Earth, Solar System objects, and brown dwarfs; they are rapidly emerging as a major theme in the study of hot Jupiters, super-Earths, and directly imaged exoplanets.

2.2.2.2.1 Constraints from the transit light curve

The spectroscopically active molecules of an atmosphere typically contribute spectral features in the infrared, but these molecules are often minor constituents of an atmosphere (by mass). The knowledge of the pressure scale height⁴, set by the mean molecular weight, temperature, and surface gravity is of central importance in interpreting an exoplanetary atmosphere. *Because the atmospheric scale height depends on gravity, it can only be determined for planets which mass has been (precisely) measured, such as the CHEOPS targets.* The mean molecular weight is determined by the dominant molecule (by mass). On Earth and Titan, the dominant (and inert) molecule is molecular nitrogen (N₂); on Venus and Mars, it is carbon dioxide (CO₂); in gas giants like Jupiter, it is molecular hydrogen (H₂). Analyses of the spectrum of hot Jupiters often assume the atmosphere to be hydrogen dominated (Madhusudhan & Seager 2009). For telluric exoplanets with secondary atmospheres, the mean molecular weight is difficult to estimate. A robust way to infer the mean molecular weight is to measure the transits at two visible wavelengths (Benneke & Seager 2012) to retrieve the slope due to Rayleigh scattering, which is typically increasing towards short wavelengths (λ) as λ^{-4} . CHEOPS will make only one broadband measurement of the transit depth in the visible; however, this measurement will be systematically available and it will be used to constrain the Rayleigh slope when used in combination with infrared spectrophotometry, which cannot provide any constraints on atmospheric scattering. Broadband visible data thus provides an important complement to the analysis of infrared data of exoplanetary atmospheres. Identifying the dominant scattering process and inert molecule in an atmosphere has significant implications for inferring its thermal structure and spectrum, as the inert component often exert an indirect influence on the spectroscopically active molecules via processes such as pressure broadening and collision-induced absorption. In addition, the thermal dynamics and cloud abundance in an exoplanetary atmosphere can be constrained with phase curves.

2.2.2.2.2 Constraints from the phase curve

Phase curves represents the flux of the star + planet system as a function of orbital phase (see Figure 2), which may be deconvolved to obtain the flux versus longitude on the exoplanet, known as a “brightness map” (Knutson et al. 2007; Cowan & Agol 2008). Infrared phase curves contain information about the efficiency of heat redistribution from the day side to the night side of an exoplanet (Showman & Guillot 2002; Cooper & Showman 2005; Showman et al. 2009; Cowan & Agol 2011; Heng et al. 2011), as previously demonstrated for hot Jupiters (e.g., Knutson et al. 2007, 2009). In contrast, *visible phase curves* encode the reflectivity of the atmosphere versus longitude, which in turn constrains the relative abundance of clouds or hazes if they are present. The cloud or haze abundance depends on the size and number density of the particles, as well as the local velocity, density, pressure, and temperature of the flow, implying that a robust prediction of the cloud properties requires to understand atmospheric chemistry and dynamics in tandem. Examples of exoplanets where clouds are likely to be present include Kepler-7b, which has a high albedo (~0.35) and a phase curve containing a surprising amount of structure (Demory et al. 2013; see Figure 9).

The detailed shape of the visible phase curve can constrain the size of the cloud particles: sinusoidal phase curves result from large particles, while small particles produce flat phase curves (Heng & Demory 2013). The feasibility of obtaining visible phase curves for giant planets has already been demonstrated for the *CoRoT* (Snellen et al. 2009) and *Kepler* (Borucki et al. 2009) missions. Since this phase effect can be seen on almost any hot Jupiter, including non-transiting geometrical configurations (but excluding systems orbiting in the plane of the sky), the number of potential targets amongst hot Jupiters detected orbiting bright stars is significant.

In the following, we explore CHEOPS abilities to constrain the phase curve properties of highly-irradiated hot Jupiters at visible wavelengths. For the hottest planets, the dominant contributor in the CHEOPS band pass may be of thermal origin rather than optical. Remarkably, the spectral energy distribution of extremely hot planets leaks into visible wavelengths rendering the distinction between thermal emission and reflected light difficult. In such cases, complementary observations in the infrared will allow us to precisely determine how reflected light and thermal emission contribute to the total phase modulation observed by CHEOPS. We

⁴ The scale height is $H = (k_B T) / (\mu g)$, where T is the atmospheric temperature, μ the mean molar mass, g the acceleration of gravity, and k_B is Boltzmann’s constant.

use the Kepler-7b phase curve shown on Figure 9 to assess the feasibility of phase-curve observations with CHEOPS, given different science cases. Kepler-7b is a gaseous planet twice larger than Jupiter and half its mass. It orbits its host star in 5 days. The binned Kepler-7b light curve yields a precision of 20 ppm per 5 min. This precision is required to extract the phase-curve parameters (amplitude of 50 ppm, offset of 13 h) at a level that provides meaningful constraints on, e.g., global circulation models. CHEOPS photometric precision is 67 ppm per 5 minutes for a $V = 9$ target.

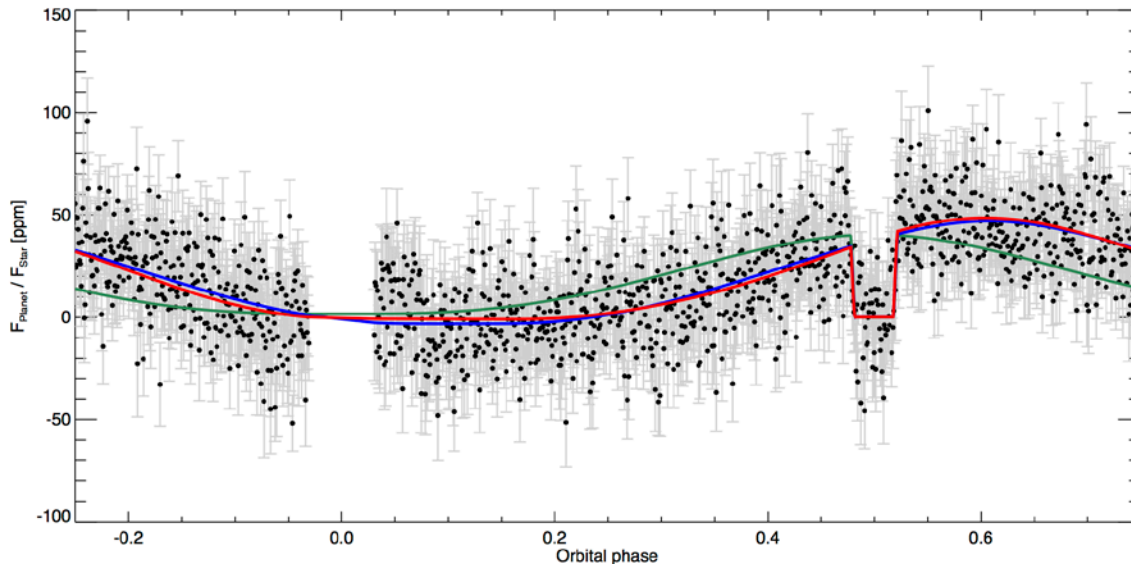


Figure 9 | Visible phase curve of the Kepler-7b exoplanet. The solid lines represent various model comparisons to the data. The phase curve peaks after secondary eclipse (the dip at an orbital phase of 0.5), suggesting an atmospheric structure in reflected light that does not follow that of thermal emission. This is strongly indicative of the presence of clouds. After Demory et al. (2013).

Using simple Gaussian scaling, we find that obtaining a phase curve similar to Kepler-7b in terms of amplitude and asymmetry for a star of the 7th magnitude, but on a 2-day revolution period (CHEOPS photometry should be stable for 48 h), would require observing 8 orbits of the planet with CHEOPS (hence, a maximum of 32 cumulated days of observations, assuming an observing efficiency of 50%). This will be possible for a handful of targets, preferentially the hottest Jupiters at very short periods.

Finally, for the most massive objects among the very hottest planets, it is possible to detect relativistic beaming and ellipsoidal variations (departures from spherical symmetry of the exoplanet due to tidal distortion) (Cowan et al. 2012; Faigler et al. 2013; Welsh et al. 2010). These effects modulate the light curve on characteristic time scales of 1/4 and 1/2 of the orbit, respectively.

2.2.2.2.3 Constraints from the occultation event

The albedo measures the fraction of starlight reflected by an atmosphere and therefore its energy budget. It is of central importance in determining the thermal structure of the atmosphere. Measuring the occultation depth of the secondary eclipse (see Figure 2) in the visible directly yields the geometric albedo (e.g., Demory et al. 2011), which is the albedo of the atmosphere at full orbital phase. By considering the geometric albedo over the entire orbit of the exoplanet (yielding the spherical albedo) and integrating over wavelength, one obtains the Bond albedo. When interpreting the spectrum of an exoplanetary atmosphere, knowledge of the Bond albedo determines both the amount of starlight and its penetration depth (Fortney et al. 2008; Heng et al. 2012) and helps determining the presence of clouds (Demory et al. 2011). Knowledge of the temperature-pressure profile then allows for the synthetic spectrum of the atmosphere to be computed accurately. For the hottest objects ($\sim 2\,000$ to $3\,000$ K), thermal emission from the exoplanet may contaminate the broadband visible data, thus confusing the measurement of reflected light versus thermal emission. The feasibility of measuring geometric albedos has already been demonstrated for the *Kepler* mission (see Figure 10).

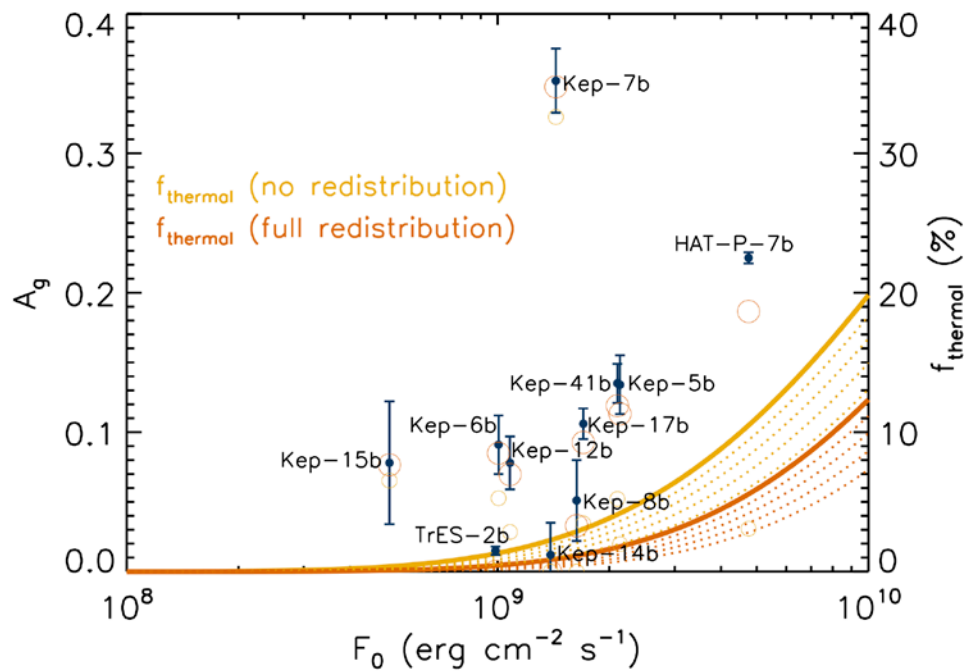


Figure 10 | Geometric albedos versus the incident stellar flux upon the exoplanet atmosphere, as measured by detecting visible occultations using Kepler. The curves attempt to estimate the amount of contamination by thermal emission leaking into the visible band pass. The small and large circles are the decontaminated values of the geometric albedos assuming no and full redistribution of heat from the dayside to the night-side hemispheres, respectively. After Heng & Demory (2013).

2.2.2.3 Atmospheric evolution of close-in exoplanets

Most exoplanets followed up by CHEOPS will have maximal orbital periods of 50 days, shorter than Mercury's (88 days). Hence, they will be submitted to extreme conditions in terms of stellar irradiation. While short-period planets around K or M dwarfs do not receive as much stellar black-body emission as they would receive around Sun-like stars, they are nonetheless submitted to extreme levels of high-energy fluxes and particles. The stellar soft X-ray and extreme ultraviolet (XUV) flux and the stellar wind plasma flow interact with the upper layers of planetary atmospheres. These energetic inputs can efficiently modify the density and temperature structure of the upper planetary atmospheres and affect finally the whole planetary evolution due to thermal and non-thermal atmospheric escape processes (Lammer 2013). Thermal atmospheric escape at Solar System planets occurs in thermospheres that are in hydrostatic equilibrium, so that the upper atmosphere experiences classical Jeans escape. Here, particles in the high-energy tail of the Maxwell distribution at the base of the exosphere (or exobase), that separates the collision-dominated region from the collisionless exosphere, can escape from a planet.

Highly irradiated exoplanets in close orbits around their host stars can experience dramatic atmospheric escape. Transmission spectroscopy of planetary transits in the UV revealed extremely extended hydrogen upper atmospheres escaping from several hot Jupiters (e.g., Vidal-Madjar et al. 2003; Lecavelier des Etangs et al. 2012; Ehrenreich et al. 2012). The observations of heavy species in the hydrogen clouds surrounding the planets (Vidal-Madjar et al. 2004; Linsky et al. 2010) show that in contrast with planets in our Solar System, the escape is hydrodynamic. The atmospheric gas envelopes, mainly composed by hydrogen, experience non-hydrostatic conditions, where radiative heating can only be compensated by an adiabatic expansion, so that the major gases in the XUV-heated thermosphere expand hydrodynamically, and carry up heavier elements such as ionised carbon (C II). Under such extreme conditions, the exobase levels can be located at several or even tens of planetary radii above a planet's surface (Erkaev et al. 2013; Lammer et al. 2013). As a result, light atoms or molecules such as H, H₂, and He can experience high thermal escape rates, of $\sim 10^{10-11}$ g s⁻¹. Such rates are negligible with respect to the gas reservoir in a hot Jupiter; however, they could be sufficient to threaten the long-term stability of lower-mass planets, such as super-Earths. There is even a possibility that the hot rocky planets Corot-7b and Kepler-10b are evaporation remnants, the remaining cores of super-Earths that once possessed a gas envelope (e.g., Lecavelier des Etangs 2007; Davis

& Wheatley 2009; Valencia et al. 2010; Ehrenreich & Désert 2011). In this frame, the simple identification by CHEOPS of the existence of a thick atmosphere on a super-Earth will constrain the efficiency of the atmospheric escape mechanism.

The atmospheric escape rate depends on the host star XUV flux (i.e., age, spectral type, etc.) and planetary parameters such as the semi-major axis, the equilibrium temperature, the gravity of the planet (hence its mass and radius), and the mean molecular weight in the thermosphere.

Figure 11 shows an estimated mass-loss evolution of hydrogen-dominated planets with initial masses between 12–95 M_{\oplus} at an orbit of ~ 0.02 au around a G-type star, based on the energy-limited hydrodynamic mass-loss rate equation (Sekiya et al. 1980; Watson et al. 1981; Erkaev et al. 2007; Lammer et al. 2009). The different colours correspond to different percentages of planetary mass loss for an integration time of 0.01–5 Gyr, from black where negligible mass-loss occurs to red where only a core with a mass of 5 M_{\oplus} remains. The XUV evolution in Figure 11 corresponds to the power law given for G stars in Penz et al. (2008). One can see that low-density hot Neptunes ($< 20\text{--}30 M_{\oplus}$) are the most affected by atmospheric evaporation.

CHEOPS will provide radii for exoplanets with already accurately known masses. *Both the planetary mass and radius are critical to interpret the observations of atmospheric evaporation.* In the frame of an energy-limited atmospheric escape, the mass-loss rate is determined by a balance between the incoming energy absorbed in the upper atmosphere of the planet and the gravitational potential of the planet (Lecavelier des Etangs 2007). The knowledge of the gravitational potential relies mainly on the knowledge of the planetary radius ($\propto 1/R_p^2$). In addition, the size of the escaping atom cloud is related to the size of the Roche lobe (Bourrier & Lecavelier des Etangs 2013), which is a function of the planet-to-star mass ratio.

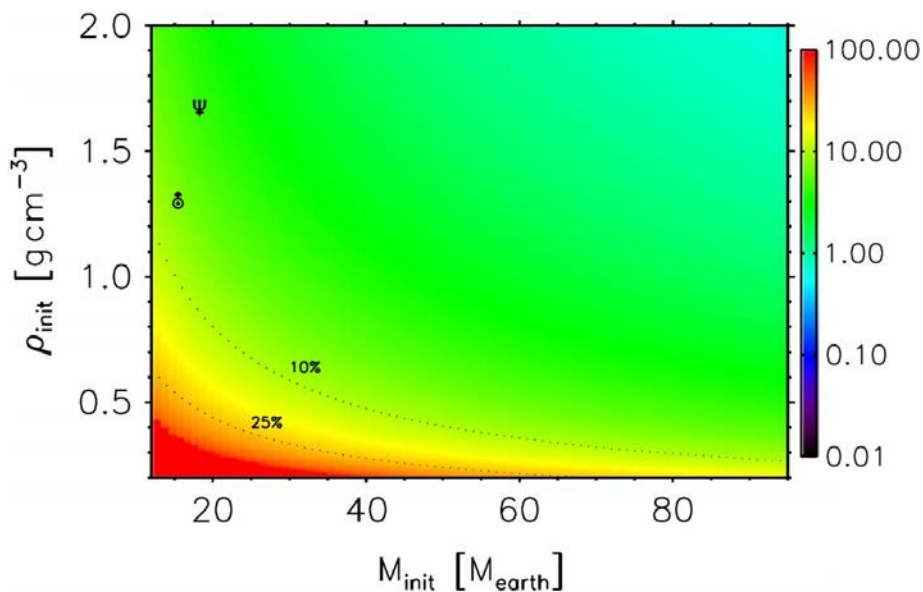


Figure 11 | Estimated mass-loss evolution caused by XUV-driven evaporation of hydrogen for exoplanets with initial masses in the range 12–95 M_{\oplus} , as a function of their mean density within a range of 0.2–2 g cm^{-3} . All planet models are located at 0.02 au around a G-type star. The colour bar ranges from negligible mass-loss (black) to a mass-loss where only the core (with a mass set to 5 M_{\oplus}) remains (red; after Leitzinger et al. 2011). The corresponding mass-loss of the two Solar System hydrogen-rich ice giants Uranus and Neptune also shown and the dotted lines illustrate the effect of assumed fraction of energy transferred into heating of the thermospheric neutral gas (the “energetic efficiency”).

The example of Kepler-11f (see Figure 3), a $\sim 2 M_{\oplus}$ exoplanet with a mean density similar to Saturn, is a tell-tale sign that super-Earths with hydrogen envelopes could exist. Such planets, with Earth-mass cores surrounded by hydrogen envelopes, which account for 0.1 to 10% of the mass, can have radii between $\sim 1.3\text{--}4.5 R_{\oplus}$ (Mordasini et al. 2012). If such hydrogen envelopes would experience a similar stellar XUV flux about 100 \times larger than that of today’s Sun – which is certainly possible at short semi-major axes – the escape rates could differ by $\sim 10^7$ to 10^{10} g s^{-1} , based only of the radius difference. From this example, which yields 3

orders-of-magnitude different thermal escape rates, one can easily understand how sensitive the atmospheric evaporation is to the planetary radius. The importance of accurate stellar and planetary parameters becomes more relevant for low-mass exoplanets because due to the low gravity and related upper atmospheric structure, the stellar XUV radiation can be deposited over a broad range of altitudes in the atmosphere, while for hot Jupiters the energy is deposited in a narrow layer close to the base of the thermosphere.

Lammer et al. (2011) pointed out that the detection and study of extended upper atmospheres around exoplanets provide promising insights into the interaction of the host star's plasma environment with the planet itself, as well as it sheds light into the evolutionary stage of these bodies, their atmospheres and possible magnetic obstacles. Therefore, by observing planetary hydrogen clouds and related coronæ of energetic neutral atoms (ENAs; Holmström et al. 2008) around transiting super-Earths and Neptunes in the far UV, we will learn more on the structure of non-hydrostatic upper atmospheres and the related thermal evaporation. In fact, the observations of exoplanetary upper atmospheres rely on the absorption detected during the transit in the stellar Lyman- α emission line of atomic hydrogen, which is located in the far UV at 121 nm. Because this line is efficiently absorbed in the interstellar medium, such observations are only possible for nearby planetary systems, typically located < 50 pc from Earth. By aiming at bright and nearby stars, CHEOPS will ensure that all its targets could be observed at Lyman- α to search for signatures of atmospheric evaporation.

Depending on the size, mass, and composition of a super-Earth, a hydrogen-rich upper atmosphere under non-hydrostatic conditions can interact with the stellar radiation pressure and the stellar wind and give rise to a huge hydrogen corona. The observations of the size of the extended upper atmospheres and related hydrogen-coronæ of transiting planets characterised by CHEOPS will be possible with the *Hubble Space Telescope*, which is planned to be operational until 2018–2019 and, later, with missions such as the *World Space Observatory-UV (WSO-UV)*; Shustov et al. 2009), scheduled for launch in 2016.

2.2.3 Orbital dynamics of planetary systems

2.2.3.1 Detection of additional planets through transit time variations

Transit time variation (TTV) is a powerful technique to discover additional bodies in a planetary system by detecting and modelling small changes in the orbital period of an already known transiting planet (Holman & Murray 2005; Agol et al. 2005). From the measured TTV signal it is possible to infer the parameters of the third body by assuming that it is gravitationally perturbing the known planet. Transit time variation analysis requires the accurate estimate of the central instant (T_0) of a large number of individual transits, and therefore it is very efficient from space-borne facilities where both temporal coverage and photometric precision is high. This was the case of *Kepler*, as it was for *CoRoT*, and it will be for CHEOPS.

Transit time variation is a dynamical technique. It provides an independent estimate of the mass of the perturbing body, thereby allowing to determine its nature (planet, brown dwarf, stellar companion, etc.). For this reason, TTVs can be exploited to confirm and characterise a multiple system discovered by transit even if radial velocity measurements are not feasible or if the precision of the measurements is too low. The most impressive case published so far is the Kepler-11 multiple planet system, with a star hosting six transiting planet candidates, of which at least the inner five were confirmed by TTV (Lissauer et al. 2011, 2013). CHEOPS can detect transits from additional unknown planets in the targeted systems, which velocimetric signal could not be detected by the current facilities. In these cases, the analysis of TTVs of the known exoplanet will be the only method to confirm the planetary nature of these detected transits. We expect that these additional planets will be quite common especially among the Neptunes and super-Earths in the CHEOPS sample, as about 20% of stars hosting planets with masses $< 30 M_{\oplus}$ are expected to host at least another transiting planet (Fabrycky et al. 2012).

On the other hand, a planet detected by TTV does not need to be necessarily transiting. Once observational biases (such as projection effects) are taken into account, about 85% of *Kepler* planetary systems are expected to be multiple (Fang & Margot 2012). When applied to CHEOPS data, the TTV technique would then allow the mission to greatly increase its discovery parameter space.

Usually, TTV signals are detected by inspecting a *O-C* (observed minus calculated) diagram. For each observed transit, the central time predicted by a linear ephemeris $C = P N + T_{\text{ref}}$ (where P is the revolution period and N the number of transits elapsed since a reference time T_{ref}) is subtracted from the measured best-

fit central time $O = T_0$. The resulting $O-C$ residual is then plotted against N (also called “epoch”), or time to search for drifts or periodic patterns. For an unperturbed two-body transiting system, we expect a completely flat $O-C$ diagram. When there is a significant amount of scatter in the $O-C$ diagram, an estimator for the amplitude is its root mean square (rms), called ΔTTV . The main quantities at play will be then ΔTTV , the error ΔT_0 with which the central instant T_0 of each single transit can be measured, and the number of observed transits N_{obs} .

To quantify the possible range of ΔTTV to be explored on realistic systems, a set of three-body simulations was performed using the TRADES numerical integrator (Borsato et al., in preparation). The simulated target is modelled after the well-known hot Neptune HAT-P-11b (Bakos et al. 2010), which has a revolution period of $P = 4.8878$ days and a mass of $\sim 26 M_{\oplus}$ and is hosted by a main-sequence K4 dwarf on a circular orbit. The third body (the outer “perturber”) is constrained on an initially circular orbit coplanar with the target orbit. Several simulations are carried out by varying each time the mass M_{pert} and period P_{pert} of the perturber. Each simulation spans about 3.5 yr (the planned CHEOPS operational window) and every transit time T_0 is extracted for constructing a synthetic $O-C$ diagram. The resulting ΔTTV is shown in Figure 12 as a function of M_{pert} and P_{pert} , after being averaged over eight different values of initial mean anomaly of the perturber. It is evident that ΔTTV is at first approximation linearly proportional to M_{pert} , while the dependence on P_{pert} is much more complex, revealing the presence of many mean motion resonances (MMRs) where P_{pert} is commensurable with the period of the targeted planet. These MMRs are known to amplify the TTV signal by several orders of magnitude (Agol et al. 2005); in our specific case, the strongest and widest ones are those at period ratios 2:1, 3:2, 4:3, and 5:4. The plot is limited to $P_{\text{pert}} > 6$ days because shorter orbits make the considered system unstable. At $P_{\text{pert}} > 11$ days, ΔTTV is simply monotonically decreasing, because resonances like 3:1, 5:2, 4:1, and higher lead to libration periods too long to be fully sampled by the 3.5 yr observing window: their effect on the data is thus negligible or misinterpreted as a linear drift, and the corresponding ΔTTV equal to the non-resonant case. Larger masses $M_{\text{pert}} > 30 M_{\oplus}$ are not probed in this context because giant perturbers would have been already detected by velocimetric follow-ups, even at much larger periods.

Interestingly, massive super-Earth and Neptune perturbers yield $\Delta\text{TTV} > 60$ s at nearly every configuration with P_{pert} shorter than 2:1, even outside resonances, while near low-order resonances, ΔTTV is boosted up to one hour or more. In the case of an Earth-mass perturber, the signal is still $\Delta\text{TTV} > 100$ s close to resonances, dropping to a few seconds otherwise. It is worth noting that resonant and especially quasi-resonant orbital configurations appear to be common amongst compact multiple systems of Neptunes and super-Earths identified by *Kepler* (Fabrycky et al. 2012).

2.2.3.2 Optimisation of the extraction of dynamical information from the light curve

The accuracy on the measurement of the central transit time T_0 is known to be influenced by many factors, including the photometric precision, the temporal cadence, the intrinsic shape of the transit light curve, the amount of correlated (red) noise and its full spectrum, and the analysis technique adopted (Kipping et al. 2010). It is fundamental to investigate what will be the limiting factors of CHEOPS, how the observing strategy need to be optimised, and, in particular, whether the nominal observing cadence (1 measurement per minute) is fast enough to exploit the full potential of this mission.

In order to estimate the timing accuracy ΔT_0 in a realistic way, synthetic planetary transits have been injected in a flat light curve of real instrumental noise, then T_0 is estimated by fitting the light curve with a model. The process has been repeated 100 times for each instrumental setup, each time injecting the transit at random phases; the rms of the differences between injected and recovered T_0 is then assumed to be the achievable timing error ΔT_0 . The JKTEBOP code (Southworth 2008) was employed to generate the synthetic transits and to fit them.

Two parallel sets of simulations were performed, corresponding to the S/N ratio expected from a $V \sim 8$ - and $V \sim 10$ -mag star (101 and 256 ppm in one minute, respectively). In each set, the sampling cadence was varied from 1 to 60 s with a 1-s step, injecting and recovering 100 transits at each step. Synthetic light curves generated at 120-, 60-, 30-, and 5-s cadences for a $V = 10$ -mag star are shown as examples in Figure 13 (left). Gaps are not included in simulated time series, while a typical real target will not be observed for at least 20% of each 101-min spacecraft orbit due to pointing constraints and passages through the South-Atlantic

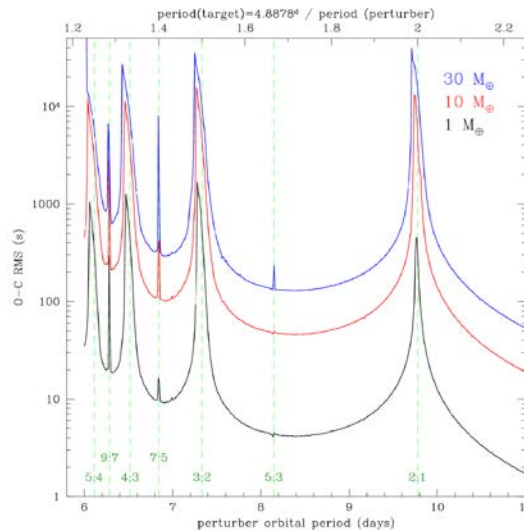


Figure 12 | Estimated O-C signal (rms) induced on a $P = 4.89$ -day, $26\text{-}M_{\oplus}$ Neptune target by an outer coplanar perturber, as a function of the perturber orbital period and for three different perturber masses (black, red, and blue curves). Most important low-order mean motion resonances (MMRs) are marked with green dashed vertical lines.

anomaly (SAA). Nevertheless, the information content on T_0 is almost exclusively concentrated on those parts of a transit light curve having a higher first derivative: that is, the transit entry (or ingress) and exit (or egress) phases (Doyle & Deeg 2004). For this reason, if a light curve is missing the ingress or egress, and assuming that the correct transit duration is known by one complete observation or multiple observations stacked together, ΔT_0 can be straightforwardly estimated by rescaling the simulation results by $\sqrt{2}$. However, once the ephemeris of a newly discovered planet is computed, an optimal follow-up strategy could be devised to observe only transits whose both ingress and egress fall within the observational windows of CHEOPS.

The simulation results (Figure 13, right) show that the $\tau = 60$ -s baseline cadence is a suitable choice that minimises the data transfer while optimising the scientific result. In fact, for longer cadences $\tau > 60$ s, additional simulations show that ΔT_0 starts to increase linearly, suggesting a significant loss of information due to the finite integration time. On the other hand, only large targets ($\geq 4 R_{\oplus}$) hosted by bright stars ($V \leq 8$ mag), especially of late spectral types, would benefit from a sampling cadence shorter than the baseline ($\tau < 60$ s).

The observing strategy needed to firmly detect a TTV (and to reconstruct the properties of the perturber) is of course dependent on the shape and amplitude of the TTV signal compared to the number, S/N ratio, and phase coverage of the measurements. Outside orbital resonances, TTV signals often show complex, multimodal shapes which make them difficult to identify and model (Veras et al. 2011). However, within or close to resonances the TTV signal shows a nice pseudo-sinusoidal shape with a period corresponding to the libration period of the three-body system. In this case the number of measurements and S/N ratio needed for an unambiguous detection is similar to what has been estimated for velocimetric studies (among others, by Cumming et al. 2004: “ $N > 10\text{--}20$ is required to be able to detect an orbit with $K = 2\text{--}4\sigma$ ”).

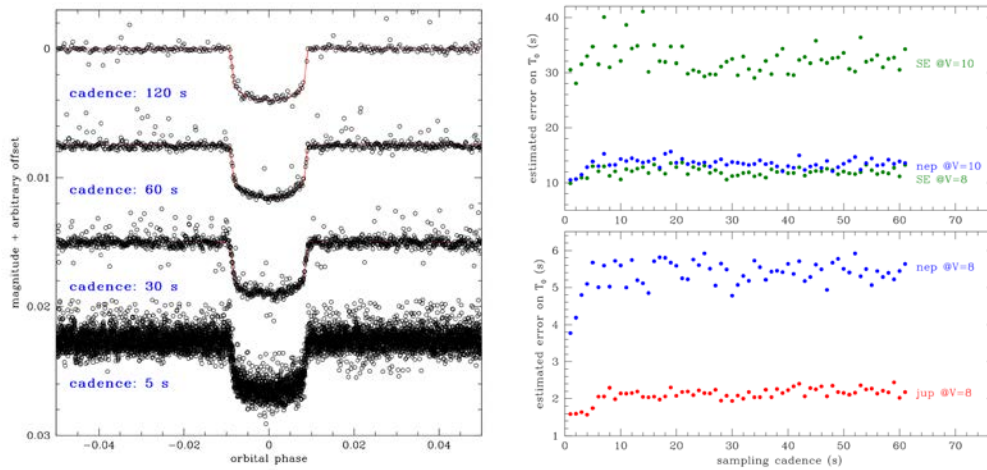


Figure 13 | **Left panel**— Synthetic CHEOPS light curves for the transit of a Neptune around a 10^{th} -magnitude star, generated at different cadences with a S/N ratio corresponding to a fixed noise of 256 ppm per min. The corresponding noise-free models are plotted with red lines. **Right panel**— Estimated timing error ΔT_0 as a function of the sampling cadence, for a $V=8$ – 10 -mag star (100–256 ppm per min, respectively) and for three different transiting planets corresponding to Earth, Neptune, and Jupiter analogues around a $G2V$ star.

A set of simulations on synthetic $O-C$ diagrams was performed by injecting a sinusoidal signal of amplitude ΔTTV in a 3.5-yr flat $O-C$, adding white noise corresponding to ΔT_0 , and selecting N_{obs} randomly spaced transits to simulate CHEOPS observations. Each $O-C$ diagram is then scanned by a GLS periodogram (Zechmeister & Kürster 2009) and the best-fit solution compared with the injected signal (Figure 14). For each pair of $S/N = \Delta TTV / \Delta T_0$ and N_{obs} , 100 different $O-C$ are generated with random signal phase and sampling times; the “detection efficiency” is defined as the fraction of “well recovered” signals. As expected, about ten transits are required to reconstruct the TTV signal at $S/N > 5$. At very high S/N ratio (and ideally even at infinite S/N ratio), at least 7–8 transits are the minimum requirement. On the other hand, three transits at $S/N \geq 2.5$ are enough in most cases to check whether the orbital period is constant or not, i.e., whether that target deserves additional observations to assess the presence of a perturber.

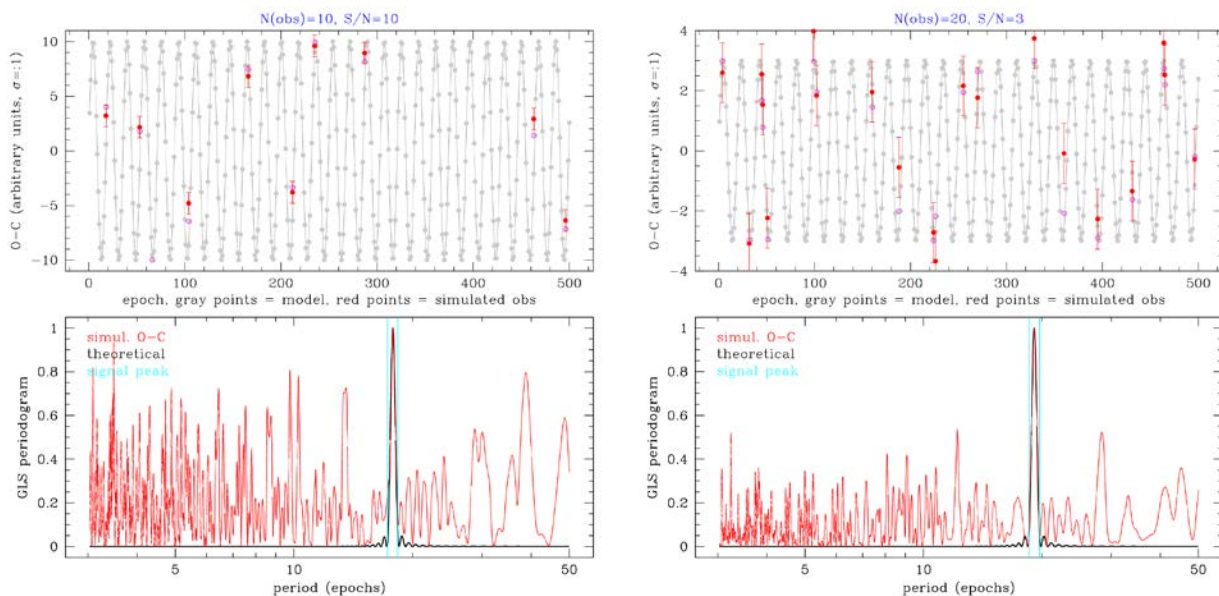


Figure 14 | Instances of simulated $O-C$ diagrams with 10 observations at $S/N = 10$ (left panels) and $S/N = 3$ (right panels), randomly sampled over a 3.5-yr span. The periodic signal is properly recovered by GLS (red periodogram in bottom panels) in both cases.

2.2.3.3 Detection of exomoons

Detection and study of exoplanet moons (exomoons) represent a completely unexplored territory in exoplanetary research. The interest in this field has been on the rise recently (e.g., Szabó et al. 2006; Simon et al. 2007; Kipping et al. 2009; Simon et al. 2012), mostly thanks to *Kepler* and its unique data on transiting exoplanets.

Generally, there are several methods for detecting an exomoon. The most important ones involve TTVs, aiming at the detection of a stroboscopic period due to the moon (Kipping 2009a, 2009b; Szabó et al. 2013). The photometric method involves the search for light curve distortions that can be explained by an orbiting companion (Simon et al. 2009, 2012) as illustrated in Figure 15 (left), where the transit of an Earth-size exoplanet plus a $0.4\times$ smaller moon is simulated when the photometric precision is set to ~ 20 ppm (the solid curve shows the underlying theoretical model). The extra “shoulders” may be detected in single transits but firm detection will require sensitive analyses of multiple transit observations. Finally, it could also be possible to search for exomoons with the Rossiter-McLaughlin effect (Simon et al. 2010).

After three years of monitoring by *Kepler*, there are yet no successful detections of exomoons. Because the sphere of gravitational influence (the Hill sphere) of a planet shrinks when the planet is close to its star, the chances to find stable moons around close-in exoplanets are small. At the exception of the 95-day-period Corot-9b (Deeg et al. 2009; Weidner & Horne 2010), almost none confirmed exoplanets is thought to have the actual possibility to host a stable moon. Our simulations show that exomoons larger than the Earth could be stable over 4 Gyr around planets with revolution periods > 16 days (Figure 15, right). Up to five transit observations of such planets could be needed during the 3.5-yr mission to unveil their moons, however these 20–50-day-period super-Earth and Neptune systems are well in the reach of CHEOPS.

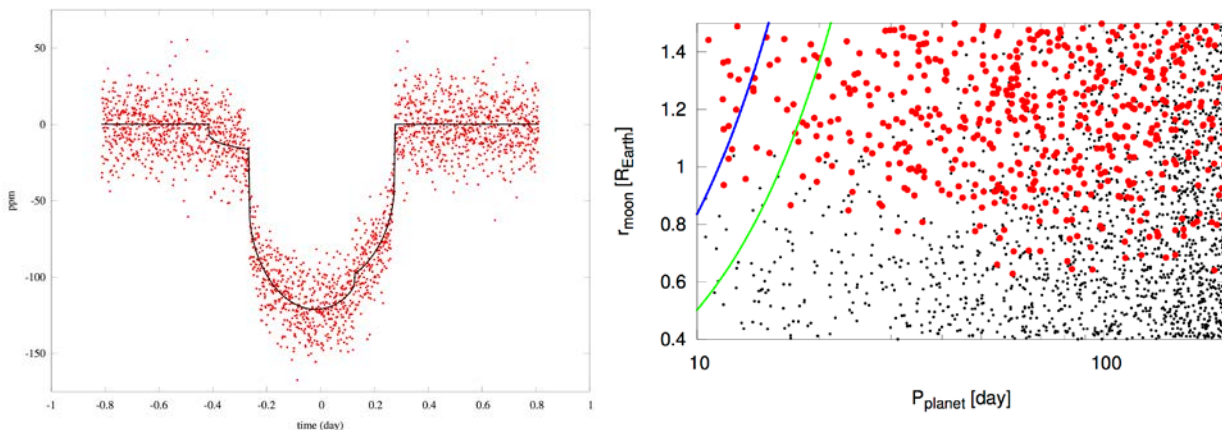


Figure 15 | Left panel— Transit of an Earth-size exoplanet plus a $0.4\times$ smaller moon is simulated when the photometric precision is set to ~ 20 ppm (the solid curve shows the underlying theoretical model). **Right panel**— Planet + moon systems have been generated with random planet periods and moon sizes (black dots). The blue and green curves show the 1- and 4.6-Gyr stability limits, respectively, of these systems (stable systems are on the right of the lines). The red dots are those systems for which the moon could be detected assuming CHEOPS observes five planetary transits.

The effects of stellar noise (photometric jitter, surface spots, granulation, etc.) should be distinguished from meaningful features in the transiting silhouette. Simulations imply that the expected precision of CHEOPS will be sufficient for meaningful detection of Earth-to-Moon-size exomoons, depending on the planet size. If an exomoon becomes suspected, either through the core observation programme of CHEOPS or through dedicated open time programmes, subsequent short observations can be scheduled to cover several individual transits. Timelines spanning several years can thus be generated, with strongly improved detection thresholds. In the coming decade or so, CHEOPS will be the prime instrument with real chances of exomoon detection.

2.3 CHEOPS targets and expected transit yield

The CHEOPS target list will be provided from:

- (i) Ground-based Doppler surveys (e.g., HARPS, HARPS-N; see §2.3.1).
- (ii) Ground-based transit surveys (e.g., NGTS; see §2.3.2).
- (iii) The *TESS* space-borne transit survey (see §2.4.2).
- (iv) Astrophysical sources proposed by the community through available open time (20%).

Some of these surveys (e.g., HARPS, HARPS-N) are already in progress and are continuously providing new targets. Other instruments (e.g. ESPRESSO, NGTS) or space missions (e.g. *Gaia*, *TESS*) are currently being developed and will start providing targets between now and the launch of CHEOPS. The target list of CHEOPS will therefore evolve with time including during the mission proper. As it grows, selecting the best objects to observe will become increasingly important. In order to prepare for such a task, it is possible to simulate, within limits, the expected yields from the various surveys. Figure 16 shows a sky projection map, where we have located super-Earths and Neptunes already known today from radial velocity surveys and orbiting bright stars (~ 60 targets) and for which CHEOPS will seek transits. In this example, we have also added super-Earths and Neptunes orbiting M dwarfs. While these stars are faint in the CHEOPS band pass, this is compensated by much larger transit depths, as described in §2.3.3. Interestingly, M dwarfs offer the opportunity for CHEOPS to detect transits of habitable planets.

Only a couple of Neptunes (HAT-P-11b and HAT-P-26b) have been discovered via ground-based transit surveys so far. This number is bound to increase significantly with surveys like NGTS (see §2.3.2). We therefore simulated a possible yield of these surveys, which will be available when CHEOPS observations start in 2018. The simulated yield of Neptunes detected by transit surveys was obtained using the following methodology. The positions in the sky (α , δ) of exoplanets detected from the ground in the southern hemisphere was taken and for each system a new random position around its observed location was drawn. The aim of this operation was to conserve (in particular) the biases linked to the stellar field densities and the duration of the night. Once new positions have been obtained for all systems, the properties of each system have been reset and drawn from the *Kepler* catalogue. We made a selection within *Kepler* targets with planetary radii ($< 8 R_{\oplus}$) and magnitudes (*Kepler* mag < 15). We applied the NGTS window function to these targets (100% chances to detect a planet with a period < 6 d, 50% chances to detect a planet with a period < 14 d, 0% chances to detect a planet with a period of 22 d) and kept only those with transit depths larger than 500 ppm.

Finally, hot Jupiters around bright stars could also be interesting targets to follow: in fact, few of these objects have been detected in transit around bright stars, whereas the few that have been became the most studied objects in the exoplanet field (HD 209458b and HD 189733b). (In addition regularly observing transits of hot Jupiters across bright and quiet stars would be useful in terms of performance monitoring of the instrument.)

Strikingly, all of the exoplanets first discovered with radial velocimetry, then detected in transit, lie in the northern hemisphere. This is likely due to observational biases and target selection effects. From this simple fact, it is clear that the CHEOPS follow-up of targets in the southern hemisphere would at least double the number of such “golden” targets for future atmospheric characterisation missions, and would do so among already known objects.

The resulting preliminary target list represents the minimum number of systems that CHEOPS could target. The total number of targets will continue to increase until the launch of CHEOPS and during the mission. Mission scenario simulations, taking the transit ephemerids of these targets into account, allows us to fill completely 60% of a year of operations, assuming each target is to be observed only once. This figure increases to $\sim 70\%$ when repeated observations of a transit are allowed (e.g., to detect TTVs). The remaining time will be easily filled with new targets from Doppler surveys (e.g., HARPS-N, ESPRESSO), *TESS*, possibly *Gaia*, and instrument characterisation programmes aiming at monitoring and understanding the instrumental behaviour of CHEOPS. Finally, up to 20% of the observing time shall also be dedicated to targets provided by the community. In the end, we believe that sufficient targets will be available to allow CHEOPS to select the most promising ones.

2.3.1 Planetary systems from ground-based Doppler surveys

The radial velocity (or Doppler) technique is at the origin of exoplanet detections (Mayor & Queloz 1995). Originally reaching a precision of $5\text{--}10\text{ m s}^{-1}$, it led to the discovery of the giant planet population around stars in the solar neighbourhood, including hot Jupiters. A paradigm shift happened in 2004 with the first detections of Neptune-mass objects on close-in orbits (Santos et al. 2004, McArthur et al. 2004, Butler et al. 2004). Thanks to an improved precision of $\sim 1\text{ m s}^{-1}$, velocimetric surveys are now able to fully explore the domain of super-Earths and Neptunes with semi-major axes up to 1 au. Several tens of objects of this kind are known today from these surveys, orbiting nearby, bright stars in the solar neighbourhood. Many of these planets are part of systems with complex dynamical architectures (e.g., HD 10180; Lovis et al. 2011). The existence of a large population of low-mass planets has been confirmed by Nasa's *Kepler* mission which has found thousands of small planet candidates within a survey of 150 000 stars (e.g., Batalha et al. 2013).

As of today, on-going velocimetric surveys are focusing on two main objectives:

- (i) Characterising the statistical properties of the exoplanet population as a whole down to the mass of the Earth.
- (ii) Detecting potentially transiting low-mass planets around nearby, bright stars for internal structure studies and subsequent atmospheric characterisation.

These two avenues of research are expected to be continued in the coming years, with a growing emphasis on the search for transiting planets in the solar neighbourhood.

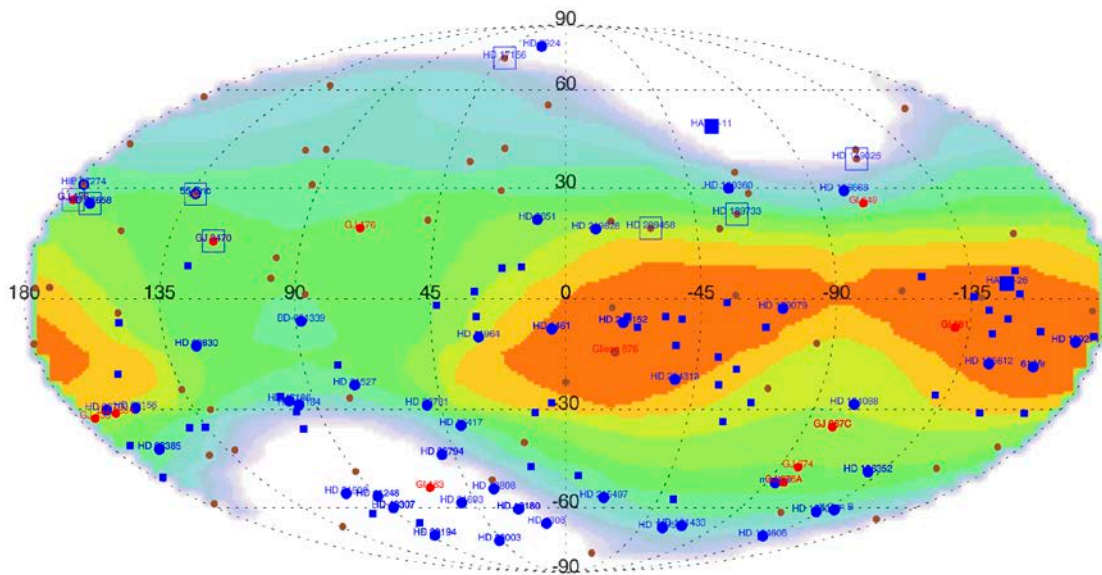


Figure 16 | Example of a preliminary target list for CHEOPS displayed on a Mollweide sky projection. The symbols correspond to different types of targets and are described in Table 2. Symbols framed in blue are planets discovered with radial velocimetry that have already been detected in transit. No such cases have been reported in the southern hemisphere yet. The colour gradient indicates the time that CHEOPS could spend pointing at given coordinates, taking into account pointing restriction due to the Sun exclusion angle (120°), occultation by the Earth for an orbital altitude of 800 km, a stray light exclusion angle of 35° , and requiring that CHEOPS is able to observe for at least 50 min during each orbit. White regions cannot be observed due to the Sun, while orange regions can be observed for 2000+ hours per years.

Table 2 | Possible types of CHEOPS targets shown in Figure 16.

Targets	Mass limit (M_{\oplus})	Mag limit (V)	# Targets	Symbol in Figure 16
Super-Earths & Neptunes detected by RV surveys	< 30	< 9	62 known	
Neptunes detected by ground-based transit surveys	< 60	< 12	2 known 60 simulated	 
Planets detected by RV surveys around M dwarfs	< 30	< 13	18 known	
Hot Jupiters detected by RV surveys around bright stars	> 30	< 9	54 known	

The combination of a velocimetric survey and a photometric follow-up campaign to search for potential transits has proved very successful in recent years. The transiting super-Earths 55 Cancri e (Winn et al. 2011; Demory et al. 2011) and HD 97658b (Dragomir et al. 2013), as well as the transiting Neptunes GJ 436b (Gillon et al. 2007) and GJ 3470b (Bonfils et al. 2012), have all been discovered in this way. While the transits of both Neptune-like exoplanets could be detected from the ground, the space-borne *MOST* and *Spitzer* telescopes were necessary for the super-Earths due to their shallow transit depths. It must be noted that the derived uncertainties on the planet radius remain significant for these small planets and often hamper the precise measurement of their bulk densities. A dedicated, space-borne facility such as CHEOPS will make it possible to overcome this issue.

We now examine more closely the prospects of finding further low-mass transiting objects with the existing and planned radial velocity surveys in conjunction with CHEOPS. As of September 2013, 80 Doppler-detected exoplanets were known with minimum masses below $30 M_{\oplus}$ and orbital periods shorter than 50 days. This number includes 62 G and K dwarfs brighter than the 9th magnitude and 18 M dwarfs brighter than the 13th magnitude. Computing the cumulative transit probability of this population, we estimate that 4–5 of them should be transiting. Since 3 planets (55 Cnc e, HD 97658b, GJ 3470b) are already known to be transiting (see above), more radial velocity discoveries are needed to further increase the chances of catching new transiting objects.

2.3.1.1.1 On-going velocimetric surveys

The major on-going velocimetric surveys that have yielded the vast majority of low-mass planets are the ESO/HARPS and Keck/HIRES surveys. HARPS itself has been the most productive thanks to its sub-meter-per-second precision. This explains why most presently-known planets are located in the southern hemisphere. Both surveys have been targeting several thousands of F, G, K, and M dwarfs over the past decade, although not necessarily at the required precision and cadence to detect the weak signals of Neptunes and super-Earths. In fact, only a few hundred stars (200–300) have been followed in an appropriate way as of today. HARPS and HIRES will continue to expand this sample until the launch of CHEOPS and beyond. Based on the on-going programmes and their time allocation, one can estimate that another ~150–200 nearby, bright stars can be searched, yielding 60–80 new planets among which 4–5 will be transiting bright stars.

2.3.1.1.2 Upcoming velocimetric surveys

New velocimetric facilities have just started operations or will come online in the near future. HARPS-North (HARPS-N) has now reached its nominal performances and is expected to monitor about 50 nearby stars across various observing programmes, which should yield ~20 new planets. The SOPHIE spectrograph is

being refurbished and should deliver improved velocimetric precision. Another ~200 stars can be monitored with this facility, which has an efficiency 2 to 3 times lower than HARPS, yielding another ~25–40 planets. Importantly, HARPS-N and SOPHIE will extend the known exoplanet population in the northern hemisphere, which suffers from sparse coverage at the moment. These new instruments are expected to discover between 105 and 140 low-mass planets, yielding 5 to 7 additional planets transiting bright stars.

On slightly longer timescales (still compatible with CHEOPS), the VLT/ESPRESSO instrument is expected to monitor ~100 more targets on the lower main sequence (K and M dwarfs) with unprecedented accuracy and efficiency. Furthermore, two instruments are currently under development to specifically survey nearby M dwarfs, including late-M dwarfs: CARMENES and SPIRou. Although evaluating their contribution is more speculative at this stage, it seems reasonable to include another 100–200 targets to be monitored by these facilities, yielding 80–100 extra new planets, with ~5 expected in transit across K or M dwarfs.

In terms of observability by CHEOPS, the future Doppler-detected planets are expected to be uniformly spread over the whole sky. Moreover, velocimetric surveys could in principle define their search sample in a way that is optimised for the CHEOPS visibility zones. Scheduling of the transit windows for Doppler-detected planets is therefore expected to be relatively smooth for CHEOPS.

Since 2004, the number of low-mass planets with revolution periods lower than 50 days has doubled every three years. The above estimates follow this trend, as we expect this number to almost triple within 5 years. It thus means that CHEOPS will be able to find about 10 new transiting Neptunes and super-Earths coming from velocimetric surveys. These ten “golden targets” will be the very best ones available in terms of characterisation potential. In other words, each one of them could become a “Rosetta stone” for their exoplanet families and play a similar role for super-Earths and Neptunes as HD 209458b and HD 189733b played for hot Jupiters. The availability of a versatile space-borne follow-up facility like CHEOPS, entirely dedicated to hunt transits (in contrast with *Spitzer*) with excellent photometric performances (much better than, e.g., *MOST*) will significantly increase the efficiency of velocimetric surveys in identifying these benchmark objects.

2.3.2 Planets from ground-based transit surveys

Ground-based surveys have provided, with a few notable exceptions, the bulk of the sample of confirmed transiting planets with bright host stars. Surveys such as the Hungarian Automated Telescope Network (HATNet) and the Wide Angle Search for Planets (WASP) have been extremely successful in detecting Jupiter- and to some extent Saturn-sized objects (as well as a couple of hot Neptunes). They highlighted the diversity amongst these planets and the need for new physics to understand them. In the future, ground-based surveys are being developed towards the detection of:

- (i) Planets with brighter hosts (e.g., KELT, MASCARA, WASP-S).
- (ii) Smaller planets (for ice giants: HAT-S, SuperWASP, QES, NGTS; for super-earths: NGTS).
- (iii) Planets with longer periods (e.g., SuperWASP, NGTS).

To reach these goals, understanding the causes of the systematic noise error budget has been instrumental in reaching the necessary precision. For example, in the case of NGTS, the experiment aims at detecting transits of one-millimagnitude (1-mmag) in depth. This precision is needed to reach the sensitivity required to detect super-Earths and Neptunes around the late K and M spectral types that the survey is sensitive to. The prototype instrument developed has shown that through careful selection of instrumentation and observation strategy, systematic noise is well below 1 mmag.

Within the CHEOPS consortium, we are participating in the NGTS, SuperWASP/WASP-S and QES surveys, and have links to KELT and MASCARA. SuperWASP has already started collecting data in the best CHEOPS visibility zones in the equatorial and northern regions of the sky.

2.3.2.1.1 Current Planet Yield

As of July 2013, the WASP (SuperWASP/WASP-S) total stands at around 104 confirmed planets but is steadily rising as candidates are spectroscopically examined. Over the last few years the number of Saturn-mass planets has been steadily increasing as the benefits of multi-season observations have aided transit confirmation. Other experiments (including space based) increase the total to around 300. However, limiting

our sample to those with $V < 11.5$, then the sample drops to 61 targets. With few exceptions these are nearly all gas giants (5 are Neptunes or super-Earths).

2.3.2.1.2 Expected planet yield in 2014–2017

The expanded QES and MASCARA networks will come on line at the start of this period. At this stage their levels of systematic noise remain to be assessed and so their planet catch is uncertain. However, the original QES has published 2 (large gas-giant) planets so it is likely that further discoveries will be forthcoming. Even if MASCARA is successful, its expected planet catch will be low as it is aimed at substantially brighter stars ($4 < V < 8$ mag) and primarily for atmospheric analysis.

The KELT survey of the southern hemisphere is also still to produce results. But as the data has already been taken and the analysis tools developed for the northern datasets, it is likely that additional large planets around bright southern host stars will be identified.

As noted earlier, the upgraded SuperWASP is now targeting equatorial fields that are favoured by the CHEOPS orbit. The upgrade has led to a substantial reduction in systematic noise and hence the observations can now benefit from the short cadence resulting from staring observations (at the expense of the effective field of view from cycling around a number of fields). While simulations show that the instrument will produce significant numbers of low-mass planets, the actual planet catch will depend on the long-term systematic noise of the instrument (probably a better idea by mid-2014 when the first season of results will be examined).

In this period, the NGTS surveys will be finding planet candidates that are well matched for confirmation from HARPS and, from 2016, ESPRESSO at ESO. The NGTS surveys will provide CHEOPS with a significant number of Neptunes and super-Earths with host stars having $V < 11.5$ mag. NGTS will cover the best CHEOPS visibility area (see Figure 17). Detailed modelling shows that the initial NGTS survey will be comparable to *Kepler* in a single pointing (but with a brighter stellar population and cadence) so that over a four-year mission, with a relatively small amount of HARPS time, around 20 (mainly) Neptunes will be confirmed. The advent of ESPRESSO will lead to a $15\times$ increase in this and 40 new confirmed super-Earths, of which at least 20 will be brighter than $V = 11$ mag.

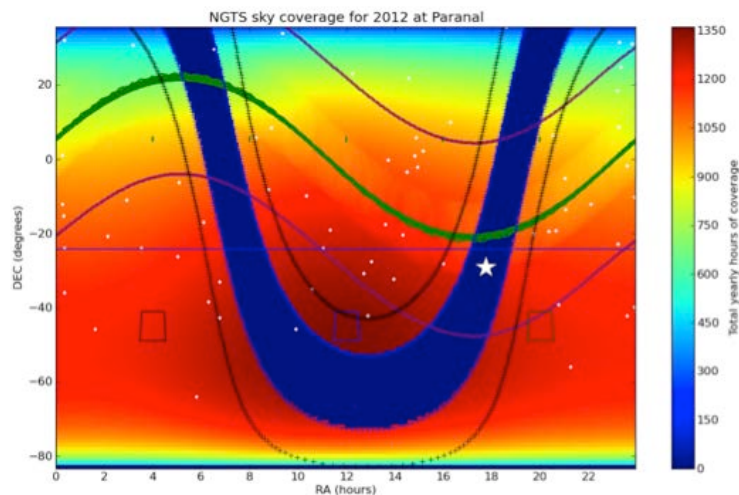


Figure 17 | Visibility plot for NGTS assuming historical weather characteristics for Paranal and several visibility constraints (lunar position, etc.). (Bento, private communication.)

2.3.3 M dwarfs in CHEOPS target list

The small, cool M dwarfs present particularly compelling advantages for the detection and characterisation of low-mass planets. Compared to solar-type stars, their lower masses and smaller radii translate into much larger Doppler and transit signals for the same planetary parameters. This is well illustrated by GJ 436b and GJ 3470b, two Neptune-mass planets transiting nearby M dwarfs and for which ground-based telescopes of only 60-cm aperture were necessary to detect the transits (Gillon et al. 2007; Bonfils et al. 2012). The small size of M dwarfs maximises also the potential for detailed follow-up of transiting planets, as exemplified by

the on-going atmospheric characterisation of GJ 1214b (Charbonneau et al. 2009), the only super-Earth so far for which a constraining transmission spectrum has been obtained (e.g., Fraine et al. 2013 and references therein). Last but not least, the small luminosity of M dwarfs translate into habitable zones that are much closer than for solar-type stars, making the putative transits of habitable planets much more probable and frequent. This is an interesting perspective for CHEOPS considering the arguments of Alibert (2013) about the maximum radius for a planet to be habitable.

Several optical Doppler surveys targeting nearby early-type M dwarfs are presently in operation, the most successful of them using the HARPS spectrograph to monitor several hundreds of M0 to M4 dwarfs (Bonfils et al. 2013). This HARPS survey has notably revealed that the frequency of short-period (< 10 days) super-Earths around early M dwarfs is $36_{-10}^{+25}\%$. In this period range, the mean transit probability is of about 4%. Combining both numbers leads to 1–2% of early M dwarfs having a transiting short-period super-Earth. Considering the optical Doppler surveys in operation now or in the near future, we estimate that in 2017 at least two super-Earths out of the ten objects predicted (cf. §2.3.1) will be transiting M dwarfs.

Thanks to its superb photometric precision and its ability to point at nearly any location in the sky, CHEOPS will be the optimal observatory to detect the transits of any planet discovered by optical Doppler surveys around a nearby early-type M dwarf. Among the ones with at least one planet detected by HARPS, the faintest in the optical is GJ 3470 with $V = 12.3$ mag. According to the CHEOPS noise budget, it will be possible to reach precisions better than 100 ppm per hour for V -magnitudes up to 13, making possible the firm detection ($> 5\sigma$) of Earth-size planets for the majority of the M dwarfs surveyed by Doppler surveys. This shows that the potential of CHEOPS will not be limited to solar-type (G) stars and K-type stars, and that it will also efficiently explore the terrestrial regime for early M-dwarfs. (Because of their extreme faintness in the optical, this conclusion does not hold for mid- to late-type M dwarfs.)

Of course, CHEOPS will also have a huge potential for the photometric follow-up of planets previously detected in transit in front of bright early-type M-dwarfs like GJ 436b or GJ 3470b. Its high photometric precision will yield a better characterisation of the planets, notably by improving the precision on the transit and physical parameters (e.g., Gillon et al. 2007b; Demory et al. 2013), by allowing the detection and modelling of spot-crossing events able to reveal the spin-orbit angle (e.g., Sanchis-Ojeda et al. 2011), and by searching for transit timing variations (TTVs) able to reveal a second planet (e.g., Nesvorný et al. 2013). Such follow-up precise observations by CHEOPS will be possible not only for transiting planets detected around bright M dwarfs from the ground but also the ones detected by *TESS*.

2.3.4 CHEOPS target stellar properties

2.3.4.1 Stellar spectroscopic analysis for CHEOPS targets

The derivation of accurate stellar parameters for the planet host stars is of uttermost importance for an accurate determination of the properties of the transiting planets. For instance, precise (or if possible, accurate) stellar radii are critical if we want to measure precise values for the radius of a transiting planet (see, e.g., Torres et al. 2012). The determination of stellar radii depends upon the quality of the derived stellar parameters such as the effective temperature. The bulk chemical composition of a planet is also likely to be related to the chemical composition of the proto-stellar cloud, reflected on the composition of the stellar atmosphere (Guillot et al. 2006; Fortney et al. 2007; Bond et al. 2010) as evidenced by the solar system. The precise derivation of stellar chemical abundances thus gives us important clues to understand the planets and their observed properties.

The derivation of precise stellar parameters (such as the effective temperature and the chemical abundances) is often achieved through the analysis of high-resolution spectra. Indeed, and contrarily to the case of most *CoRoT* and *Kepler* objects, CHEOPS targets will be bright and thus easily observable with high resolution spectrographs. This will provide measurements of effective temperatures and metallicity for CHEOPS targets three times more precise than those achieved for most *Kepler* targets (Molenda-Zakowicz et al. 2013). It is thus important to understand what are the different relevant stellar parameters (mass, radius, effective temperature, surface gravity, and chemical abundances) that can be derived through this analysis, as well as the typical uncertainties that can be expected.

2.3.4.1.1 Main sequence stars with F, G, and K spectral types

The effective temperature (T_{eff}) is the key ingredient in the derivation of the stellar radius and stellar mass (the latter through model comparison). Different methods have been used to derive values for T_{eff} , each of them having its own advantages and drawbacks. More important perhaps is the fact that the results derived from the different methods show some spread. For example, methods based on spectral synthesis (and using well defined spectral regions/lines) were shown to provide results that are very dependent on the estimate of the surface gravity (Torres et al. 2012); a problem not encountered by other methods (e.g., Tsantaki et al. 2013). In any case, the best estimates for the effective temperature have typical relative errors of the order of 50 K. Possible systematic errors exist that are difficult to quantify. For F, G, and K stars, comparisons with results from the “standard” infrared flux method (IRFM; see Figure 18) show that these are of the a similar order of magnitude (Tsantaki et al. 2013).

The derivation of the surface gravity (g) of a star, in combination with an estimate for its mass, is in principle a good starting point for the derivation of the stellar radius. However, contrary to the effective temperature, the derivation of precise surface gravity values is usually difficult from the analysis of high-resolution spectra. Typical uncertainties exist that are of the order of 0.1 dex or higher (e.g. Tsantaki et al. 2013). Another approach is to derive the stellar density (ρ_*) directly from the transit lightcurve (Seager & Mallén-Ornelas 2003). If the stellar radius (R_*) is known to a good precision (see §2.3.4.2), it is then possible to determine the value of $\log g$. An even more promising approach to obtain the stellar mass for bright stars is through the precise measurement of the stellar luminosity or the asteroseismic “large separation”, as described in §2.3.4.2. With typical values for the stellar density and the effective temperature, and assuming the stellar metallicity (see below), precise values for the stellar radius (with typical uncertainties below 10%) and mass can be derived.

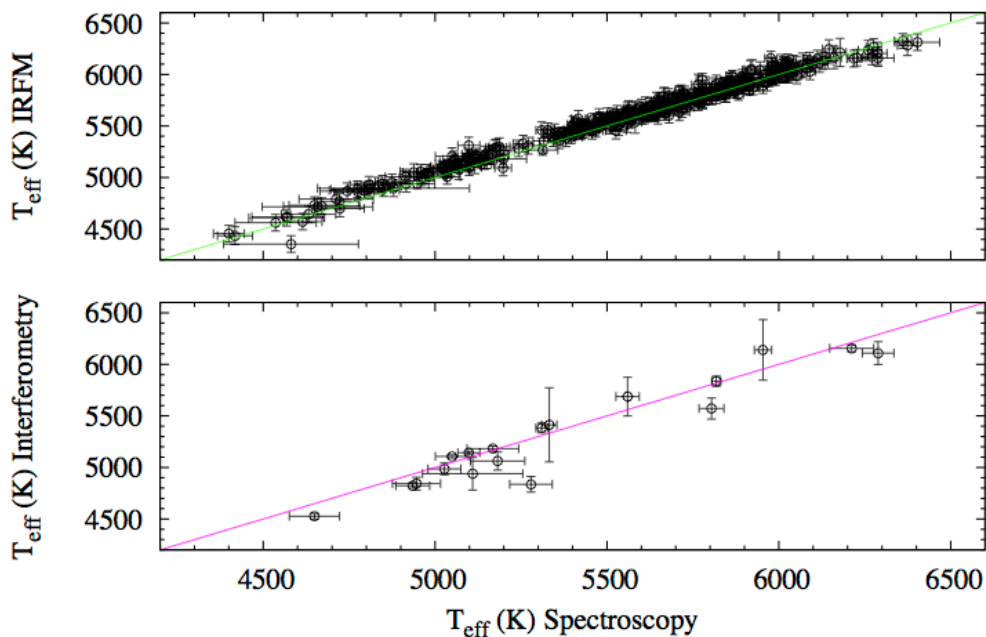


Figure 18 | Comparison of the effective temperatures derived using a detailed spectroscopic analysis with values derived using the infrared flux method (IRFM; top panel) and with values derived using interferometry (bottom panel). The results show a very good agreement over the whole range of temperatures compared, giving great confidence to the parameters derived using the spectroscopic analysis. From Tsantaki et al. (2013).

If different methods exist that can derive stellar parameters such as the effective temperature and surface gravity, the chemical abundances for a star (including iron) are best determined through a detailed spectroscopic analysis. Typical uncertainties on the iron abundance ($[\text{Fe}/\text{H}]$) are of the order of 0.05 dex or better if a high S/N ratio, high-resolution spectrum is available (e.g., Sousa et al. 2008). Uncertainties of the same order of magnitude (and certainly below 0.1 dex) are possible for the abundances of other species like silicon (Si) and magnesium (Mg) that are well represented in a stellar spectrum (e.g., Adibekyan et al. 2012).

However, the results strongly depend upon the number of available spectral lines for the analysis. Elements such as carbon and oxygen, for example, are more delicate to analyse. In such cases the uncertainties in $[X/H]$ (where X is the element) can increase up to 0.10–0.20 dex (Écuillon et al. 2006).

To illustrate the usual precision that can be obtained on the final mass and radius of the star, we can use the mass and radius calibrations of Torres et al. (2010) that make use of the effective temperature, surface gravity, and metallicity. Using typical parameters for a solar-type star and uncertainties of 50 K, 0.03 dex (from the light curve), and 0.05 dex for these three variables, respectively, we derive typical 1- σ uncertainties of $0.04 R_{\odot}$ and $0.02 M_{\odot}$. These errors do not take into account systematic effects. In practice, for example, including model uncertainties and adopted helium abundance errors, typical errors in the stellar mass of $0.1 M_{\odot}$ can be expected (Fernandes et al. 2011).

2.3.4.1.2 *The peculiar case(s) of M dwarfs*

The derivation of M dwarf atmospheric parameters is a challenging task. Due to the difficulty in deriving precise values for the effective temperature and metallicity based on spectral fitting procedures, most determinations are based on calibrations using colours (e.g., Neves et al. 2012) or spectroscopic indices (e.g., Rojas-Ayala et al. 2012). This implies that the errors in M-dwarf parameters (namely on T_{eff} and metallicity) are usually much higher than the ones we can achieve for F, G, and K dwarfs.

Due to the above mentioned problems, uncertainties in the derived $[Fe/H]$ values for M dwarfs are typically of the order of 0.1 dex, or even higher, with different calibrations providing also different zero points. Uncertainties in the derived effective temperatures are also higher than for F, G, and K dwarfs, with errors of the order of 100–200 K. Progress in this respect is however expected to come from the analysis of high resolution optical and near-infrared spectra (Neves et al. 2013; Önehag et al. 2012), which also bring the promise of precise abundances for large sets of elements.

2.3.4.2 *Characterisation of the masses, radii, and ages of the host stars*

To improve the precision (in %) but also the accuracy (proximity of the measurement to the true value) of the stellar mass and radius determinations from spectroscopy described just above (§2.3.4.1), several methods from stellar physics are available: the classical method based on direct comparison with evolutionary models, and asteroseismology. The latter provides very precise knowledge of the stellar mass and radius, even with a basic knowledge of the pulsation spectrum of the star. Stellar physics methods (both classical method and asteroseismology) also provide the age of the star, precious information since it is expected to be equal to the age of the planetary system.

2.3.4.2.1 *Classical method from stellar physics*

For a given physics, spectroscopic estimates of T_{eff} and metallicity, together with the knowledge of luminosity, can be used as inputs in a stellar evolution code to obtain a stellar model (giving “evolutionary” mass, radius, and age) of the host star satisfying at best these constraints. The measured mean stellar density (ρ_{*}) and $\log g$ from transiting light curve can also be used as further constraints in the procedure. Several evolution codes are available; such as the CLES code (Code Liégeois d’Évolution Stellaire; Scuflaire et al. 2008) or the Roma ATON code (Ventura et al. 2008). This method leads to the determination of the “evolutionary” mass and radius, which can be compared to the “spectroscopic” mass and radius (see §2.3.4.1) to improve the accuracy of the stellar mass and radius knowledge.

The precision of this general method, applicable to all CHEOPS targets (F, G, K, and M stars) is closely related to the precision of the input spectroscopic parameters and of the knowledge of the luminosity (usually coming from *HIPPARCOS* measurements). Given a precision of $\sim 1\%$ on T_{eff} , the precision on the stellar mass is typically $\sim 10\%$. The precision on the stellar radius is related to the precision obtained on the luminosity, typically $\sim 10\%$. Finally, the precision on the stellar age estimate is closely related to the precision obtained for the metallicity and the luminosity. The age is usually relatively poorly constrained by this method, with a typical error of a few gigayears. This is, however, usually better than the stellar age inferred from empirical methods such as gyrochronology, decay of activity through Ca II, Mg II H & K lines, or decline in lithium (Soderblom 2010).

By the launch in 2017 and exploitation of CHEOPS data, *Gaia* will have provided parallaxes of the CHEOPS targets with an unprecedented accuracy (typically 1 000 times better than *HIPPARCOS*). From there, distances and luminosities will be extremely well known. Together with the knowledge of T_{eff} from spectroscopy, *the stellar radius should be known with a precision of 1–2%* (Liu et al. 2012). Reddening and extinction are not expected to be major issues for the CHEOPS targets.

Interferometers are also able to measure directly and with an accuracy of a few percents the diameter of close solar-type stars (Boyajian et al. 2013). In the northern hemisphere, the CHARA interferometer (Mount Wilson, 330-m baseline) is already at work both in visible and IR. The MROI interferometer (New Mexico, 400-m baseline) will be available by the launch of CHEOPS. For the southern targets, the VLTI (Chile, 120–150-m baseline) is available, especially with 3rd generation instruments in the visible. Interferometric measurements will be valuable to check the accuracy of the stellar radius determined from *Gaia* and other means.

These better constraints on radius and/or luminosity improve the classical method based on stellar evolution codes. *Gaia* and interferometry are therefore major tools for the characterisation of planet-hosting stars, to improve the precision and accuracy of stellar mass, radius, and age.

2.3.4.2.2 Asteroseismology for CHEOPS targets

Asteroseismology is the study of the oscillations of stars. The goal of asteroseismology, based on similar principles as the study of the Earth’s structure through its seismic activity, is to provide information on the stellar global parameters (mass, radius, etc.), internal structure (depth of the convection zone, envelope composition, extension of the overshooting zone, etc.), and internal rotation. In solar-type (F, G, and K) stars, oscillations correspond to acoustic waves (also called p-modes) that depend on the radially varying density and internal speed of sound in the star.

The power pulsation spectra of solar-type stars exhibit a characteristic structure, with regular spacings between the peaks. The most interesting spacing to derive stellar global parameters is called the “large separation” ($\Delta\nu$) and is directly related to the stellar mean density, which can be constrained this way to a precision of a few percents (White et al. 2011). The frequency at the maximum power, ν_{max} , is also of prime interest. These two parameters can be relatively easily measured, even if data with S/N ratio are insufficient to extract individual p-modes frequencies (see below). From the averaged large separation $\langle\Delta\nu\rangle$, the frequency at the maximum power ν_{max} , and the effective temperature T_{eff} of the star (determined from spectroscopy), stellar mass and radius can directly be determined from scaling relations (Kjeldsen & Bedding 1995). The stellar mass and radius are much better constrained this way than from the classical method described above (§2.3.4.2.1). In case of a very precise knowledge of the radius (for example from *Gaia* or interferometry), in combination with the stellar mean density (determined very precisely from the large separation or from the transit light curve itself), the stellar mass is provided with a much higher precision than the classical method and the scaling relations method. The method of combining the mean stellar density from the large separation and the precise and accurate stellar radius from *Gaia* or interferometry is probably the most accurate and less telescope-time-consuming way to obtain an accurate and precise estimate for the stellar mass. The method should be applicable for a large number of CHEOPS targets.

CHEOPS is not optimally designed for the observation of the stellar oscillations. While the CHEOPS observing cadence of 1 min is in principle ideal to detect p-modes oscillations of solar-type stars, the short time spent on the targets (< 48 h) and the limited number of repeated observations per target make it difficult to exploit CHEOPS data for asteroseismology. *Nevertheless, asteroseismologic information will be available for most of CHEOPS targets thanks to whole sky bright stars surveys such as the one that will be undertaken by the TESS mission.*

The selected NASA space mission *TESS* (§2.4.2), to be launched in 2017, aims at detecting small transiting planets around nearby, bright solar-type stars. Like *Kepler*, *TESS* includes asteroseismology in its core programme, with 27-day observations of its targets. *TESS* and CHEOPS will have targets in common, and CHEOPS will benefit from asteroseismic measurements from *TESS*: at least large separations and frequency at the maximum power, but also other seismic indicators and individual frequencies will therefore be available to characterise at best the nearby bright solar-type stars. Simulations show that for a $V = 5$

(respectively $V = 9$) magnitude star, 27-day *TESS* observations will give the large separation with a precision of 0.5% (respectively 2%; Goupil et al., in preparation).

Ground-based spectrograph like ESPRESSO at the VLT will be available to detect solar-like oscillations in the interesting southern targets (in complement of *TESS* observations). Again, accurate measurements of the large separations and frequency at the maximum power directly provide a good estimate of the stellar mass and radius from the scaling relations. If the stellar radius is more precisely known from another way (by *Gaia* or interferometry), the stellar mass is obtained with a precision of typically 2% by combining this with the precise knowledge of the mean stellar density (directly determined from the averaged large separation, also with a precision of a few percent).

2.3.4.3 Energetic (XUV) radiation environment of CHEOPS planetary systems

The high-energy environment resulting from stellar magnetic activity is a crucial factor in the development of planetary atmospheres, their chemistry, ionization, dissociation, heating, inflation, evaporation and consequently loss of crucial molecules. In particular, the atmospheric loss can play a critical role in the size evolution of close-in Neptune- to Earth-mass planets (§2.2.2.3). Given the list of processes it impacts, the knowledge of the XUV environment of an exoplanet is absolutely critical regarding the potential habitability of the CHEOPS targets. It is therefore important to characterise the host star's magnetic activity and in particular its high-energy environment in detail.

The UV range below 200 nm (FUV) is particularly important for exoplanetary atmospheres because many important molecules such as H_2O , CO_2 , CH_4 , and O_3 have large photodissociation cross sections in this range. Ultraviolet emission is, on the one hand, emitted as part of the stellar photosphere and this radiation sensitively depends on the stellar spectral type, being rather unimportant for the coolest main-sequence stars. On the other hand, magnetically-induced line emission from the chromosphere and the transition region, such as lines of C IV and in particular H I Lyman- α (important for the characterisation of the upper atmospheres, see §2.2.2.3), depends on the stellar activity level, which itself is determined by the stellar rotation rate and therefore the age for a given stellar spectral type. The fractional ratio of FUV to the near-ultraviolet (NUV) flux is therefore strongly dependent on spectral type, with ratios particularly high in M dwarfs due to magnetic activity (1 000 \times solar; France et al. 2013). This ratio is especially important for the O_2 and O_3 production in planetary atmospheres.

The strong hydrogen line of Lyman- α at 121 nm is of particular importance as it provides approximately 50% of the ultraviolet flux in late-type active stars ($\sim 1\,000$ times the Sun's fraction; France et al. 2012). In habitable zones around M dwarfs, the Lyman- α flux may easily exceed the modern Sun's value by 1–2 orders of magnitude (Linsky et al. 2013). Its evolutionary behaviour is therefore crucially important for exoplanetary atmospheric modelling (e.g., Ehrenreich et al. 2011), and it is well understood for solar-analogue stars; its flux at 1 au is expected to vary like $F = 19.2 t_9^{-0.72} \text{ erg cm}^{-2} \text{ s}^{-1}$, where t_9 is the stellar age in Gyr (Ribas et al. 2005). Work for later-type stars is being conducted, but will require better calibration of stellar ages (France et al. 2013, Linsky et al. 2013). The core of the Lyman- α line needs to be reconstructed from observations because it is completely absorbed by the interstellar medium. The reconstruction is nevertheless possible using the wings of the line (Wood et al. 2005; Ehrenreich et al. 2011; France et al. 2013) and its flux can also be scaled from Mg II fluxes that are easier to observe (Wood et al. 2005). Furthermore, there is a relatively tight correlation with X-ray flux (Linsky et al. 2013). For other UV bands, similar evolutionary decay laws are available, with power-law indices around -0.6 to -1.0, indicating a decay by a factor of 10–30 over the main-sequence evolution of a solar-like star (Ribas et al. 2005; Claire et al. 2012).

The X-ray range at 0.1–10 nm (0.1–10 keV of photon energy) reveals the strongest evolutionary dependence for solar-analogue stars. X-rays are emitted by the hot, magnetised corona of a star, containing plasma with temperatures between 1 and 50 MK. The radiation decays by a factor of about 1 000 on main-sequence evolutionary time scales; the decay law for the luminosity of a solar analogue reads $L_X = 3 \times 10^{28} t_9^{-1.5} \text{ erg s}^{-1}$, where t_9 is again the stellar age in Gyr and the expression applies for approximately $t_9 > 0.1$ for solar analogues. Stars around this limit and younger are rotating sufficiently rapidly so as to bring magnetic activity into saturation, where $L_X \approx 10^{-3} L_{\text{bol}}$ (bolometric luminosity). Similar decay laws have been measured for other spectral types from open-cluster studies. Toward later-type stars, the saturation age limit is higher and may be up to a Gyr or beyond for some M dwarfs (Güdel 2004). For atmospheric studies of exoplanets,

it is important to know the X-ray hardness as well, because of different penetration depths for photons of different energy. A relatively tight correlation exists between L_X and the coronal temperature (hence spectral hardness) and therefore with any other evolutionary activity parameter, so that the incident X-ray spectrum can be predicted based on other activity properties (Telleschi et al. 2005).

The intermediate EUV range is more difficult to observe due to severe photoelectric absorption in the interstellar medium. Only for nearby stars, such as the CHEOPS targets, is sufficient spectral information available. However, EUV can partly be modelled from extrapolation of X-ray spectra and UV spectra because the EUV range contains many lines forming at similar temperatures in the stellar atmospheres. The evolutionary flux decay laws derived from observations are indeed intermediate between X-rays and the UV, with power-law indices in t of order -1.20 to -1.0 (Ribas et al. 2005; Sanz-Forcada et al. 2011).

Flares are of particular importance in all UV/EUV/X-ray wavelength regimes and could also have major impact on the habitability of a close-in exoplanet. While the optical emission of flares may contaminate transit observations significantly, their large and variable fluxes modulate the energy input into upper planetary atmospheres considerably. Enhanced EUV and X-radiation leads to enhanced heating and therefore atmospheric inflation and enhanced atmospheric mass loss rates, accompanied by an expanded absorbing gas layer around the planet. A possible flare-induced enhancement of hydrogen absorption in the exosphere of HD 189733b was indeed seen in joint observations with *HST* (UV) and *Swift* (X-rays) during the transit (Lecavelier des Etangs et al. 2012).

The CHEOPS mission will provide great opportunities to not only characterise exoplanets based on their masses and radii, but to model and predict possible ranges of atmospheric properties because in contrast to *CoRoT* or *Kepler*, the XUV environment of the CHEOPS targets will be much easier to characterise, including time histories of atmospheric development based on the roughly known evolution of UV/EUV/X-ray stellar fluxes. In this respect, we are in a favourable situation because relevant observing opportunities will be available. Apart from archival data (in particular from the *International Ultraviolet Explorer* satellite), the Cosmic Origins Spectrograph (COS) and the Space Telescope Imaging Spectrograph (STIS) on board *HST* cover these wavelength ranges. The *World Space Observatory (WSO-UV)* will be dedicated to observations in the 100–320 nm range. Photometric UV information will also be available from the sensitive Optical Monitor on board *XMM-Newton*. For X-ray studies, two large satellites are presently available and both are likely to be operational in the CHEOPS time frame; these are ESA's *XMM-Newton* and NASA's *Chandra* X-ray Observatories, both equipped with sensitive CCD cameras (with energy resolution) and high-resolution grating spectrometers. Additional large data archives exist in particular for the *ROSAT* mission, both for pointed observations and the – albeit less sensitive – *ROSAT* All-Sky Survey. For 2014, JAXA plans to launch its *ASTRO-H* X-ray observatory.

2.4 Synergies with other missions

2.4.1 Golden targets for atmospheric characterisation with *JWST*

Understanding the true nature of super-Earth planets requires not only precise measurements of their mass and radius, but also a study of their atmospheric properties. This is only possible for planets orbiting bright-enough stars to permit high signal-to-noise spectro-photometric observations. This last condition is drastically more stringent for low-mass planets than for gas giants, leading to the conclusion that only the few dozens of super-Earths that statistically transit the brightest stars within the solar neighbourhood will ever be suitable for a thorough characterisation with future instruments (e.g., Seager et al. 2009). This has been nicely demonstrated in the case of the planet 55 Cancri e. This $8-M_{\oplus}$ planet is the only one transiting a star visible to the naked eye. First detected by Doppler measurements, transits were later detected by the *Spitzer* and *MOST* space telescopes (Demory et al. 2011; Winn et al. 2011), revealing a planet with a size of $\sim 2.1 R_{\oplus}$. Owing to the brightness of its host star ($V = 6$, $K = 4$), very high signal-to-noise occultation photometry was possible with *Spitzer*, leading to the detection of the thermal emission of this super-Earth (Demory et al. 2012).

The *James Webb Space Telescope (JWST)*, launch scheduled for October 2018) will be the premiere general purpose infrared space observatory in the next decade. It will enjoy unprecedented thermal infrared sensitivity and a suite of diverse and capable instruments with which to take advantage of this. As a result, *JWST* will provide powerful capabilities to study transiting planets (Deming et al. 2009). All four of its

infrared instruments (NIRCam, NIRISS, NIRSpec, and MIRI) will attempt transit observations. While no other facility from ground or space will match the sensitivity of *JWST* in the infrared from 1 to 28 μm , *JWST* does not operate below 600 nm and was not designed for precision photometric stability. NIRCam, NIRISS, and NIRSPEC will provide a number of modes to obtain light curves as well as spectroscopic data from 1–5 μm to the stability enabled by the platform (currently unknown, but speculated to be at least as good as 100 ppm as found by *HST* and *Spitzer*). MIRI will enable studies from 5–28 μm at a variety of resolving powers. The infrared opens a unique science by allowing secondary eclipse observations thereby revealing planetary spectra in thermal emission. In the near-infrared, *JWST* will also provide transmission spectrum of exoplanetary atmospheres with an unmatched precision. *JWST* will be able to measure a handful of transit light curves at high spectral resolution ($100 < R < 1\,500$).

One of CHEOPS main science goals is to determine whether there is a limiting planetary mass for which a massive hydrogen envelope is always detected based on precision radius measurements. To achieve this, CHEOPS is carrying-out two sets of observations: (i) follow-up of exoplanetary transits discovered from the ground (see §2.3.2) with the goal of obtaining broad-band planetary radius measurements good to 10% for super-Earths; (ii) discovering which super-Earths among those known from Doppler surveys are transiting (§2.3.1). Both programs could provide *JWST* with new targets, or at least new priorities to select them from the growing list of transiting exoplanets.

The first programme will precise radii of Neptunes from detection (e.g., 3σ) to a S/N ratio of 10 or more resulting in precise flux estimates in secondary eclipse being refined by up to factors of more than 50%. In other words, thermal emission directly detectable by *JWST* for a $3-R_{\oplus}$ planet is $1.8\times$ fainter than a $4-R_{\oplus}$ planet for a given temperature. CHEOPS will further distinguish rocky planets with thin atmospheres from gas-rich planets with thick hydrogen atmospheres (mixed with other species). Thus CHEOPS will provide vital information concerning the prioritisation of targets for exoplanet transit science programmes as well as important flux constraints for planning useful observations.

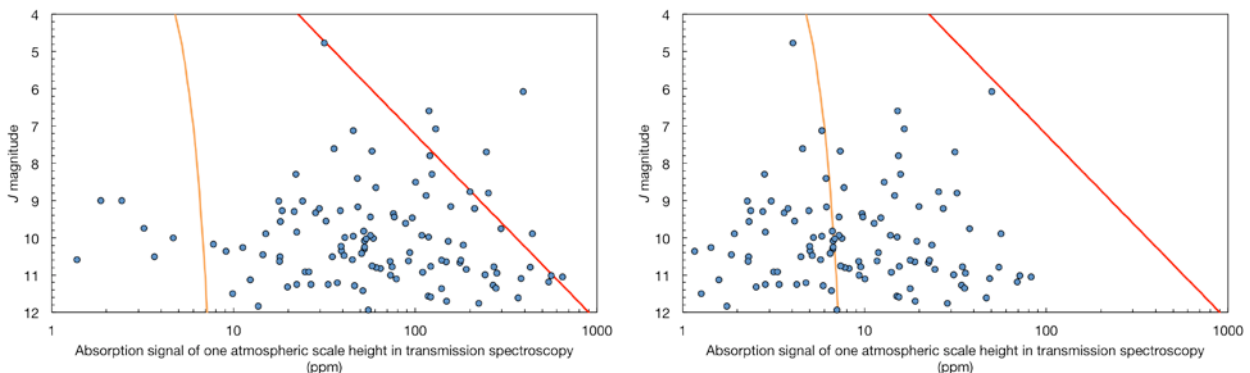


Figure 19 | Detectability of exoplanetary atmosphere in the J band in transmission spectroscopy, as a function of the J-band magnitude and the expected absorption signal caused by one atmospheric scale height. This quantity is scaled on the detection of water at 1.3 μm on the hot Jupiter HD 209458b with the *HST*/Wide Field Camera for Surveys 3 (Deming et al. 2013). The blue dots are the confirmed transiting planets. The *HST* (diameter of 2.4 m) $3\text{-}\sigma$ detection limit is represented by the red curve. The scaled *JWST* (“diameter” of 6.5 m) $3\text{-}\sigma$ detection limit is the orange curve. In the left panel, all planets are assumed to have hydrogen-dominated atmospheres ($\mu = 2.3 \text{ g mol}^{-1}$) while in the right panel, all planets are assumed to have water-dominated atmospheres ($\mu = 18 \text{ g mol}^{-1}$).

The second programme will directly yield some of the most exciting targets (“golden targets”) for *JWST*: transiting super-Earths. *JWST*, in principle, will have the sensitivity to obtain spectra for such planets, some even (theoretically) within the habitable zone (defined by the possibility of liquid water; e.g., Zsom et al 2013). Beyond whether these worlds could retain liquid water on their surface, understanding their temperature, luminosity, and composition (through spectra obtained with *JWST*) will place powerful constraints on models of their formation, and evolution, including surface/atmospheric interactions important for habitability.

JWST will not be able to conduct a very broad survey as it must satisfy many science goals in its mission, with a limited lifetime (5 years required, with a goal of 10 years). Therefore, CHEOPS will be extremely

important in helping to make the most of *JWST* exoplanet transit follow-up. The design philosophy, wavelength range and observing strategy makes CHEOPS extremely complementary to *JWST*. The fact that they will be in operation at the same time (assuming a *JWST* launch in October 2018) suggests that they will enjoy powerful synergies during mutual operation.

2.4.2 Synergies between CHEOPS and TESS

The *Transiting Exoplanet Survey Satellite* (*TESS*) is a mission designed to search for extrasolar planets using the transit method. It has been selected by NASA for launch in 2017. *TESS* observation plan is to conduct a two-year all-sky survey programme to detect transiting exoplanets around nearby and bright stars. The satellite is equipped with four wide-angle telescopes with CCD detectors. Each telescope has an equivalent collecting area of 60 cm². *TESS* mission is planned for a 2-year duration. Its observation programme is assembled to scan wide slices of the sky during 28 days and complete a full half hemisphere in one year by moving the telescope pointing direction about every months. The second year, *TESS* will scan the other hemisphere. *TESS* is designed to reach a systematics photon error of 60 ppm maximum. About 500 000 stars in a magnitude range from 4 to 12 will be observed by *TESS*. Comparison with photometric performance of CHEOPS are listed in Table 3.

Table 3 | Compared characteristics of CHEOPS and TESS. *CHEOPS can obtain light curves of stars brighter than the 6th magnitude, however there is no precision requirement in such cases. †Observation of 13th-magnitude stars with a precision allowing the transit characterisation of Neptune-size planet is a goal requirement. This magnitude can also be reached in the case of M dwarfs. ‡Most extreme possible time span between first and last observation. §Only at the ecliptic poles.

	CHEOPS	TESS
Equivalent collecting area (cm ²)	768	60
Magnitude range	6(0*)–12(13 [†])	4–12
Photometric performance on 12 th magnitude	100 ppm in one hour	300 ppm in one hour
Photometric performance on 9 th magnitude	20 ppm in six hours	60 ppm (TBC)
Data sampling	1 min	?
Most extended observation period [‡]	1 000 days	28 d or 280 d [§]
Launch date	2017	2017
Primary mission duration	3.5 yr	2 yr

TESS will observe about 40 000 stars brighter than the 9th magnitude. Extrapolating from the *Kepler* results, this should lead to the detection of about a hundred of small planets with periods less than 6 days. The 28-days limit for most of *TESS* observations make uncertain the detection of longer-period planets, excepted in small regions at the ecliptic poles where the different field of views overlap. However, only few hundred stars brighter than the 9th magnitude will be observed in these two areas. The smallest transiting planets will be found on K and M dwarfs. To get a sample of 40 000 K dwarfs, the magnitude range must be extended up to the 12th magnitude, decreasing in the same time the accuracy of each transit measurement. Without a complete simulation, it is difficult to assess the number of Earths and super-Earths that will be detected by *TESS*. One can guess a typical number between few dozens and hundred super-Earth candidates. This will be a significant increase of small transiting planet on bright stars.

Looking at the differences between *TESS* and CHEOPS, synergies between these two missions are obvious. In fact, CHEOPS is a perfect follow-up mission for *TESS* discoveries, particularly for the smallest transiting planet candidates and the long-period candidates. For most stars, CHEOPS achieves in a single transit the equivalent signal-to-noise ratio that *TESS* gets after 10 consecutive transits. That means that for any transiting system of period longer than 3 days, a CHEOPS light curve will significantly increase the accuracy

of the transit parameters. This includes as well improving the ephemerids to allow few years later for optimum follow-up. Since we know from *Kepler* that the number of small-size planet rises at least up to 20-day orbital period, the most exciting planets to be detected by *TESS* will benefit from CHEOPS follow-up.

3 Scientific requirements

This chapter describes the science requirements of the CHEOPS mission with their justification. The science requirements are divided in two levels, Level 1 (L1) and Level 2 (L2), and the flow down from L1 to L2 requirements is indicated in each case. L1 and L2 are defined as follows:

- L1 — Top level science requirements directly linked to the science objectives. These should be met by the L2 requirements.
- L2 — Derived science requirements that specify the system scientific capabilities to enable the mission to meet the L1 requirements. These requirements provide the link between L1 requirements and the system engineering requirements.

3.1 Photometric accuracy

SciReq 1.1 Photometric precision for transit detection (L1)
CHEOPS shall be able to detect Earth-size planets transiting G5 dwarf stars (stellar radius of $0.9 R_{\odot}$) with V -band magnitudes in the range $6 \leq V \leq 9$ mag. Since the depth of such transits is 100 parts-per-million (ppm), this requires achieving a photometric precision of 20 ppm (goal: 10 ppm) in 6 hours of integration time. This time corresponds to the transit duration of a planet with a revolution period of 50 days.

SciReq 1.2 Photometric precision for transit characterisation (L1)
CHEOPS shall be able to detect Neptune-size planets transiting K-type dwarf stars (stellar radius of $0.7 R_{\odot}$) with V -band magnitudes as faint as $V=12$ mag (goal: $V=13$ mag) with a signal-to-noise ratio of 30. Such transits have depths of 2 500 ppm and last for nearly 3 hours, for planets with a revolution period of 13 days. Hence, a photometric precision of 85 ppm is to be obtained in 3 hours of integration time.

SciReq 1.3 Point spread function (L2 ← SciReq 1.1, SciReq 1.2)
The point spread function (PSF) of CHEOPS shall be adjusted (e.g., defocused) as a function of the flat field precision (SciReq 1.4) and the pointing accuracy (SciReq 1.6) to reach the required photometric precision (SciReq 1.1, SciReq 1.2).

This shall ensure that the PSF shape and surface area will result from a compromise between the expected spacecraft jitter (which implies a wider PSF to reduce error contributions from the flat-field) and the need to minimize the PSF because of (i) potential stray light contamination of the signal, (ii) a possible contamination from background stars, (iii) the possibility to obtain light curves from close binaries, and (iv) the amount of cosmic rays hitting the area covered by the PSF.

SciReq 1.4 Flat-field precision (L2 ← SciReq 1.1, SciReq 1.2)
The flat field shall be measured down to a pixel-to-pixel precision of $\sigma_{\text{ff}} = 0.1\%$.

This precision results from a compromise between the size and shape of the PSF (SciReq 1.3) and the pointing accuracy (SciReq 1.6), and is necessary to reach the required photometric precision (SciReq 1.1, SciReq 1.2).

SciReq 1.5 Flat-field stability (L2 ← SciReq 1.1, SciReq 1.2)
The flat-field precision (SciReq 1.4) shall be stable over 2 days.

This duration represents the maximum time scale of an observation (and applies here to the search of a transit across a star from the radial velocity sample).

SciReq 1.6 **Pointing accuracy (L2 ← SciReq 1.1, SciReq 1.2)**
CHEOPS pointing accuracy during observations shall be better than 8 arcsec rms.

The 8-arcsec standard deviation of the jitter results from a trade-off between the size of the PSF and the flat field, necessary to reach the required photometric precision (SciReq 1.1, SciReq 1.2). This formulation is compatible with the system requirement formulation that during observations, the half cone angle between the actual and desired payload line of sight (LoS) directions shall have an absolute performance error (APE) less than 8 arcsec at 68% confidence, using the temporal statistical interpretation.

These last four L2 requirements (SciReq 1.3, SciReq 1.4, SciReq 1.5, SciReq 1.6) are tied together. The effect of the spacecraft jitter causes a displacement of the PSF onto different detector pixels, introducing extra noise due to pixel-to-pixel variations. This extra noise depends on the flat-fielding accuracy and can be mitigated by obtaining a flat PSF without a central peak very sensitive to inter-pixel variations. Trades are therefore possible between the flat-field precision, the extent of the PSF, and the pointing accuracy, provided the overall precision is maintained.

3.2 Sky coverage

SciReq 2.1 **Transit search on stars with small planets (L1)**
50% of the whole sky shall be accessible for 50 (goal: 60) cumulative (goal: consecutive) days of observations per year and per target with observation duration longer than 50% of the spacecraft orbit duration (>50 min for 100-min spacecraft orbital period).

This requirement is associated with the detection of shallow transits (SciReq 1.1). CHEOPS is a follow-up mission; therefore it is absolutely critical that it is able to observe stars with Doppler-detected planets on the largest possible fraction of the sky. The 50% of the whole sky results from a trade-off with the maximum revolution period of the planets we want to observe: a period of 50 days corresponds to a planetary orbit at the inner edge of the habitable zone of K stars. The transit of an Earth-size planet with a revolution period of 50 days across a 0.9- R_{\odot} star has a depth of 100 ppm and lasts for 6h. Since the transit measurement is essentially differential, it is necessary to monitor the star before, during, and after the transit, which for such transit duration requires to observe during several (9 to 12) consecutive spacecraft orbits. The consecutive coverage of one target could be extended up to 48 h (28 orbits) depending on the transit ephemeris precision for this given target. The coverage need not be strictly continuous: given the noise budget (~150 ppm/min) expected for a V=9 magnitude star, the required rms (SciReq 1.1) can still be achieved if 50% of the transit is covered with the observing time evenly dispatched among all spacecraft orbits. Therefore, it shall be possible to observe the star during at least 50% of each spacecraft orbit. The 50 days of visibility with >50% of the spacecraft orbit shall be as consecutive as possible to allow for a transit coverage at any time during the window, depending on its predicted ephemeris.

Note that the shallow transits of planets with shorter revolution periods will also be shorter (4h for P=15 days), hence for these planets two transits will be needed to obtain the requested signal-to-noise ratio. Note also that for small-size transiting objects, the time of the in/egress is too short to be of any use to constrain the planet size through comparison with the precise measurement of the contrast. Missing in/egress (occurring during interruptions) would not affect the performance of the mission to detect the transit and measure the size of small planets.

SciReq 2.2

Follow-up of stars with transiting planets (L1)

25% of the whole sky, with 2/3 in the southern hemisphere, shall be accessible for 13 days (cumulative; goal: 15 days) per year and per target, with observation duration longer than 80% of the spacecraft orbit duration (>80 min for 100-min spacecraft orbit).

This requirement is related to the observation of transiting hot Neptune planets on stars with V magnitudes < 12 (goal: 13) (SciReq 1.2). The sky coverage need not be as complete for these as for the Doppler targets, since for example NGTS will target only a fraction (10%) of the southern sky. The revolution period of 13 days (goal: 15 days) is linked to the window function of the Next Generation Transit Survey, which will be effective in detecting Neptune-size planets with revolution period up to 15 days. Such a transit across a 0.7-R_⊙ K-type star has a depth of 2500 ppm and lasts for 3h. In order to characterise this transit with a S/N_{transit} of 30, the noise rms after 3h of integration should be <85 ppm (SciReq 2.2). Contrary to shallow transits of Earth-size planets (SciReq 1.1), these transits are short enough to be missed in case of large interruptions during spacecraft orbits. Any of these transits by planets with revolution periods <13 days can be completely covered within two spacecraft orbits, and detected with the requested S/N_{transit}= 30, provided that the observations are carried out during at least 80% of each spacecraft orbit (<20% of interruptions).

3.3 Target observability

The following conditions shall be met for a target to be observable:

SciReq 3.1

Earth occultation (L2 ← SciReq 2.1, SciReq 2.2)

For the observing time to be scientifically valid, the target shall have a projected altitude from the surface of the Earth equal or higher than 100 km.

The margin of 100 km is taken to avoid atmospheric glow.

SciReq 3.2

Earth stray light exclusion angle (L2 ← SciReq 1.2, SciReq 2.1, SciReq 2.2, SciReq 4.1)

In order to limit stray light contamination, the minimum angle allowed between the line-of-sight and any (visible) illuminated part of the Earth limb, the so-called *Earth stray light exclusion angle* shall be 35° (goal: 28°).

This angle value is driven by the faint magnitude limit (SciReq 4.1). For brighter targets, this constraints could be relaxed.

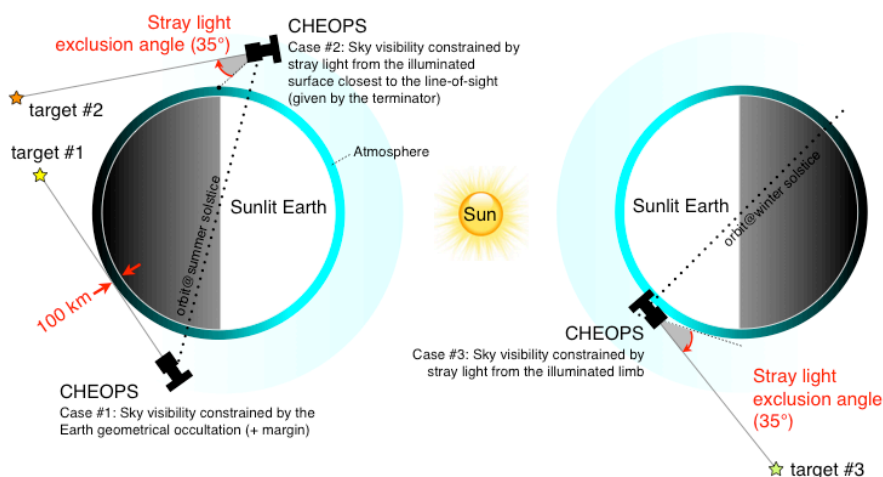


Figure 20 | Illustration of the pointing constraints introduced by SciReq 3.1 and SciReq 3.2.

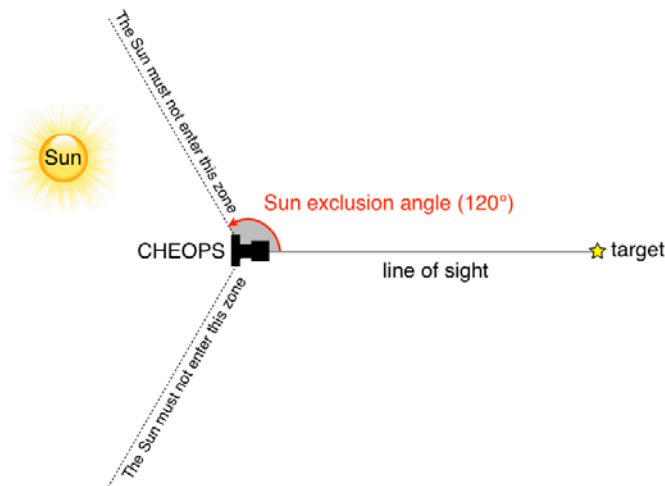


Figure 21 | Illustration of the pointing constraint introduced by SciReq 3.3.

SciReq 3.3 Sun exclusion angle (L2 ← SciReq 2.1, SciReq 2.2)

The Sun must be outside the cone around the line-of-sight (LOS) of the telescope having a half-angle, the so-called *sun exclusion angle*, of 120°.

This angle will in particular insure that the radiators are never illuminated by the Sun. A Sun exclusion angle < 120° (goal) would enable better sky coverage capabilities.

SciReq 3.4 Moon exclusion angle (L2 ← SciReq 2.1, SciReq 2.2)

The bright Moon must not be inside a cone around the line-of-sight of the telescope having a half-angle, the so-called *moon exclusion angle*, of 5°.

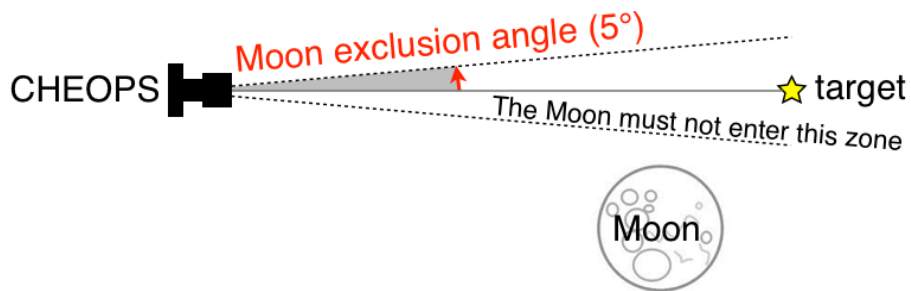


Figure 22 | Illustration of the pointing constraint introduced by SciReq 3.4.

3.4 Magnitude range of targets and exposure times

SciReq 4.1 Bright-to-faint target magnitudes (L1)

CHEOPS shall be able to observe bright to faint stars with V-band magnitudes in the range $6 < V < 12$ mag with the photometric precisions given in SciReqs 1.1 & 1.2.

SciReq 4.2 Very bright target magnitudes (L1)

CHEOPS shall be able to obtain light curves from very bright stars down to a V-band magnitude of $V = 0$ mag.

There is no requirement on the photometric precision for such targets.

SciReq 4.3 Exposure times (L2 ← SciReq 4.1, SciReq 5.1)
The exposure times for targets in the magnitude range defined in SciReq 4.1 shall range from 1 to 60 seconds.

The shortest exposure times should allow avoiding saturating the 6th -magnitude targets, while the longest exposure times are set by the temporal sampling of the measurements (SciReq 5.1).

3.5 Time sampling & precision of the light curves

SciReq 5.1 Temporal resolution of the measurements (L1)
CHEOPS shall be able to provide one photometric measurement per minute (goal: one per 30 seconds) in order to characterise the transit light curves of Neptune-size planets (SciReq 1.2).

In particular, this requirement will allow a proper mapping of the ingress and egress phases, which will lift the degeneracy between the impact parameter and the transit duration.

SciReq 5.2 Time stamp uncertainty (L1)
CHEOPS shall be able to provide photometric measurements with time stamp (UTC) uncertainties of 1second (goal: < 0.01 second) for transit light curves. The goal value is set to provide a better time stamp precision for ancillary (non-transit) science.

Given the expected durations of the transits (from one to several hours), this time stamp uncertainty is sufficient to obtain the central time of the transit with a good precision, allowing for instance the analysis of transit timing variations.

3.6 Lifetime

SciReq 6.1 Mission duration (L1)
The nominal duration of the mission shall be 3.5 years (goal: 5 years).

Transit detection on bright stars identified by Doppler surveys will need about a minimum total of 600 days of satellite life for 150 targets (expecting 2 days of observation time per target with 50% efficiency; SciReq 2.1). For bright to faint targets from ground-based transit surveys (NGTS), some of them requiring the observation of up to 10 transits, a total of 180 days of mission is foreseen (expecting an observing time of 12 hours per transit and 80% efficiency; SciReq 2.2). Observations to detect the planets directly in reflected light will be possible for a handful of hot Jupiters and would require 75 days of mission (for a sample of 5 hot Jupiters). In total these programs combined require ~500 separate target pointings. Assuming 0.3 hours per pointing for acquisition and 10% margin on each program, the mission duration is estimated at ~950 days or 2.6 years. Adding to this duration the open time allocation (up to 20% of the observing time) and the commissioning phase of 0.2 years, the total required duration of the CHEOPS mission is estimated to be 3.5 years. An extended mission (5 years) would potentially allow to significantly enhance the science impact of the mission. The rate of exoplanet discovery in the past years show that new exciting targets are likely to be discovered within the next 5 years (e.g., the impact of a mission such as TESS). Furthermore, no other mission similar to CHEOPS is planned in this time frame, making CHEOPS a unique follow-up machine of wide astrophysical interest.

4 Payload and Performance

The CHEOPS mission payload consists of only one instrument, a space telescope of 33 cm clear aperture, which has a single CCD focal plane detector. This telescope, along with all the detector and support electronics, instrument computer, and thermal regulation hardware, is called the CHEOPS Instrument assembly System (CIS).

4.1 Instrument Description

The CIS telescope tube assembly is passively cooled and thermally controlled with on-board heaters. The telescope feeds a re-imaging optic, which supports the straylight suppression concept, by providing a position for a field stop and reducing the impact of scattering from the baffling system (vanes edges) reaching the detector directly.

The baseline detector for CIS is a 13- μm pixel $1\text{k} \times 1\text{k}$ CCD (E2V CCD47-20 AIMO). This detector will be operated at a nominal temperature of -40°C . A mid-band coating is specified to enhance the quantum efficiency.

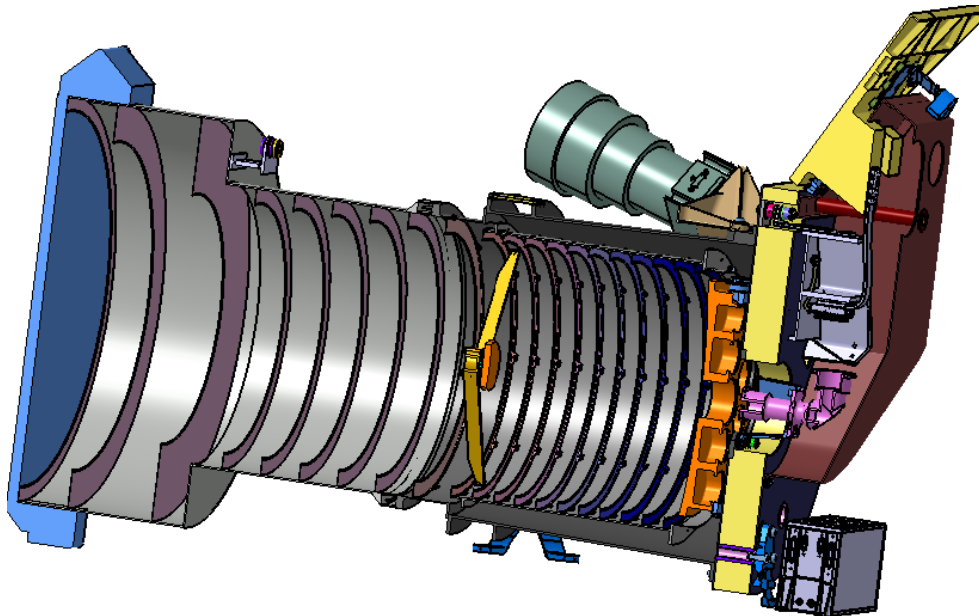


Figure 23 | A cutaway view of the CHEOPS flight instrument showing components.

The CHEOPS Instrument (CIS) consists of four major hardware units described below. Each unit will be independently mounted on the spacecraft (S/C).

4.1.1 Optical Telescope Assembly (OTA)

This is the structure carrying the telescope, the Focal Plane assembly Module (FPM), and the radiators. The structure is made of near-zero CTE sandwich panels (CFRP-Al). The optical bench supports the FPM and back end optics. The Star Trackers (ST) will be mounted on the isostatic mounts of the OTA.

4.1.2 Baffle and Cover Assembly (BCA)

Baffle including protective cover and release mechanism. The main structure is made of Aluminium.

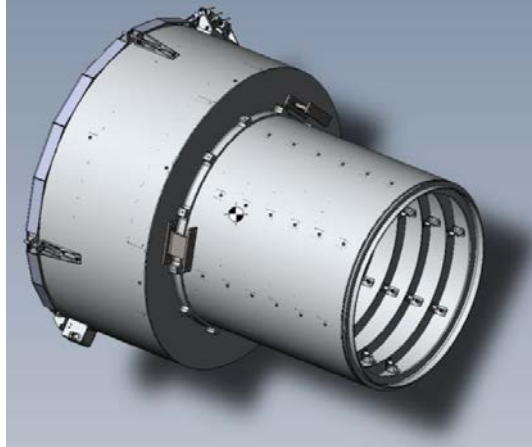


Figure 24 | BCA current design.

4.1.3 Back-End Electronics Box (BEE) and Sensor Electronics Module (SEM)

The BEE is the electronics box including the DPU and power converters with aluminium housing. It contains two redundant DCDC converters and two redundant instrument computers (DPU). The BEE will be installed inside the S/C structure. The sensor electronics module contains the digital electronics and interfaces to the DPU. The SEM is attached to the S/C panel.

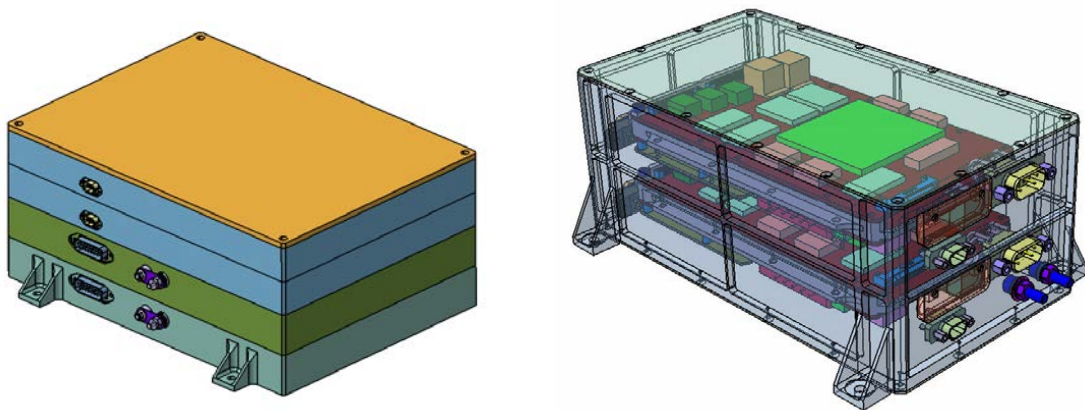


Figure 25 | CIS instrument Back End Electronics Box (BEE, left) and Sensor Electronics Module (SEM, right).

4.2 Design Challenges

The key challenge of the mission is to achieve ultra-stable photometry at the 20 ppm level. To meet this goal a number of effects have to be controlled:

- Temperature dependence of CCD sensitivity and quantum efficiency (QE): thermal control of detector
- CCD pixel-to-pixel response non-uniformity (PRNU) and spacecraft jitter (jitter noise): calibrate the flatfield to 1000 ppm and spread the Point Spread Function (PSF) over many pixels to compensate for pointing errors
- Gain stability of analog amplifiers: low noise and very stable readout electronics
- Stray light varies over one orbit: very good stray light attenuation
- Stability of the PSF in flight: thermal stabilization of telescope tube and very stable mechanical structure

The CIS optical design is intended to produce a relatively wide PSF at the detector plane. The width of the PSF is a trade-off between reducing the jitter noise (pushing to large PSFs) and the increased susceptibility to straylight contamination within the PSF. Other factors also play a role (see noise budget).

The optical elements are mounted in a structure of carbon-fibre reinforced polymer, which is used to reduce the susceptibility of the instrument to thermal variations, which might be significant in near-Earth orbit. The target operational temperature is -10°C for the telescope structure. The change in distance between the primary and secondary mirrors (the parameter with the largest impact) should be within the $< 22 \mu\text{m}$ needed, if the PSF is to be maintained constant to an appropriate level. Prior characterisation of the CFRP (CTE $< 0.2 \text{ ppm/K}$ in plane) suggests that the telescope therefore needs to be temperature-stabilised to $\Delta T < 10 \text{ K}$. Heaters (requiring $\sim 20\text{--}25 \text{ W}$) will be placed on the telescope structure to elevate and stabilise the temperature. A further key issue during the preliminary design phase is the distortion by CFRP moisture release in vacuum.

Straylight (primarily from the Earth) is potentially a major noise source and hence the telescope must be baffled. The instrument baffling takes account of the rotation of the spacecraft, which maintains the Earth to one side of the spacecraft at all times. Concerns over cleanliness and contamination has led to the introduction of a door cover (which is light and dust tight).

The temperature stability of the Focal Plane Assembly (FPA) must be maintained to a level of $\sim 10 \text{ mK}$ and the gain of the readout electronics must be stable at the 5-ppm level. The FPA and the readout electronics require radiators to meet their operational temperatures and allow for a thermal control approach, which avoids use of energy intensive thermo-electric or Sterling coolers. The radiators will passively cool to temperatures below the target temperature and the FPA will be heated in a control loop to the specified value.

The sensor electronics module (SEM) supports the readout electronics and interfaces to a digital processing unit (DPU), which is part of the back-end electronics assembly (BEE). The DPU will control all aspects of the instrument and will allow image acquisition over a range of framing rates. The DPU will also analyse data in real-time autonomously and pass the centroid of the stellar images to the spacecraft AOCS thereby allowing more accurate control of the spacecraft pointing (requirement of $< 8''$ jitter). This is needed to reduce the jitter of the system and thereby reduce noise arising from the error in the knowledge of the flat-field. The BEE also contains a power unit (DCDC), which converts the input voltage from the spacecraft to the voltage supplies necessary for the instrument.

4.3 Instrument Decomposition

The product tree for the CHEOPS instrument is shown in the right panel of Figure 26. The payload is logically divided into several functional components as described in the functional block diagram in the left panel. The division of responsibilities in the CMC is shown in Table 4.

Table 4 | CMC member contributions to the payload

<i>Subsystem</i>	<i>Acronym</i>	<i>Organisation</i>
Instrument Prime	CIS	UBE
Outer baffle and door	BCA	CSL
Telescope Structure and Optical Bench	OTA	UBE
Telescope optical design and optical components	TEL	INAF
FPA and FEE Radiators	RAD	KON
Focal plane, thermal control, and proximity electronics	FPM	DLR
Sensor electronics module	SEM	DLR
DCDC Power converter	DCDC	IWF
Detector	CCD	ESA

Payload Computer	DPU	IWF
Science Calibration	CAL	UGE

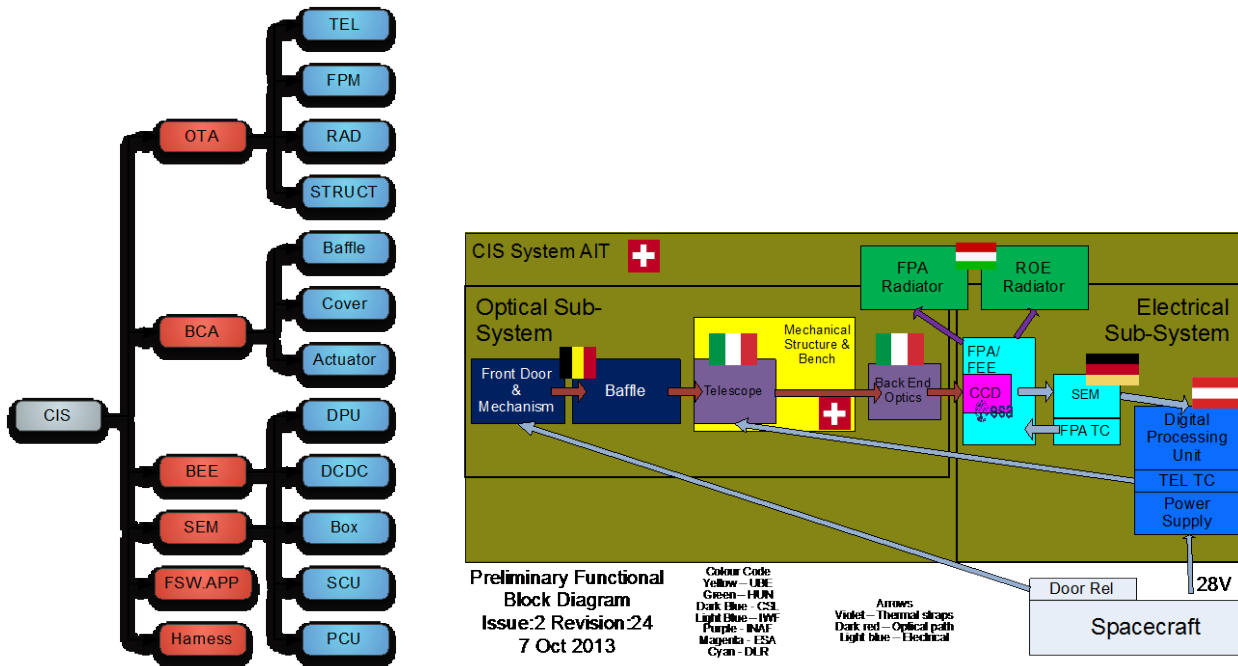


Figure 26 | Top level CHEOPS Instrument Product Tree (left) and functional block diagram (right).

4.4 CIS Design

4.4.1 Telescope optical design

The optical configuration consists of a Ritchey-Chrétien telescope. The main design drivers are related to the compactness of the optical system and to the capability to reject the straylight.

The entrance pupil is located at the primary mirror and has a diameter of 320 mm. The central obstruction has a diameter of 68 mm (equal to the secondary mirror diameter), giving a relative central obstruction diameter of 0.2125. The effective collecting area is 76793 mm² (about 8.64% more than the required one corresponding to an unobstructed telescope having a diameter of 300 mm). This redundancy has been maintained to provide for possible lack of throughput efficiencies. If this is not required, the entrance pupil diameter could be reduced.

In the baseline design, the distance between the primary mirror and the secondary mirror is 300 mm maximising launch fairing compatibility.

The telescope effective focal length is 1 600 mm, giving a telescope focal ratio $F/5$.

The focal plane has a diameter of 11.23 mm corresponding to a field of view (FoV) of 0.4°. At this location, a focal plane mask of the same size is envisaged for the attenuation of the straylight background.

An estimation of the background contribution due to direct illumination of the focal plane by the sky has been computed. The result is that this background is negligible with respect to the other background sources. As a consequence, no internal baffling for focal plane shielding is required.

The telescope parameters are reported in Table 5. A layout of the telescope (including a conceptual scheme of internal baffling) is shown in Figure 27.

Table 5 | Telescope parameters.

	Radius of curvature [mm]	Thickness to next surface [mm]	Conic constant	Aperture diameter [mm]
Primary mirror	-742.75	-300.00	-1.026	320.00
Secondary mirror	-185.90	307.464	-2.869	68.00
Telescope focal plane	Infinity			11.23

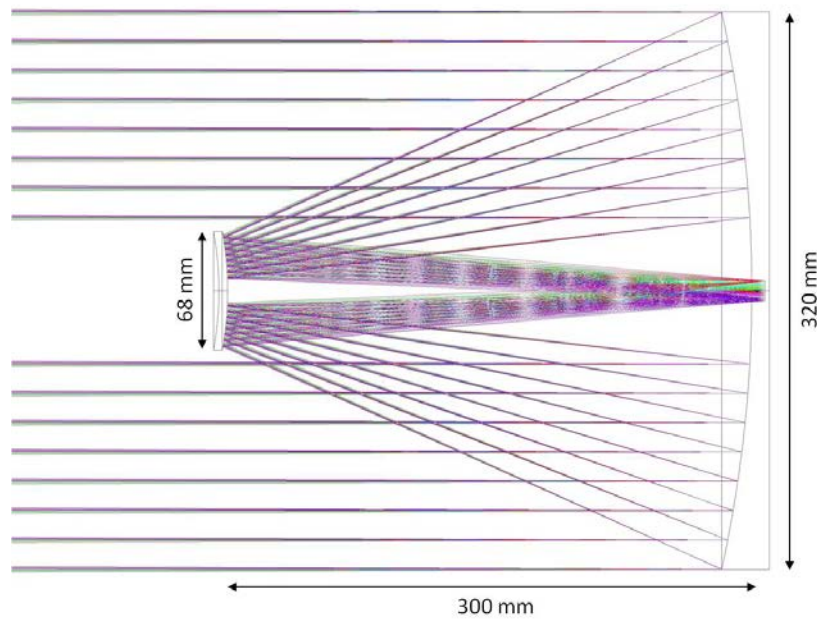


Figure 27 | Telescope optical layout.

4.4.2 Back-End Optics design

The main purpose of the Back-End Optics (BEO) is to re-image the telescope focal plane on the detector and to provide an intermediate pupil, at which location a mask is placed for the straylight rejection. Moreover, at the intermediate pupil, a PSF shaper (holographic diffuser or lenslet array) can be placed.

The BEO is basically composed by three elements: a collimator which forms an intermediate pupil, a flat fold mirror which is inserted to minimise the envelope of the whole optical system, and a camera that reimages the focal plane at the required plate scale.

The BEO has been optimised on a field of view having diameters 0.32° as shown in Figure 28. The detector area of interest is 200×200 pixels and its location will set inside the optimised Field of View. During the optimisation, all the wavelengths in the range 400-1100 nm have been associated the same weight, that is, the efficiency of the system has been assumed to be the same at all wavelengths.

The current design of the collimator and the camera is based on two spaced achromatic doublets. The goal is to maintain the system as simple as possible, and in compatibility with the performances.

4.4.2.1 Glasses selection

The glasses selection for the two doublets has been driven by considerations related to performances, spectral transmissivity and the CHEOPS space environment.

In particular, we have assumed a Total Integrated Dose (TID) of less than 10 krad over the mission profile. This assumption is supported by the fact that the lenses are not directly exposed to the external environment and that they are surrounded by the telescope and by the spacecraft structure. Moreover, it is possible to

shield the lenses in the tube where they are mounted with properly radiation resistance material (such as tantalum).

As a second driver, the transmissivity in the blue part of the spectrum (400–500 nm) has to be the same as for the other wavelengths. This requirement is in contrast with almost all the cerium enhanced glasses.

For these two reasons, we have currently selected the two glasses S-FPL51 and BPH5. They give satisfactory performance in terms of lateral colors control, they are moderate-radiation-resistance glasses and they have a good transmissivity (>96% for 10 mm thickness) over the whole spectral range.

4.4.2.2 Optical design

The collimator has been designed to form an intermediate pupil, which diameter has been set to 10.87 mm.⁵

The location of the fold mirror is expected to be between the intermediate pupil and the camera. The final location will be defined on the basis of mechanical considerations, in particular, to minimise the instrument envelope and to allow for detector accommodation.

The camera has been designed to set the system effective focal length equal to 2 681 mm, meeting the required plate scale at the nominal focal plane (1 arcsec/pixel).

Even if it is not required, currently the camera has been designed to have a small non-telecentricity angle (the exit pupil location stands at about 1 600 mm in front of the focal plane).

The overall thickness of the BEO from the telescope focal plane to the camera focal plane is currently about 298 mm (without fold mirror). In the case of defocused PSFs option, the detector focal plane will be defocused by about 3.5 mm in order to obtain a PSF spread over about 30 pixels in diameter. The lens mass has been estimated to be about 22 g.

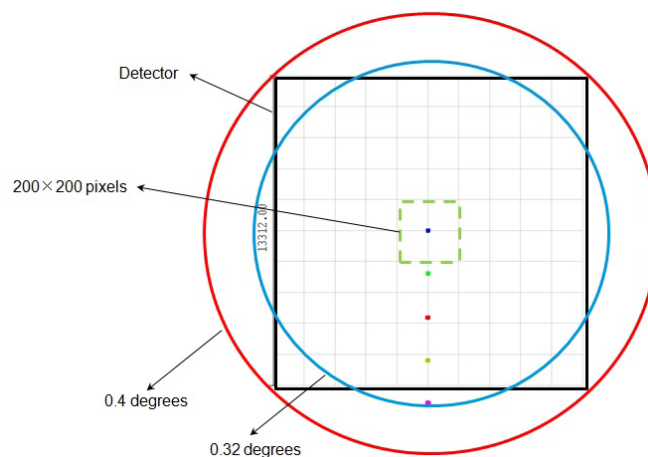


Figure 28 | Field of View: the circle at 0.4 degrees corresponds to telescope FoV optimisation, while the circle at 0.32 degrees corresponds to BEO FoV optimisation.

The BEO parameters are reported in Table 6, while a layout is shown in Figure 29.

⁵ This value allows the option to insert in this location a holographic diffuser or a lenslet array. In particular, for this size the holographic diffuser needs a diffusing angle of about 0.25° in order to spread uniformly the PSF over a circle having diameter 30'' and the lenslet array with the same spreading properties. If none of these options is adopted, there will be almost no impact on the BEO design, but the pupil size may be included as free parameter in the BEO optimisation. The current baseline does not require any beam-shaping devices.

Table 6 | BEO parameters.

		Radius of curvature [mm]	Thickness [mm]	Diameter [mm]	Glasses
telescope FP			52.02		
Collimator	s1	47.21	5.97	22	S-FPL51
lens 1	s2	-19.16	1.10	22	
Collimator	s1	-17.93	2.00	22	BPH5
lens 2	s2	-36.07	57.44	22	
Pupil			86.20		
Camera	s1	42.83	4.57	26.4	S-FPL51
lens 1	s2	-50.17	1.22	26.4	
Camera	s1	-42.95	3.00	26.4	BPH5
lens 2	s2	-145.67	84.46	26.4	
FP					

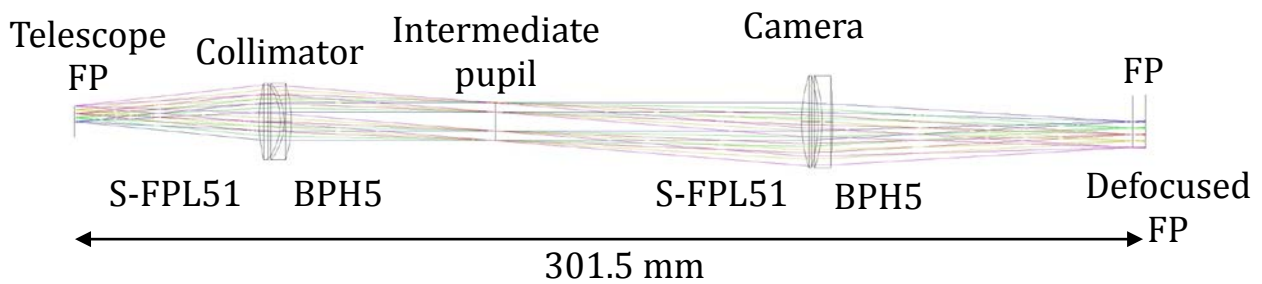


Figure 29 | Layout of BEO system.

4.4.3 Defocused PSFs performance

The theoretical PSF shape is a top-hat cylinder having diameter of about 30 arcsec (i.e., 30 pixels). The figure of merit to evaluate the performance has been derived by considering the optical PSFs, the jitter effect and the flatfield performances. The result of the simulations has pointed out that a defocused PSF gives sufficient performance to meet the requirements. Here we presented the defocused optical PSFs delivered by the baseline optical system.

PSFs have been generated at the defocused focal plane (about 3.5 mm from the nominal focal plane) with a flat spectral wavelength between 400 and 1100 nm with a spectral sampling of 50 nanometers. They have been spatially sampled with a subpixel size of 1.3 micron corresponding to 1/10th of the nominal detector pixel size.

The images of PSFs at the centre of the field of view (0,0) degrees, and for the fields (0,0.012) degrees, are shown in Figure 30, while the profiles passing through the centre along x-direction and y-direction for several positions are shown in Figure 31.

Moving from the center of the field of view to the edge, anisotropy starts to affect PSFs while at the very edge the PSF starts to be dominated by aberrations. As expected, in the PSF the feature due to the telescope central obstruction and to the Poisson spot can be clearly seen.

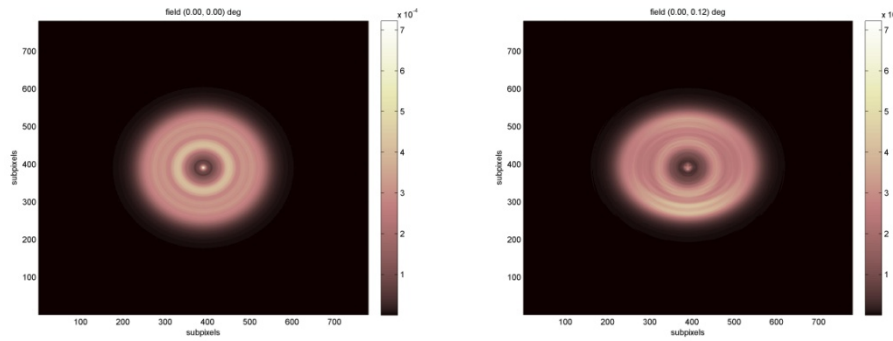


Figure 30 | Images of the PSFs for the fields (0,0.00), and (0,0.12) degrees sampled with subpixels of 1.3 μm .

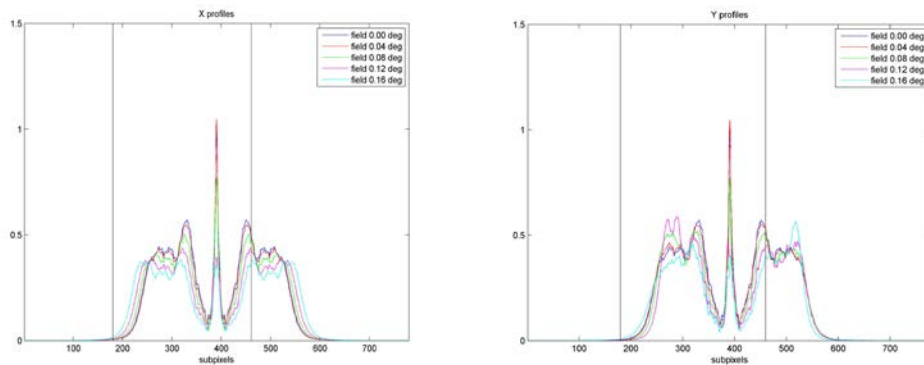


Figure 31 | Profiles of the PSFs crossing the centre for the fields (0,0.00), (0,0.04), (0,0.08), (0,0.12), (0,0.16) degrees along x-direction (left) and y-direction (right).

4.4.4 Baffle and Cover Assembly

The Baffle and Cover assembly (BCA) is the key to the stray light mitigation strategy of the CIS. The baffle design as well as the cover and actuator are of *CoRoT* heritage. The purpose of the cover is to provide a light tight lid as well as contamination control for the OTA integration prior to launch. The cover release mechanism is based on a spring-loaded hinge and a launch lock mechanism. The launch lock is based on a Frangibolt actuator design. This solution provides reliability and also avoids contamination issues during launch and early orbital phase. The baffle was designed following the constraints given in Figure 32 together with the resulting baffle geometry.

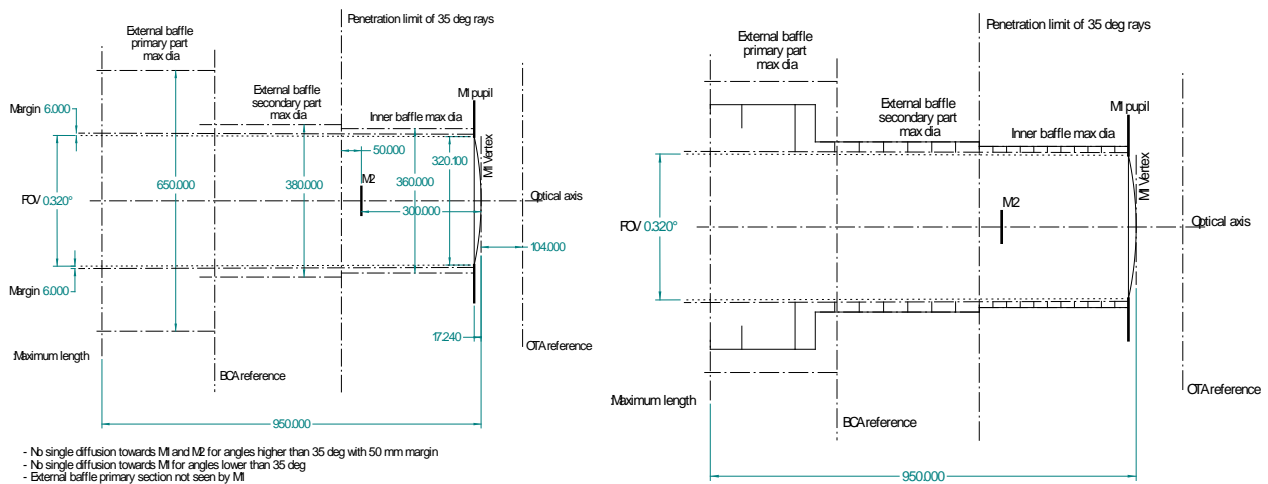


Figure 32 | Summary of constraints used to construct the baffling system (left) and the resulting baffle geometry (right).

4.4.5 Telescope Stray light analysis

Because of the required photometric sensitivity of the CIS instrument, a straylight analysis of the optical telescope and baffle assembly has been performed. The results of this initial study are shown in Figure 33, which indicates a design reaching the required straylight suppression to within an order of magnitude. Further work is expected to result in an optimised baffle design.

An important contributor to stray light is the contamination of the optics. We are targeting a cleanliness level of CL200 for the mirrors and the back-end optics which is very difficult to achieve. However, the OTA is designed in such a way that it can be kept closed for practically all integration activities, except the alignment of the optics and the final combination of OTA and BCA. Even the OTA-BCA alignment can be done with a sealed OTA. Applying the CL200 contamination to mirrors and back end optics increases the PST by about a factor of 5. Using this contaminated PST, the sky coverage is still within specifications (>50% of the sky observable).

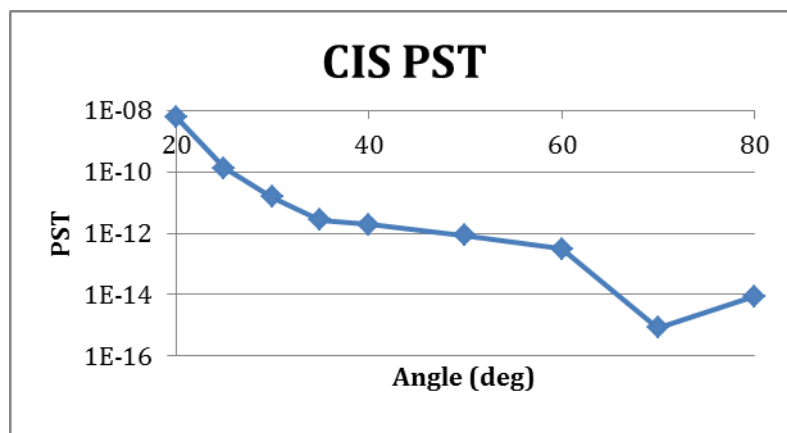


Figure 33 | Point Source Transmittance (PST) data for baseline design.

4.4.6 CCD Detector

The detector selected is an e2v CCD47-20 (AIMO). The CCD will nominally be operated at -40°C . The flight model (FM) CCD will be characterised prior to installation in the PFM instrument. The CIS will then be calibrated. Other tests are done on lot level, such as radiation tests and related qualification tests.

The CCD main parameters are:

- e2v CCD47-20 (AIMO)
- Back-illuminated
- 1024 by 1024 1:1 Image Format
- Image Area 13.3×13.3 mm
- Frame Transfer Operation
- $13 \mu\text{m}$ Square Pixels
- Symmetrical Anti-static Gate Protection
- Very Low Noise Output Amplifiers
- Gated Dump Drain on Output Register
- 100% Active Area
- Advanced Inverted Mode Operation (AIMO)
- Read noise: $2 \text{ e}^- \text{ rms}$ @ 20 kHz, $6 \text{ e}^- \text{ rms}$ @ 200 kHz
- Wavelength range: 400 – 1100 nm
- Gain sensitivity vs. temperature: assumption 1000 ppm/K (CCD773)
- Dark current $<0.08 \text{ e}^-/\text{pixel}/\text{sec}$ @ -40°C

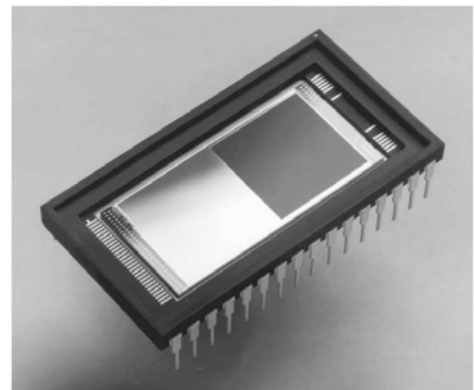


Figure 34 | The CIS detector: CCD 47-20 AIMO.

4.4.7 Focal Plane Module and Sensor Electronics Module

There are two physically separated modules for controlling and interfacing the CCD detector, the FPM and the SEM. The FPM (Focal Plane Module) contains the FPA (Focal Plane Assembly) where the CCD is located on, and the FEE (Front-End Electronics) both with two separate interfaces to the radiator. The SEM as a physically separated module and electrical harness to the FPM/FEE contains a SCU and a PCU (Power Conditioning Unit) interfacing the platform DPU (Data Processing Unit) and the PSU (Power Supply Unit). Both, the DPU and PSU are integrated in the BEE (Back-End Electronics).

This architecture is mainly driven by the thermal design having 3 different categories reflecting the requirements of thermal control.

1. Focal Plane Assembly (FPA) with CCD and proximity electronics operating at 233 K nominally stabilised by heating against a dedicated radiator,
2. Front-End Electronics (FEE) with mostly ADC and clock driving operating between 253–273 K stabilised by heating against a dedicated radiator,
3. Sensor Electronics Controller and Power Conditioning Unit (SCU & PCU), including FPGA - based digital electronics for sensor and data handling at standard temperatures without stabilisation needs.

Due to the sensitivity of signals and clocks against cross talk and disturbances the analogue electronics according 1 and 2 is organised in close vicinity.

The FPA is located at the optics port thermally connected to a radiator for cooling down the FPA, especially the CCD down to at least -40°C , radiation shielded by its housing and thermally stabilised. Figure 35 shows the FPA on the instrument preliminary model. Near the CCD the FEE is located thermally connected within the FPM housing to a separate radiator cooling down the electronics to about -20 to 0°C , and also thermally stabilised. Some electronics PCBs are placed around the FPA/CCD. The FPM/FEE is electrically interfaced to the SEM by an external harness between the two separate modules. The SEM contains mainly the digital controller and power conditioning electronics on the SCU and the PCU.

According to the concept of the telescope, the focal plane is organised in rectangular position related to a base plate in parallel to the M1 mirror. This is done by a 90° -fold mirror in front of the detector together with a back-end lens system. Due to the strongly diverging operating temperatures, there is no direct mounting interface of the detector to the telescope foreseen; instead an iso-static mount onto the base plate parallel to M1 is planned.

Figure 35 shows the SEM with 4 PCBs and harness inside including cold redundancy. This box is mounted on the S/C panel. Its temperature at the mounting point will be about -5 to $+30^{\circ}\text{C}$ (TBC) while in operation and -20 to $+50^{\circ}\text{C}$ when it is OFF (i.e., non-operational, TBC).

The SEM box has connectors to the FEE and heater, as well as connectors to the BEE (DPU and PSU). Figure 36 shows the block diagram of the FPM and SEM.

4.4.7.1 FPM mechanical and thermal design

The mechanical FPM design is shown in Figure 37. The concept is that the CCD is iso-statically mounted on the FPA and thermally coupled as much as possible to the dedicated radiator. It is supported on the structure for FEE accommodation, which simultaneously creates a thermally defined environment for the FPA/CCD, e.g. 2 thermal stages -40°C (233K) at CCD and about -20 to 0°C at FEE (baseline is about 5°C). The massive FEE body shall react thermally inert and therefore serve as the basis for the temperature control of FEE/ADC. Figure 37 shows the FEE as 3 PCBs, main and redundant analog chain (left and right) and one PCB containing the CCD clock driver electronics.

Some harness will connect the FPM/FEE with the SEM as separate box. Additionally the heater and some temperature sensors are located within the FPA/FEE assembly interfaced also to the SEM. Harness, heater, and temperature sensor are not shown in Figure 37.

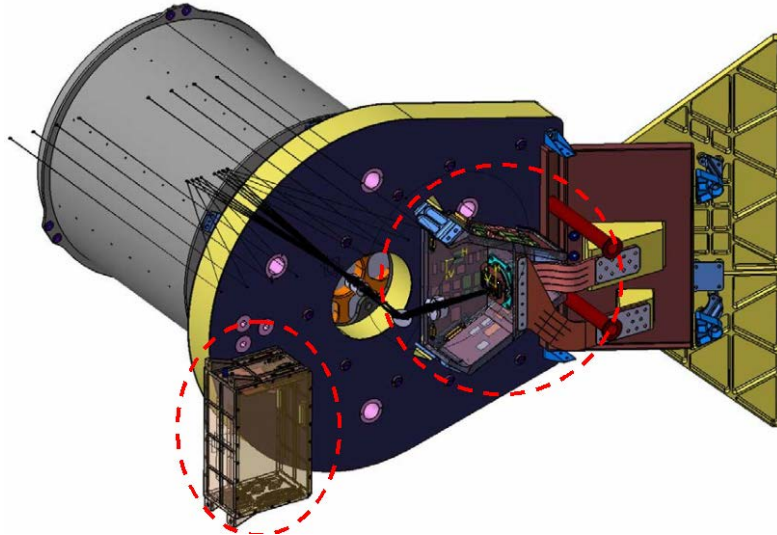


Figure 35 | FPM and SEM on CHEOPS instrument.

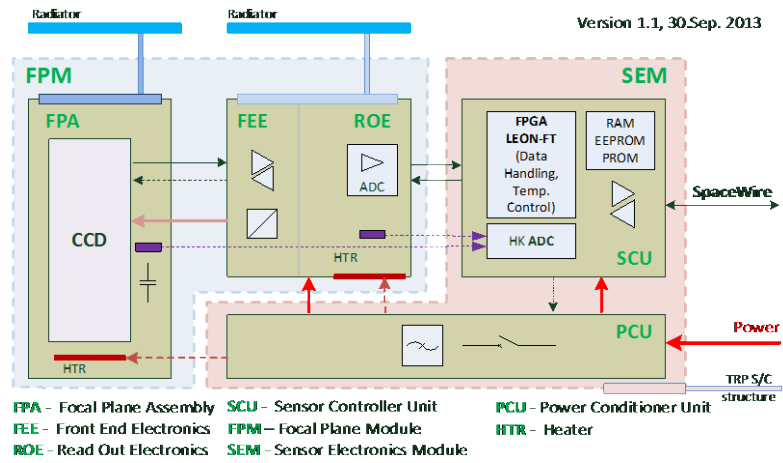


Figure 36 | FPM and SEM block diagram.



Figure 37 | FPM with FEE, FPA, and dedicated radiator straps.

Since the CCD has to be cooled down lower than 233 K but the package is of standard design, an intermediate structure acting as a cold block has to be developed as shown in Figure 38. It provides the interfaces to the radiator heat link, realises a mounting interface for heater and thermal sensors, and carries a few parts of proximity electronics and the CCD itself. The latter can be performed in different ways (hybrids, ring PCB etc.) but has to end up in any case with a flex link towards FEE for thermal decoupling. For thermal efficiency this unit shall be kept small to reduce radiating surfaces and cooling power. However the CCD standard package does not have any mounting interfaces so thermal transfer will be determined by gluing at plane-to-plane interfaces. A small size thermal isolating bracket is holding the CCD block to the FEE structure.

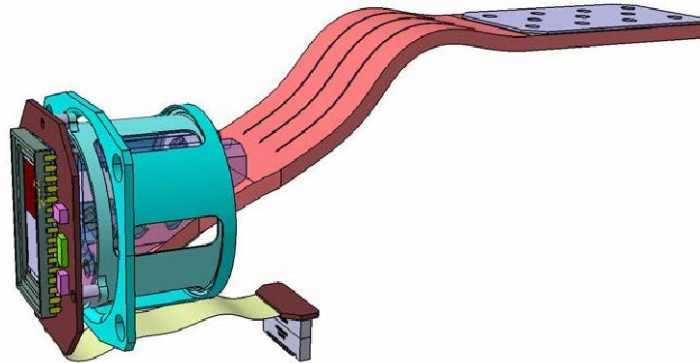


Figure 38: FPA with CCD, spider, and radiator strap.

4.4.7.2 FEE and FPA Electrical Design

The FEE is an analogue electronics with a 16-bit ADC providing digital data to the SCU. Furthermore, it provides BIAS voltages, clocks etc. to the CCD. The FEE will provide low noise reading-out, clocking and supplying the CCD. An accuracy of the electronics chain of 14–15 bit is the goal to achieve, having a low part of the system noise budget in total. Therefore EMC design aspects e.g. grounding or low distance between FEE and CCD are design drivers. Additionally the selection of qualified EEE parts, the highly accurate temperature stabilization and a low ADC clock jitter are important aspects for designing a reliable low noise FEE.

4.4.7.3 SEM electrical design

The SEM contains the SCU and the PCU.

The SCU electronics are designed in standard manner and stored within a box on a PCB with one ACTEL FPGA including a controller/processor functionality on it. The SCU interfaces with both the FEE via digital interfaces controlling/reading-out the CCD and the DPU via SpaceWire. One connector is available as technological interface for development and debugging purposes.

A slow 26-bit ADC with differential input converts analogue housekeeping (temperatures, voltages) from the FPA, FEE, and SCU itself with high precision. Some control lines are provided by the FPGA for PWM switching and filtering of heater supply for thermal control of FEE and CCD on the PCU.

There is a SDRAM (128 Mbyte) available for intermediate storage of CCD image data and as program code/data memory for software execution. SDRAM access is protected by an EDAC to correct SEUs in memory online and to detect double failure.

The FPGA and the LEON-FT core runs at 21 MHz. The implemented SpaceWire core supports 10,5 MHz (or optional 21 MHz) SpaceWire interface signal clock rates.

There are two software modules on the SCU, a Primary Boot Software (PBS) stored in a PROM (32 kbyte) which runs at power-on to boot a second or Application Software (APS) from, and stored and unloadable in EEPROM (2 Mbyte). This allows any flexibility for sensor and thermal control as an intelligent but small sensor front end with a SpaceWire interface only to the DPU. The software or command/data protocol should be CCSDS compatible equal to the DPU to platform protocol.

The power Conditioning Unit (PCU) contains some auxiliary electronics, e.g. filters, LDOs (TBD), and power switches for heater control. It interfaces the BEE/PSU for input voltages and provides voltages to all SEM and FEE electronics as well as for the CCD.

4.4.7.4 Data transfer to DPU

The SCU delivers the following data to the DPU via SpaceWire:

- CCD data as 200×200 window packet
- CCD data as 1024×1024 full window packet
- Housekeeping: temperature of CCD, FEE, SCU and PCU
- Housekeeping: voltages to supply CCD, FEE, SCU
- Housekeeping: status information as e.g. mode, CCD image/window counter, etc.
- Timestamp of CCD data and housekeeping at the time when they are acquired from the interface - Events: error, warnings

Different modes have been identified to define the SEM output data rate via SpaceWire applicable for the DPU as maximum and minimum input data rate:

- Mode SCIENCE (nominal fast: bright star): ~640 kbps i.e. 200-kHz CCD read-out rate, (200×200 pixels×16bit) every > 1s + auxiliary data (excluding averaging by SCU)
- Mode SCIENCE (nominal slow: faint star): ~11 kbps i.e. 200-kHz CCD read-out rate, (200×200 pixels×16 bit) every ≥ 60 s + auxiliary data (excluding averaging by SCU)
- Mode FULL_CCD (test/calibration nominal: full image): ~3200 kbps i.e. 200-kHz read-out rate, (1024×1024 pixels×16 bit) / 5.3 s + auxiliary data

It is assumed to have a 16-bit ADC sending 16 bit/pixel as signed data to the DPU. 10.5 Mbit/s is sufficient to cover all operation modes including fast test modes with a net data rate of 3.2 Mbit/s.

4.4.8 CIS Computer (DPU) and Power distribution (DCDC)

The instrument computer (DPU) is housed in the BEE along with the instrument power conditioning unit (DCDC). The BEE housing is attached as one of the four CIS units to the spacecraft bus and conductively cooled. The CHEOPS DPU, actually two DPUs, are integrated in a common box together with the power supply. The individual frames for DPU and power supply shall be stacked onto each other. Figure 39 below indicates a schematic for the DPU baseline. Both SpaceWire and MIL 1553 I/F to the S/C can be implemented depending on the final S/C selection.

The DPU carries 4 Gbit of usable memory as FLASH that allows for 3 day operation without ground contact. In hardware, 16 Gbit of FLASH will be protected by EDAC. To increase the reliability, in particular for the back-up of the application software, it is recommended to keep more than one copies, located at different pages. The flash device is 3D-Plus component. Eight standard chips are combined to a stack, packed into a ceramic package. The total height of the stack is approximately 12 mm. Due to this configuration it is unlikely that one high energetic particle would hit a similar address range on all pages at the same time.

The DC-DC converter will have dedicated DC-DC converters for the DPU and the SEM. In addition, switches are provided to control up to four external heaters used to stabilize the telescope. The S/C interface includes an EMC filter, solid state switches for ON/OFF control, and the status monitoring.

The baseline is currently a double string cold redundant DPU as well as power supply (DCDC) as illustrated in Figure 40.

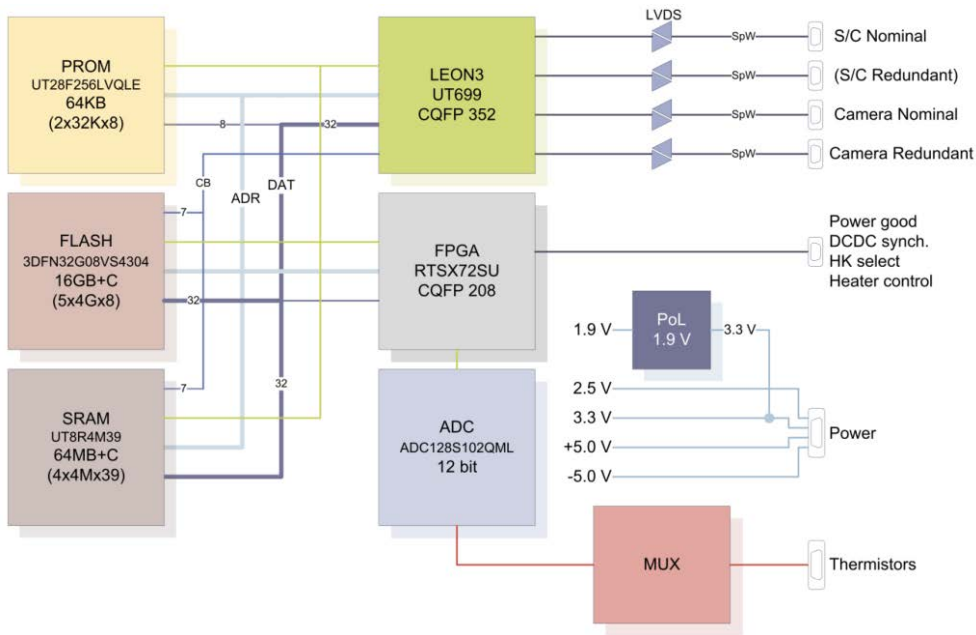


Figure 39 | DPU schematic for LEON 3 core.

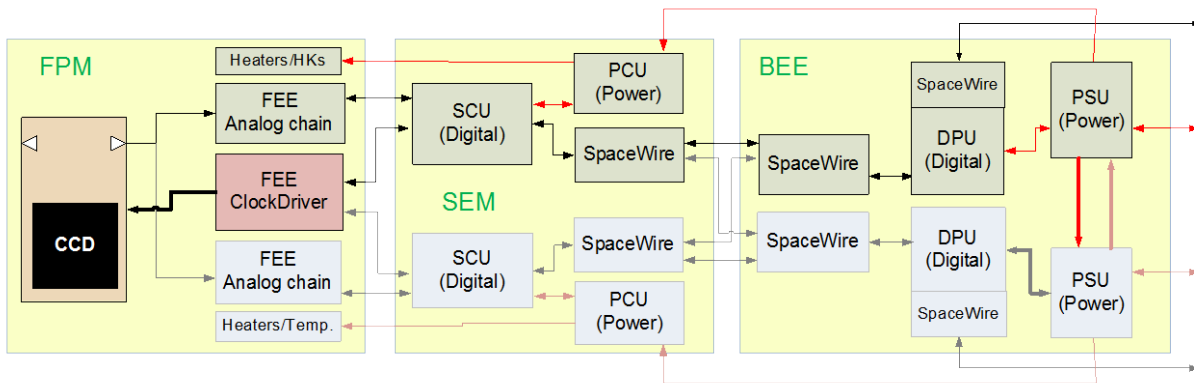


Figure 40 | Fault tolerance architecture. Note that cross strapping at the SpaceWire I/F SEM-BEE is currently TBD.

4.5 Interfaces and resource requirements

4.5.1 Mass

Table 7 lists the current mass of the instrument and its subsystems. The OTA mass is without star trackers. All unit and system margins are at 20% level for I-SRR, only the OTA unit margin is slightly smaller due to the smaller margins of the basic components (e.g. screws).

4.5.2 Power Budget

Table 8 summarises the average primary power consumption of CIS and its breakdown per unit for nominal operating mode. Note that the contingency factors are weighted average numbers based on sub-unit level input. The average and peak power requirement for CIS are 60 W and is <70 W, respectively.

Table 7 | CIS mass budget.

Instrument / Unit	Basic Mass [kg]	Unit/System Margin [%]	Nominal Mass [kg]
UNIT Level			
OTA	24.8	20	29.6
BCA	10.3	20	12.4
SEM	1.4	20	1.6
SEM-FPA harness	0.8	20	1.0
BEE	3.0	20	3.6
Harness & shielding	0.6	20	0.7
Sum			48.9
System Level			
CIS	48.9	20	58.7

Table 8 | CIS power budget.

Instrument / Unit	Basic Power [W]	Unit/System Margin [%]	Nominal Power [W]
UNIT Level			
OTA	0		0
BCA	0		0
FPM	2.5	20	3.0
SEM	3.5	20	4.2
DPU	3.8	20	4.6
DCDC (conversion loss)	0.6	20	0.7
Sum Unit	10.4		12.5
UNIT thermal control			
FPA TC	3.3	20	3.9
OTA TC	24.0	20	28.8
FEE TC	3.5	20	4.2
Sum	30.8		36.9
System Level			
Units	12.5		
Thermal heater	36.9		
Total Power	49.4	20	59.3

4.6 Instrument Performance and Noise Budget

4.6.1 Noise Model

A detailed noise budget has been computed for the instrument. To do so, the noise sources have been classified in the following categories:

1. Random noises: These noises are assumed to reduce with time averaging and/or repeated sampling. These errors can be combined quadratically and reduced by acquiring multiple images.
2. Systematic noises: These noises are likely non-random, and predominantly periodic, possibly synchronised with the period of the chosen orbit. These errors might not be reduced by time averaging and/or increasing the number of samples. The sources of these noises is in the system, therefore pre-flight instrument characterisation is likely to enable some degree of correction.
3. Environmental noises: These noises are likely non-random, and might not be reduced by increasing the number of samples. These noise sources are again likely periodic, synchronised with the chosen orbit. As they are related to the spacecraft environment, characterisation pre-flight will not be possible, and characterisation in flight will be required. These errors cannot be reduced by summation although we assume that the errors are independent so that they can be added in quadrature. It is also probable that noise from some of these sources will have a periodic component with a period close to that of the effects we are seeking to study, in particular Earth stray light contributions.

The total error budget is the combination of all the photometric errors, namely:

- shot noise;
- zodiacal light (sky background);
- read-out noise;
- quantisation noise;
- jitter combined with flat-field errors (jitter+FF);
- temperature induced variability of the dark current;
- quantum efficiency (QE) variation of the detector with temperature;
- gain variation of the proximity electronics;
- stray light contributions (stellar and Earth);
- bad pixels;
- cosmic ray hits.

In addition to the aforementioned noise categories, we differentiate two different noise estimation techniques:

1. Noises that can be assessed using an analytical noise model (e.g., shot noise, readout noise).
2. Noises that have to be estimated by doing complex computer simulations (e.g., stray light and jitter+FF noise).

For the first kind we compute the noises in a spread sheet. For the second kind, detailed simulations are performed and a certain value is allocated to this noise. For instance, jitter+FF noise is allocated 10 ppm in the noise budget. Allocated noises are:

- gain variability: 5 ppm;
- quantum efficiency variation: 0.1/112 per K;
- stray light for bright stars: 10 ppm;
- stray light for faint stars: 70 ppm;
- jitter+FF noise: 10 ppm.

The noise values chosen for the stray light are compliant with the observable sky requirements and the current baffle performance.

Table 9 lists the parameters for the noise budget baseline.

Table 9: Adopted values for the calculation of the noise budget

PSF	1257 px
Implied Radius of the PSF	20 px
Read Noise	6 e-/px
Jitter	8 arcsec rms
Quantisation	14 bits
Pixel Size	13 μm
Angular scale	1 arcsec/px
Pixel Full Well Cap.	60 000 e-
Image Size	200 \times 200 px
Operating Temperature	233 K
Temp Stability	0.01 K
Dark Current	0.08 e-/px/s
Flat Field Knowledge	0.1%
Zodiacal Light	4.8 e-/px/s
Gain Variability	5 ppm
QE variation per K	0.1/112
Residual electronics	5 e-/readout
Timing error	2 ppm/sec

4.6.2 Noise Budget

The mission has different requirements for bright stars (mag 6 to 9 in the V band) and faint stars (up to mag 12 in the V band). For bright stars, the requirement is to obtain 20 ppm precision over 6 hours; for faint stars the requirement is to reach 85 ppm over 3 hours. The final noise budget for stars of magnitude 6, 9, and 12 is shown in Table 10.

The current noise budget is compliant with the science requirements (cf. §3).

Table 10: Noise Budget. Dominant noise terms are highlighted in boldface.

Case Number	A	B	C
V-band magnitude (+spectral type)	6 (G)	9 (G)	12 (K)
Exposure time [s]	1	10	60
Integration time [h]	6	6	3
Read out noise [ppm]	0.1 [6.9]	0.6 [26.8]	4.3 [57.3]
Shot noise [ppm]	1.9 [282]	7.6 [355]	38.7 [519]
Quantization noise [ppm]	0 [3]	0.1 [4.7]	0.8 [10.1]
Background (inc. dark) noise [ppm]	0 [3.2]	0.2 [7.4]	2.3 [31]
Jitter + Flat Field noise [ppm]	10	10	10
Dark current variation noise [ppm]	0	0	0.1
Gain variability noise [ppm]	5	5	5
Stray light (Earth) noise [ppm]	10	10	70
QE change [ppm]	8.9	8.9	8.9
Residual Electronics [ppm]	0.4	0.6	1.3
Timing error [ppm]	2	0.2	0
Error time average [ppm]	17.7	19	81.4

5 Mission design

5.1 Operational orbit and mission profile

The nominal CHEOPS operational orbit is a circular Sun-synchronous orbit (SSO) with an altitude of 800 km and a local time of the ascending node (LTAN) of 6 am; the orbit inclination is about 98° , the orbital period is ~ 100 min, while the maximum allowed variation of LTAN is ± 20 min. A LTAN of 6 pm (as opposed to the nominal 6 am) would also be acceptable, although less favourable from a science point of view, due to the need to ensure a better coverage of the southern hemisphere to take full advantage of ground-based observations.

This nominal orbit has been preferred to alternative scenarios (e.g., higher altitude SSO, GTO with increased perigee altitude) as it provides a more stable thermal environment, good visibility from the baseline ground station as well as a good instantaneous sky visibility at a manageable delta-V cost. Moreover it also favourable in view of identifying a shared launch opportunity for CHEOPS, as Sun synchronous orbits with this altitude range and LTAN are typically used by Earth observation missions.

Given the boundary conditions applicable to Small missions, CHEOPS needs to make use of a shared launch opportunity to reach the operational orbit. In order to maximise compatibility with the largest possible number of launch opportunities, the S/C is designed to be compatible with an altitude range of 650 to 800 km.

The total launch mass of about 250 kg is fully compatible with a shared launch scenario with typical small or medium-size launch vehicles, such as VEGA, Soyuz, but also PSLV or Rockot. The S/C is designed to maintain compatibility with a variety of launchers, both in terms of launch environment as well the fairing envelope.

Depending on the selected launcher and on the requirements of the main flight passengers, the operational orbit will be reached either with a direct injection to the nominal altitude and LTAN, or following dedicated orbit adjustment manoeuvres performed by the last stage of the launcher. As an alternative, and depending on the specific shared launch scenario and launcher performance, CHEOPS could increase its orbit altitude by own propulsion means. No orbit maintenance maneuvers are planned in addition to the correction for the launcher dispersion, since, by optimising the initial parameters, the spacecraft orbit remains compatible with the nominal LTAN for the complete mission lifetime within the specified ± 20 min. Orbital altitude losses from 800 km are low (typically less than 5 km over the nominal 3.5 yr lifetime) given the low area-to-mass ratio of the spacecraft and the low solar activity expected between 2018 and 2021.

The total delta-V demand is driven by the orbit altitude and the need to comply with the orbit debris mitigation measures applicable to CHEOPS. The total delta-V budget for the nominal altitude of 800 km is about 110 m/s, including launcher dispersion correction, collision avoidance manoeuvres and de-orbiting at the end of the nominal mission lifetime in view of re-entry within 25 years. Dedicated analysis demonstrated that CHEOPS, in view of the small size and low mass, meets the space debris mitigation regulations without requiring controlled re-entry.

The nominal mission lifetime is 3.5 years, with a possible extension to a total of 5 years enabled by appropriate sizing of the consumables budget.

The maximum expected eclipse duration is less than 20 min, occurring in winter time for LTAN = 6 am.

The design of the spacecraft, thanks to a dedicated Sun-shield, is compatible with large pointing excursions around the average anti-Sun direction (X axis, yaw, $\pm 180^\circ$) and considerable rotations in pitch (around the transversal Y axis, $\pm 60^\circ$) and roll (around the longitudinal Z axis, $\pm 60^\circ$). Such pointing excursion capability allows us to guarantee the required sky visibility throughout the mission lifetime, in line with the science requirements and in particular the capability to cover 50% of the sky with a minimum cumulative duration of 50 days per year, and a maximum cumulative interruption of 50 min/orbit (goal 20 min/orbit). Compliance with such requirements has been validated via a dedicated analysis, taking into account all instrument operational and pointing constraints (see Figure 41). The results of the analysis are summarised in Figure 42.

Table 11 | Characteristics of 650 km and 800 km Sun-synchronous orbits

Orbit altitude	650 km	800 km
Orbital period (min)	97.73	100.87
Inclination (°)	97.99	98.60
Maximum eclipse duration (min)	20	17.5

Table 12 | CHEOPS ΔV budget as function of initial altitude for a spacecraft with an area-to-mass ratio of 0.01 m²/kg being in orbit from 1/1/2018 to 30/6/2021 (3.5 years). No margins.

Altitude	600	620	650	700	800
Launcher correction	19	19	19	19	19
Orbit maintenance	11	0	0	0	0
Collision avoidance	3.5	3.5	3.5	5	7
Reorbit	0	0	16	36	76
Total	33.5	22.5	38.5	60	102

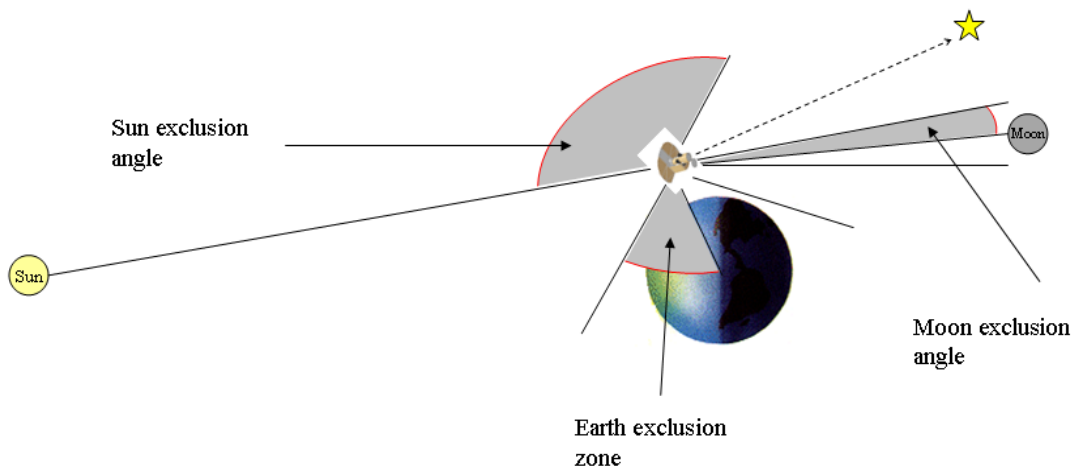


Figure 41 | CHEOPS sky visibility constraints

5.2 Environment

The energetic particle environment relevant to CHEOPS consists of geo-magnetically trapped charged particles, solar protons and galactic cosmic rays. The main components of the radiation environment are listed below.

Radiation Belts

The radiation belts encircle the Earth and contain electrons (e⁻) and protons (p⁺) that are trapped in the geo-magnetic field. An inner relatively stable belt contains mostly protons with energies up to several hundred MeVs that varies with the solar cycle, with higher levels encountered during solar minimum. An outer, highly dynamic, belt consists primarily of energetic electrons with energies up to a few MeVs.

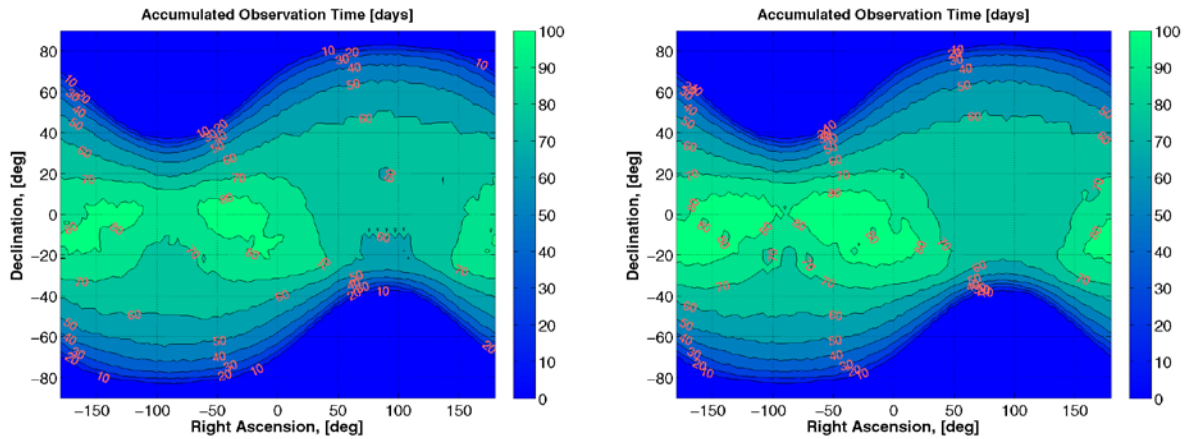


Figure 42 | Accumulated sky coverage over one year for SSO650 (left) and SSO800 (right). All pointing constraints have been taken into account in the analysis (see Figure 41).

Solar Particle Events

Events of strongly enhanced fluxes of primarily protons originate from the Sun, usually with a duration of the order of a couple of days. These events occur randomly and mainly during periods of solar maximum (~7 years of the 11-year solar cycle).

Galactic Cosmic Rays

A continuous flux of very high-energy particle radiation is received from outside the heliosphere. Although their contribution to the total dose is insignificant, they are important when analysing single event effects.

A dedicated CHEOPS environmental analysis has been performed for the nominal operational orbits, included in the range of considered orbit altitudes (650–800 km). The analysis showed that under standard equipment shielding assumptions, no concerns exist for both instrument and platform equipment. The total expected ionising dose under 5 mm Al shielding is of order 3.5 krad. At the detector location the actual focal plane design offers further shielding, leading to a total dose below 2 krad over the mission lifetime.

In correspondence to the South Atlantic Anomaly passes, instrument operations will continue, but science data will be discarded as soon as the flux of protons with energy > 50 MeV will exceed 2 p⁺/cm²/s. The corresponding impact on sky visibility has been taken into account. The geographic region corresponding to such a p⁺ flux is reported in Figure 43.

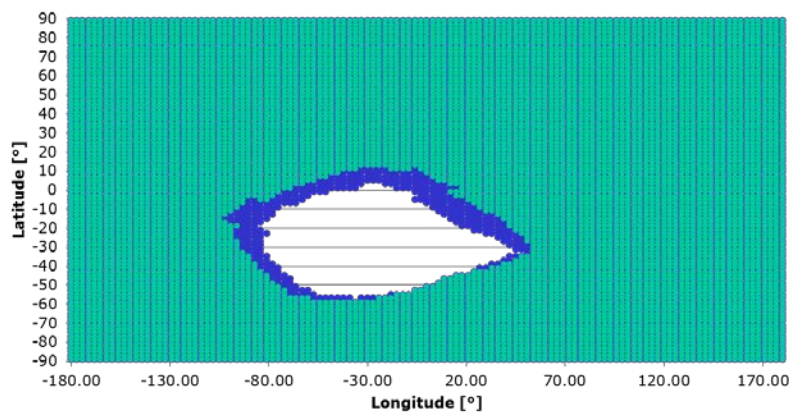


Figure 43 | Geographic region where the flux of > 50 MeV protons is less than 2 /cm² s⁻¹ at altitudes of 650 km (blue) and 800 km (green).

5.3 Spacecraft design

The design of the CHEOPS spacecraft is driven by the need to use existing small platforms based on a flight qualified design, with minimum mission specific changes. This is a key and binding requisite in order to be able to remain compatible with the mission programmatic constraints (ESA cost at completion < 50 M€ at 2012 economic conditions and launch by 2017). As mentioned before, another key requisite is compatibility with shared launch configurations inside the launcher fairing.

Typical small standard platforms offer a “payload deck” or interface plate on which the telescope can be mounted. The CHEOPS telescope is horizontally mounted on this plate also in view to meet the launcher volume constraints. The main instrument units (Baffle Cover Assembly and Optical Telescope Assembly) are mechanically fixed to the “payload deck” via iso-static mountings, while ensuring thermal isolation. The instrument electronic units are accommodated in the platform and thermally coupled to it.

In addition to existing design heritage and horizontal accommodation of the telescope, the spacecraft configuration is driven by the need to protect the instrument radiators from direct Sun illumination over a large pointing range by means of a fixed Sun-shield. The Sun-exposed surface of the shield is used as support to the solar cell arrays, in a body mounted configuration. This overall configuration offers simple and clean interfaces between the platform and the instrument, thus favouring a fully decoupled development as well as simplified integration and testing.

Figure 44 shows the CHEOPS instrument accommodation and spacecraft configuration as resulting from the phase 0/A study conducted after the proposal selection in November 2012. Figure 45 shows the CHEOPS spacecraft inside the VESPA adapter of VEGA, again as from the initial ESA study. Very similar S/C configurations have been finalised by the competing contractors during the course of the phase 1 activities.

The basic characteristics of the mission are summarised in Table 13 below. The main sub-systems are described in Table 14. It should be noted that during the competitive definition phase, the platform designs of each contractor differ on a number of specific issues.

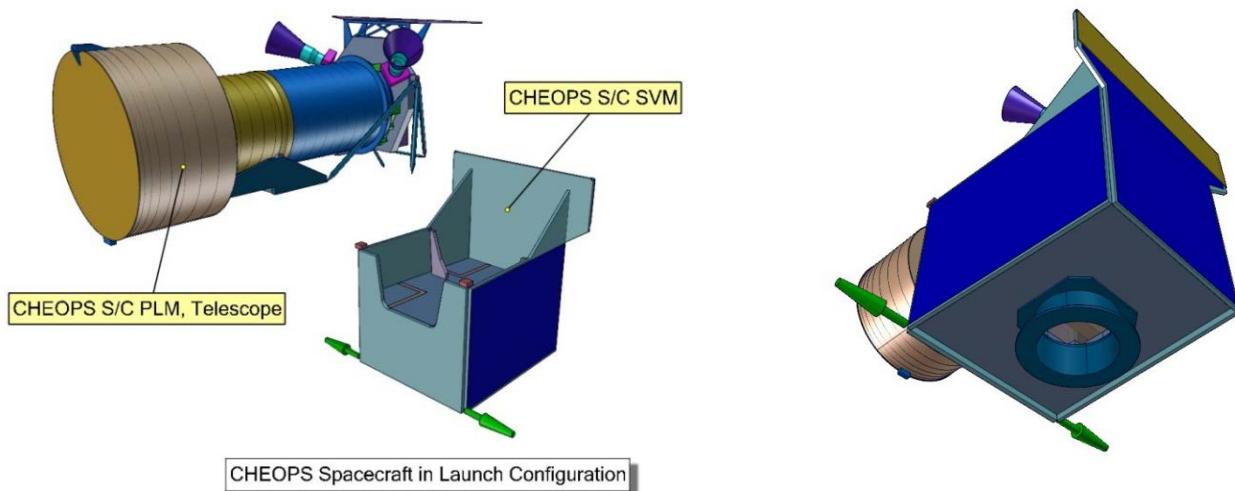


Figure 44 | CHEOPS spacecraft and instrument accommodation (ESA study).

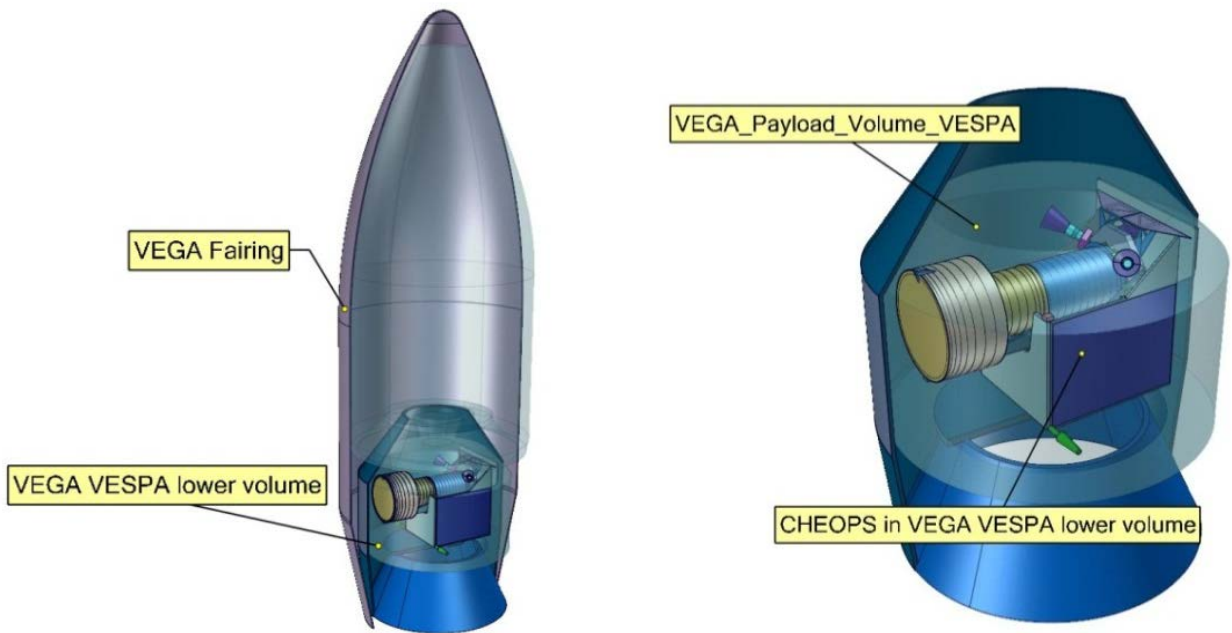


Figure 45 | CHEOPS inside VEGA VESPA launcher volume (ESA study).

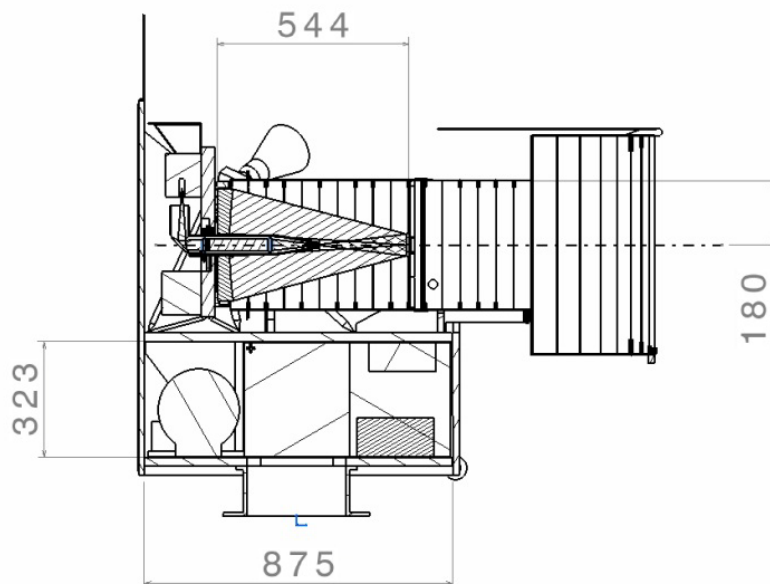


Figure 46 | CHEOPS cross-section view (ESA study).

Table 13 | CHEOPS mission summary.

Mission description		
Launch	Launcher	Vega (shared launch, under VESPA adapter) Shared launch, under ASAP-S Compatible with other LV's (e.g. PSLV).
	Launch date	End of 2017
Orbit	Orbit type	Circular Sun - synchronous
	Altitude range	650 – 800 km
	LTAN	6 am (nominal option, with 6 pm as back-up depending on launch opportunities) ±20 min deviation in LTAN acceptable
Lifetime	Nominal 3.5 years in the operational orbit	
Overall system characteristics		
Mass	Wet mass	~ 250 kg (excluding LV adapter)
Delta-V	Depends on orbit altitude: 35 m/s for 650 km, 110 m/s for 800 km	
Dimensions	~ 1.5 m × 1.4 m × 1.5 m	

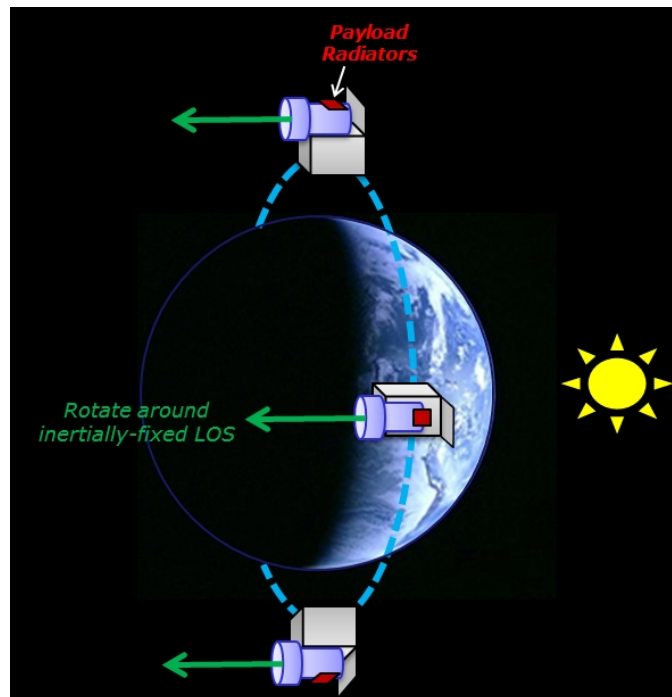


Figure 47 | CHEOPS attitude: roll around inertially fixed LOS direction, required to ensure constant pointing to cold space of the instrument radiator.

Table 14 | CHEOPS payload and subsystems summary.

Payload and subsystems	
Payload	<p>Single instrument – high precision photometer operating in the visible range.</p> <p>Telescope: single aperture (dia 33 cm), Ritchey – Chrétien</p> <p>FOV: ~ 19' × 19' (need to acquire target + background sampling)</p> <p>CCD detector (e2V CCD 47-20) in the Focal Plane Assembly (FPA)</p> <p>60 kg, 60 W (including margins)</p>
AOCS	<p>Instrument measurements in the attitude control loop to ensure 8 arcsec APE (rms) during observations. Attitude: roll around inertially fixed LOS direction</p> <p><u>Baseline sensors:</u></p> <p>2 × 3 – axis Magnetometers</p> <p>6× miniaturised analogue Sun Sensors</p> <p>2× Autonomous Star Trackers</p> <p><u>Baseline actuators:</u></p> <p>3× Magnetorquers</p> <p>4× Reaction Wheels</p>
Communications	<p>2 S-Band receivers in hot redundancy</p> <p>2 S-Band transmitters in cold redundancy</p> <p>2 S-Band LGA</p>
Data Handling	<p>Data Handling Dual – redundant DHS bus and S/C DPU</p> <p>Alternative bus protocols (CAN, MIL-1553, SpW)</p>
Power	<p>3 body mounted solar panels, total area ~ 1.85 m²</p> <p>Average power: 138 W</p> <p>Unregulated bus, MPPT.</p>
Propulsion	<p>Dual branch hydrazine propulsion system: 2 1N thrusters, 1 PEPT – 260 mm diameter tank, 6.83 kg hydrazine</p>
Programmatic aspects	<p>Design based on existing, flight qualified small platforms.</p> <p>Easy and quick P/L to platform integration and P/L calibration and verification.</p>

5.3.1 Spacecraft resource budgets

The mass and power spacecraft resource budgets are reported in the tables below (based on the results of the ESA internal study).

Table 15 | CHEOPS Mass Budget (ESA study)

CHEOPS - Spacecraft						
Dry mass contributions	Without Margin		Margin		Total kg	% of Total
	kg	%	kg	%		
Structure	38.44 kg	20.00	7.69		46.13	26.70
Thermal Control	2.60 kg	20.00	0.52		3.12	1.81
Mechanisms	1.90 kg	10.00	0.19		2.09	1.21
Communications	4.30 kg	5.00	0.22		4.52	2.61
Data Handling	5.00 kg	10.00	0.50		5.50	3.18
AOCS	12.65 kg	5.00	0.63		13.28	7.69
Propulsion	5.75 kg	9.17	0.53		6.28	3.63
Power	13.43 kg	8.10	1.09		14.51	8.40
Harness	10.00 kg	20.00	2.00		12.00	6.95
Instruments	54.27 kg	20.37	11.05		65.33	37.81
Total Dry(excl.adapter)	148.34				172.75	kg
System margin (excl.adapter)		15.00 %			25.91	kg
Total Dry with margin (excl.adapter)					198.67	kg
Other contributions						
Wet mass contributions						
Propellant	6.83 kg	N.A.	N.A.		6.83	3.32
Adapter mass (including sep. mech.), kg	14.20 kg	0.00	0.00		14.20	0.06
Total wet mass (excl.adapter)					205.50	kg
Launch mass (including adapter)					219.70	kg

Table 16 | CHEOPS Power Budget (ESA study).

		POWER	THERMAL	DHS	AOCS	COMMS	PROP	MEC	INS - Structure	INS - Mech	INS - Thermal	INS - DHS	Sub Total	Margin	Harness	Distrib	Total
Launch Mode	1													20%	2%	1%	
40 min	Pon (W)	9 W	0 W	22 W	22 W	2 W	0 W	0 W	0 W	0 W	38 W	0 W	93 W	19 W	2 W	1 W	115 W
	Pstby (W)	0 W	0 W	22 W	0 W	2 W	0 W	0 W	0 W	0 W	0 W	0 W	24 W	5 W	1 W	0 W	29 W
	D.C. (%)	100%	0%	0%	100%	0%	0%	0%	0%	0%	50%	0%	73%				73%
	Pavg (W)	9 W	0 W	22 W	22 W	2 W	0 W	0 W	0 W	0 W	19 W	0 W	74 W	15 W	2 W	1 W	91 W
Energy (Wh)	6 Wh	0 Wh	15 Wh	15 Wh	1 Wh	0 Wh	0 Wh	0 Wh	0 Wh	13 Wh	0 Wh	49 Wh	10 Wh	1 Wh	1 Wh	61 Wh	
Initialization & Rate Red	2																
94 min	Pon (W)	9 W	0 W	22 W	22 W	8 W	0 W	0 W	0 W	0 W	38 W	0 W	99 W	20 W	2 W	1 W	122 W
	Pstby (W)	0 W	0 W	22 W	0 W	2 W	0 W	0 W	0 W	0 W	0 W	0 W	24 W	5 W	1 W	0 W	29 W
	D.C. (%)	100%	0%	0%	100%	2%	0%	0%	0%	0%	50%	0%	67%				67%
	Pavg (W)	9 W	0 W	22 W	22 W	2 W	0 W	0 W	0 W	0 W	19 W	0 W	74 W	15 W	2 W	1 W	92 W
Energy (Wh)	14 Wh	0 Wh	34 Wh	35 Wh	3 Wh	0 Wh	0 Wh	0 Wh	0 Wh	30 Wh	0 Wh	116 Wh	23 Wh	3 Wh	1 Wh	143 Wh	
Safe Mode	3																
60 min	Pon (W)	9 W	0 W	22 W	22 W	40 W	0 W	0 W	0 W	0 W	38 W	0 W	131 W	26 W	3 W	2 W	162 W
	Pstby (W)	0 W	0 W	22 W	0 W	2 W	0 W	0 W	0 W	0 W	0 W	0 W	24 W	5 W	1 W	0 W	29 W
	D.C. (%)	100%	0%	0%	100%	2%	0%	0%	0%	0%	50%	0%	48%				48%
	Pavg (W)	9 W	0 W	22 W	22 W	2 W	0 W	0 W	0 W	0 W	19 W	0 W	75 W	15 W	2 W	1 W	92 W
Energy (Wh)	9 Wh	0 Wh	22 Wh	22 Wh	2 Wh	0 Wh	0 Wh	0 Wh	0 Wh	19 Wh	0 Wh	75 Wh	15 Wh	2 Wh	1 Wh	92 Wh	
Operations Mode	4																
20 min	Pon (W)	9 W	0 W	22 W	22 W	8 W	0 W	0 W	0 W	0 W	38 W	13 W	112 W	22 W	3 W	1 W	138 W
	Pstby (W)	0 W	0 W	22 W	0 W	2 W	0 W	0 W	0 W	0 W	0 W	0 W	24 W	5 W	1 W	0 W	29 W
	D.C. (%)	100%	0%	0%	100%	2%	0%	0%	0%	0%	50%	100%	72%				72%
	Pavg (W)	9 W	0 W	22 W	22 W	2 W	0 W	0 W	0 W	0 W	19 W	13 W	87 W	17 W	2 W	1 W	108 W
Energy (Wh)	3 Wh	0 Wh	7 Wh	7 Wh	1 Wh	0 Wh	0 Wh	0 Wh	0 Wh	6 Wh	4 Wh	29 Wh	6 Wh	1 Wh	0 Wh	36 Wh	

5.3.2 Modifications to Standard Platforms

Although the re-use of existing platform designs is necessary, a small number of modifications are required to enable their use on CHEOPS. The key changes are summarised in this section:

- The accommodation of the payload has to be individually assessed for each platform, and may require some structural/thermal modification, in particular in relation with the location of the CoG.
- Adaptations to the AOCS software are required to enable “instrument in-the-loop” operations.
- Higher quality Star Trackers are required in order to fulfil the pointing stability requirements.

- A propulsion system able to provide the required ΔV is needed. This may imply to upgrade the existing propulsion system (e.g. use of a larger tank) or to implement a new one (e.g. replacement of hot Xenon resisto-jet by hydrazine).
- A sunshield is required.
- The power generation capability of the existing solar array configuration needs to be verified against the CHEOPS needs.
- Due to the fact that the orientation of the spacecraft is not nadir locked, the location of the antennas on-board (S-band, GPS) may have to be modified.

The results of the definition phase studies have confirmed that these changes are well in line with the capabilities of the existing platform designs and compatible with the relevant programmatic constraints of a small class mission, namely reduced budget and high level of technology readiness, including full qualification status.

5.4 Definition phase activities

Following the ESA study completed at the end of 2012, the Invitation To Tender (ITT) for the industrial activities on the CHEOPS spacecraft was issued at the end of March 2013. The ITT covers two distinct phases, namely a competitive definition study (phase 1) and the actual mission implementation (phase 2). The start of phase 2 is subordinated to mission adoption by SPC.

In June 2013 ECE-CASA (ES) and SSTL (UK) have been selected as spacecraft contractors for the competitive definition phase (A/B1). The work started at the beginning of July 2013, leading to the mission-level Preliminary Requirements Review in December 2013 and to the System Requirements Review in March 2014. The selection of the S/C prime in charge of phase 2 is expected by April 2014.

The main characteristics of the ESA ITT are: a) the full responsibility of the contractor for the integration of the instrument and platform, with the delivery of a fully qualified satellite; b) the delivery of a ‘turn-key’ spacecraft including the corresponding Mission Control System to the benefit of the MOC; c) the selection of space qualified platform design solutions with a large flight heritage; d) the integration in the implementation phase of the AIT services procured via the CHEOPS Mission Consortium.

5.4.1 Industrial studies

The S/C solutions offered by ECE-CASA and SSTL are based on existing platform designs with a large flight heritage, respectively the AS-250 platform developed by Astrium and the SSTL-150 platform developed by Surrey Small Satellite Limited. In both cases, the overall design is largely similar to that anticipated during the ESA study, with a compact S/C body, fixed Sun-shield, fixed solar panels and an AOCS design including “instrument-in-the-loop” performance. Compatibility under the VESPA (VEGA) and ASAP-S (Soyuz) adapters is explicitly requested and ensured by design. Following a dedicated trade-off analysis, the optical heads of the star-trackers have been installed on the Optical Telescope Assembly of the instrument, so as to minimise misalignment effects induced by thermo-elastic distortion.

During the study specific emphasis has been applied to the early consolidation of all the interfaces between instrument and platform. Such a consolidation was required in order to progress quickly with the finalisation of the platform design, and in order to decouple and de-risk the development and design efforts of industry and instrument team. Both contractors have achieved such early interfaces definition by performing a number of thermal, electrical and mechanical analysis. The analysis has been enabled by the provision of detailed Finite Element and Thermal Mathematical Models of the instrument to both contractors. Most significant aspects of such analysis effort are: a) the demonstration of compliance with the thermal control requirements of the instrument (with the CCD operating at -40°C with a stability better than 10 mK); b) demonstration of compliance with mechanical stiffness requirements (with the first instrument mode at a frequency above 90 Hz).

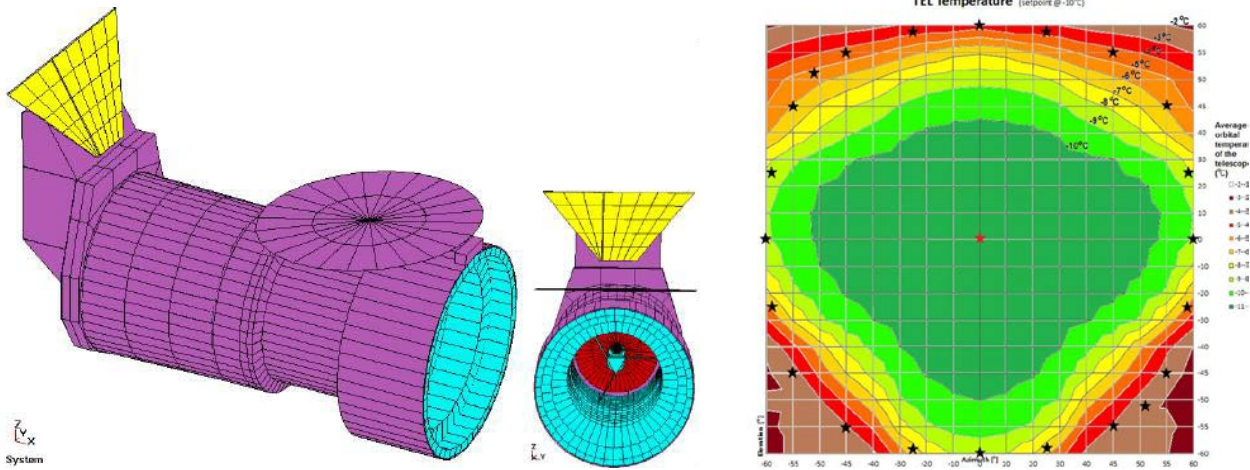


Figure 48 | Thermal model used to define the Instrument-to-P/F thermal interfaces.

Figure 49 below shows the spacecraft architecture as proposed by SSTL, while the corresponding ECE-CASA design is illustrated in Figure 50.

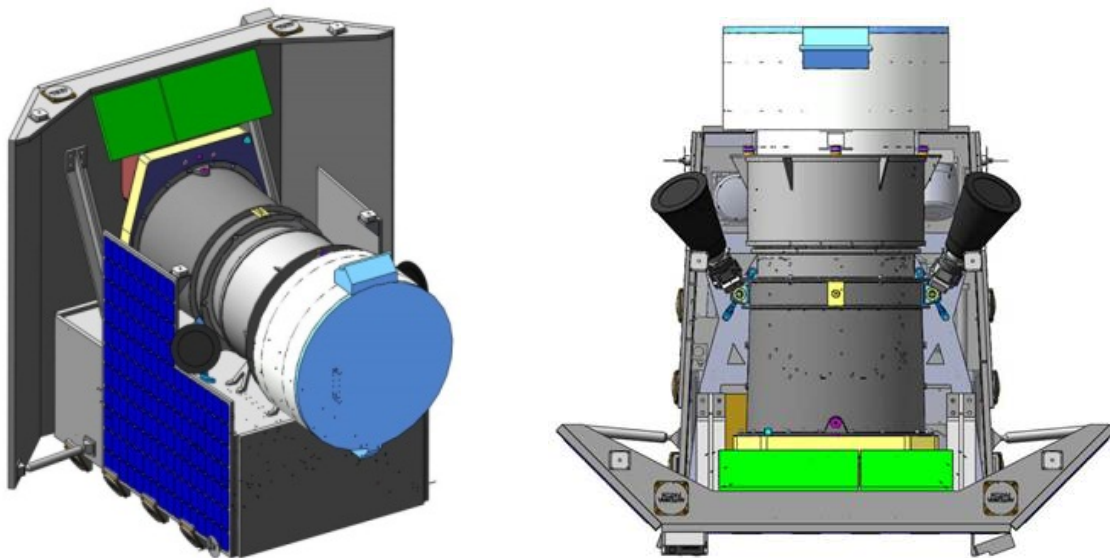


Figure 49 | CHEOPS spacecraft – SSTL design.

The SSTL design is characterised by an elongated cuboid platform and by the presence of two lateral solar panels; the total dry mass is approximately 235 kg (including margins). The total power budget is about 160 W (including margins). A large degree of flight heritage is ensured to CHEOPS by several missions which made use of the SSTL-150 platform. Such a heritage translates into flight proven solutions with a mature qualification status. In the case of the SSTL proposed design, the area mostly affected by CHEOPS specific changes is related to the demand of a total delta-V of about 110 m/s.

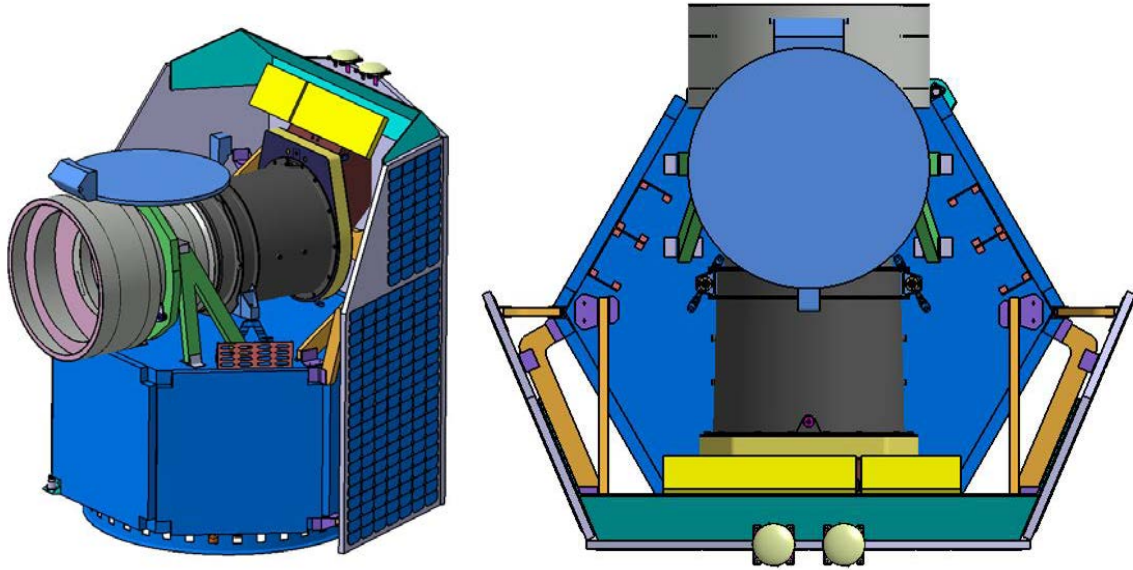


Figure 50 | CHEOPS spacecraft – CASA design.

The CASA design is characterised by an hexagonal shape platform, with lateral solar panels canted with respect to the S/C-Sun direction; the total dry mass is approximately 255 kg (including margins). The total power is about 210 W (including margins). A large degree of flight heritage is ensured to CHEOPS by several missions which made use of the AS-250 platform. In the case of the CASA proposed design, the area mostly affected by CHEOPS specific changes is related to an overall down-sizing of the structure previously used for AS-250 based missions (e.g. SEOSAT).

5.4.2 Compatibility with different launcher vehicles

The activities conducted during the definition phase have taken into account the need to remain compatible with a number of different small and medium-size launcher vehicles. Such a requirement is not unusual for small missions targeting a shared flight opportunity, which is typically secured only at a later stage in the overall development programme as requiring the identification of suitable co-passengers.

The compatibility with several LV is ensured by identifying a set of envelope requirements for the launch environment and for the volume available to the S/C inside the different fairings (see Figure 51 for this latter case).

Both contractors have been specifically requested to guarantee compatibility with a set of different launchers, including VEGA, Soyuz, PSLV, DNEPR, Rockot and Falcon and to date the approach followed was shown to be consistent with a launcher selection carried out before CDR.

5.5 Programmatic aspects

5.5.1 Contributions from consortium

The original CHEOPS proposal included a number of potential contributions to the spacecraft, namely : a) provision of a deployable Sun-shield; b) provision of high-accuracy star trackers; c) provision of AIT services (discussed in a separate section). Such potential contributions would be delivered through ESA as Customer Furnished Items to the S/C contractor, following their procurement by the CHEOPS Mission Consortium. The possibility of such provisions has been included in the ESA ITT for the S/C procurement as possible options, soliciting their consideration by the potential contractors.

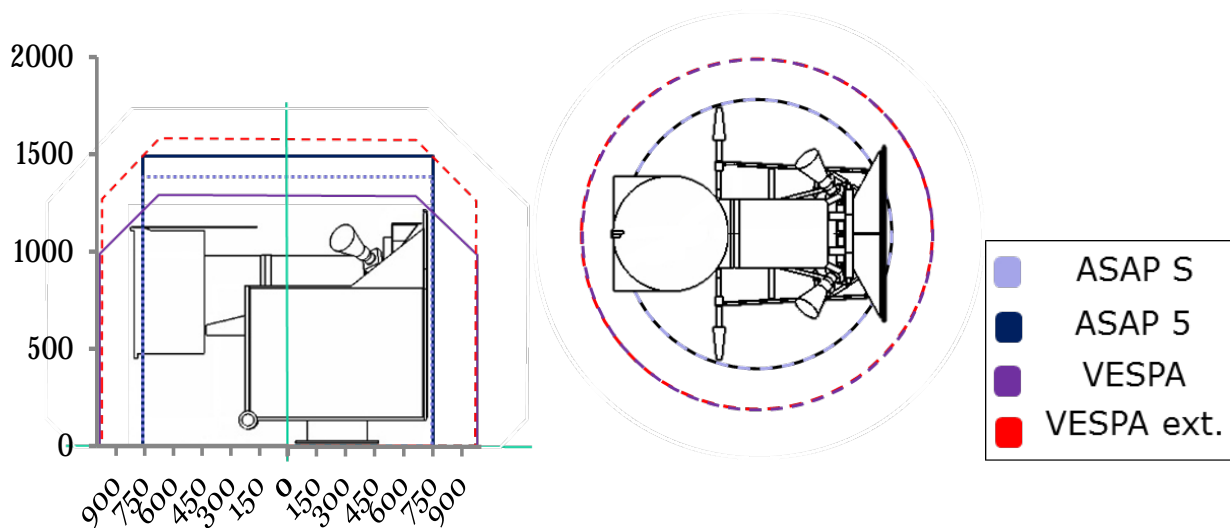


Figure 51 | Example of launcher volume envelopes accommodating CHEOPS (figure refers to the ESA design as explored during the phase 0/A study - dimensions in mm).

Following the evaluation of the responses to the ITT and dedicated technical analysis, it has been concluded that:

- A deployable Sun-shield is not required as the instrument radiators can be shielded by a fixed panel.
- The high accuracy star trackers offered by the selected contractors meet the mission requirements while having the advantage of fully defined interfaces.
- The AIT services can be integrated in the implementation activities, although the selected S/C contractor will maintain full responsibility for all AIV activities.

5.5.2 Provision of AIV services

The provision of AIT services from the company RUAG Space CH (RSSZ) is a national contribution to CHEOPS. In order to adequately define the interfaces between each potential S/C contractor and the AIT services provider, a number of meetings have taken place during the phase 1 activities, leading to the definition of a draft statement of work between RSSZ and each contractor candidate, to be applied during phase 2. The results of these discussions can be summarized as follows:

- The S/C contractor shall maintain complete responsibility and authority for all AIV activities and deliver a fully qualified satellite to ESA;
- A small number of RSSZ staff shall be co-located at the S/C contractor premises and become part of an integrated AIT team;
- Assembly & Integration activities shall take place at the S/C contractor premises;
- The mechanical vibration tests at satellite level (PFM) shall take place at RSSZ, including ancillary pre-test and post-test activities (e.g. abbreviated functional tests).

5.5.3 Interface to MOC

In order to simplify the interfaces between S/C and MOC, the ESA ITT has included the delivery by the S/C contractor of a complete and self-standing mission control system, to be installed at the MOC. Dedicated documentation has been produced to define the associated interfaces, including a Space-to-Ground Interface Control Document produced by the CHEOPS Mission Consortium, and specific Spacecraft-to-Ground Segment Interface Requirements Documents produced by the S/C contractor.

5.5.4 AIV approach and model philosophy

The CHEOPS schedule imposes the adoption of a streamlined model philosophy. In particular, the use of an “existing platform” with minor modifications, justifies a proto-flight approach, based on a Proto-Flight Model and on an Electrical Functional Model. The introduction of a Structural Model is also possible, depending on the S/C contractor design solutions, and on the level of changes with respect to the existing product line.

The instrument payload is a new development requiring a hybrid approach which includes STM, PFM and EFM. This approach implies that for structural parts and mechanisms an STM shall be manufactured and tested and for equipment and electronics EQMs shall be delivered.

In addition, at satellite level, an Electrical and Functional Model (EFM), representing platform and payload, is needed for functional development, software development, procedure validation, preparation of flight test programme, and closed loop tests.

Procurement of critical components (sensors, EEE, radiation hard and high reliability parts, and other long lead items) needs to start early and in sufficient quantities (i.e. including spare items) to alleviate the possibility that late deliveries jeopardise the schedule. Indeed in the case of the instrument some procurement actions have been already started, including the ESA procured CCD.

5.5.5 Project schedule and equipment qualification status

Given the tight CHEOPS development schedule, the extensive use of qualified equipment is a key requirement, in particular for the platform procurement (while the instrument follows a separate qualification path, being a newly designed item). In order to verify the actual qualification status of the platform equipment a three-step approach has been adopted:

- Definition of the qualification status has been requested in the bid produced in response to the ESA ITT for the S/C procurement.
- A more detailed qualification status review is part of the system level PRR activities on the basis of the designed proposed by the contractors at the end of phase 1.
- Formal Equipment Qualification Status Reviews will be held with the S/C contractor and with equipment suppliers in the early part of phase 2.

5.5.6 Approach to LV selection

A shared launch is a mandatory element of the CHEOPS mission to remain compatible with the existing programmatic boundaries. Such an approach forces to a later selection of the launch vehicle, given the need to identify suitable co-passengers and flight opportunities. The approach followed for the identification of a shared flight opportunity for CHEOPS is the following:

- in the initial study phases, compatibility with several launchers is ensured by design, imposing an envelope of launch environment requirements;
- a Request for Information concerning possible shared launch opportunities has been forwarded to several Launch Service Providers in April 2013, triggering a number of preliminary contacts and the potential inclusion of CHEOPS in corresponding launch manifests;
- a prioritised list of possible LV's is expected at the end of phase 1, taking into account the results of the study activities and the associated technical conclusions;
- additional contacts with the short-listed Launch Service Providers will continue after mission adoption in view of finalising the choice before the system level CDR, and possibly by the end of 2014.

5.5.7 Risk assessment summary

A summary of the CHEOPS technical risk assessment is presented below. The CHEOPS mission is considered successful if the customer, technical and programmatic objectives are met. The success criteria are collected in Table 17 below.

Identified risks that may jeopardise and/or compromise the CHEOPS mission are ranked in terms of likelihood of occurrence and severity of consequence. The scoring scheme for the CHEOPS study with respect to the severity of consequence on a scale of 1 to 5 is established in Table 18.

The results of the risk assessment are summarised in the two sections below, respectively on Payload related risks and Platform related risks. Only the higher severity risks are discussed.

Table 17 | CHEOPS mission success criteria.

Science	Search for exo-planetary transits by means of ultrahigh precision photometry on bright stars already known to host planets
Mission/ Technical	Use of existing spacecraft solutions Limited development Shared launch
Schedule	Launch in 2017 (S-Class ESA mission constraint)
Cost	ESA contribution below 50 M€(S-Class ESA mission constraint) on 150 M€total budget

Table 18 | Severity categorisation

Severity	Schedule	Science	Mission (ECSS-Q-ST-30 & 40)	Cost
Catastrophic 5	Launch opportunity lost	Failure leading to the impossibility of fulfilling the mission's scientific objectives	Safety: Loss of system, launcher or launch facilities. Loss of life, life-threatening or permanently disabling injury or occupational illness; severe detrimental environmental effects.	Cost increase result in project cancellation
Critical 4	Launch delayed (TBD) months	Failure results in a major reduction (70-90%) of mission's science return	Dependability: Loss of mission. Safety: Major damage to flight systems, major damage to ground facilities; major damage to public or private property; temporarily disabling but not life-threatening injury, or temporary occupational illness; major detrimental environmental effects.	Critical increase in estimated cost
Major 3	Launch delayed (TBD) months)	Failure results in an important reduction (30-70%) of the mission's science return	Dependability: Major degradation of the system. Safety: Minor injury, minor disability, minor occupational illness. Minor system or environmental damage.	Major increase in estimated cost
Significant 2	Launch delayed (TBD) months	Failure results in a substantial reduction	Dependability: Minor degradation of system (e.g., system is still able to control the consequences)	Significant increase in estimated cost

Severity	Schedule	Science	Mission (ECSS-Q-ST-30 & 40)	Cost
		(<30%) of the mission's Science return	Safety: Impact less than minor	
Minimum 1	No/ minimal consequences	Minimal consequences	No/ minimal consequences.	No/ minimal consequences.

5.5.7.1 *Payload Risks*

A number of risks have been identified in the programmatic area in relation to the very short development schedule and the fragmentation of the instrument consortium, determining an increase of organisational complexity. There are also risks related to the national funding and procurement process, often prone to delays. A rigorous and pro-active schedule management will be applied in order to mitigate such a risk. The largest possible level of decoupling between platform and instrument activities will also be enforced to avoid propagation of delays between parties.

The main risk related to instrument manufacturing, handling and operation is the potential exposure to contamination, a risk which is mitigated by the application of a cover. Another potential risk is the loss of performance due to the material and/or components degradation in space environment, such as CCD damage induced by radiation, loss of alignment in the optical telescope, and misalignment between the baffle and the telescope tube due to thermal and/or mechanical stresses. As a mitigation, several design solutions have been introduced to reduce the likelihood of this failure.

The last source of potential performance reduction is stray light effects, which is mitigated via a dedicated and realistic analysis to identify effective mitigation measures.

5.5.7.2 *Platform Risks*

Also in the case of the platform, a number of risks are related to programmatic aspects. The budget constraints impose a shared launch as “auxiliary payload”, with a related risk on the availability of an adequate launch opportunity by the end of 2017. As mitigation measure, the S/C is designed to be compatible with several vehicles so as to maximise the launch opportunities.

The CHEOPS project and the platform procurement rely on a number of external interfaces, in particular for the provision of the MOC and for specific AIT services. The management of such interfaces adds complexity to the programme. This risk is mitigated via an early and detailed definition of interfaces and responsibilities.

A risk is related to the actual use of “standard platforms”. The CHEOPS specific requirements require some re-design and customisation activities, with related programmatic impacts. As mitigation measure, the changes to the existing platform design are reduced to the minimum possible, and adequate contingencies on the schedule are taken into account.

Another area of concern is related to the fault tolerance architecture implemented in some of the existing small “standard platforms”, and their compatibility with ECSS standards (e.g. ECSS-Q-ST-30C). As mitigation measure, deviations are discussed case by case and relevant standards may be tailored, bearing in mind that the deviations have a direct effect on the risk assumed by the project.

6 Ground Segment

6.1 Overview

The CHEOPS Ground Segment will be developed, operated and maintained under the responsibility of the CHEOPS Mission Consortium. The CHEOPS Mission Consortium as a whole is described in section 7 of this document. The Ground Segment consists of the following elements:

- The Ground Station(s)
- The Mission Operations Centre
- The Science Operations Centre

which will be supported by:

- The Instrument Team
- The CHEOPS Science Team.

The development of the MOC and the SOC will be coordinated by the GS manager, who is a member of the Swiss Project Office.

6.1.1 Ground Stations

The Ground Station(s) will support the telemetry and telecommand communications with the spacecraft.

6.1.2 Mission Operations Centre

The MOC will be responsible for:

- operation of the ground stations and MOC infrastructure;
- reception of tracking data from the Ground Station(s);
- telecommanding;
- reception and archiving of telemetry;
- spacecraft orbit determination and maintenance;
- on-board S/W maintenance;
- monitoring of the spacecraft health and safety;
- execution of predetermined nominal and contingency procedures to safeguard the spacecraft;
- the mission planning system;
- the low level data processing system and first level validation of the observation execution;
- data and operations information dissemination to the SOC.

6.1.3 Science Operations Centre

The Science Operations Centre (SOC) is located at the Astronomical Observatory of the University of Geneva, Switzerland. It is developed under Geneva's responsibility with contributions from other members of the CHEOPS Mission Consortium.

The SOC will be in charge of the following tasks:

- science operations system requirements, design, implementation and management;
- scientific mission planning;
- science Instrument operations and calibration;
- data processing from level 0 to level 2;
- data archiving and access to the CHEOPS data products and documentation;
- supporting ESA in the preparation of the open time AOs by providing documentation and technical support;
- mission management after in-orbit commissioning.

To fulfil these responsibilities, the SOC will closely collaborate with the CMC Instrument Team, the MOC and ESA. The SOC will store the data and maintain the public access to the archive for 10 years after the end of the mission operations.

6.1.4 Orbit and ground contacts

With the chosen Sun-synchronous low Earth orbit and the available ground stations, one to two short contacts per day will be available for nominal telecommand uploading and telemetry downloading between the ground segment and the spacecraft. Hence, the spacecraft has to be autonomous for the majority of the operations timeline and has to provide sufficient on-board storage for the science and housekeeping telemetry. The overall data rate of 1 Gbit per day is compatible with S-band transmission of the telemetry between the spacecraft and the Ground Stations given the available contact time.

6.2 Mission Operations

The Mission Operations aspects of the CHEOPS mission are described in the following sub-sections. Figure 52 gives an overview of the operations concept.

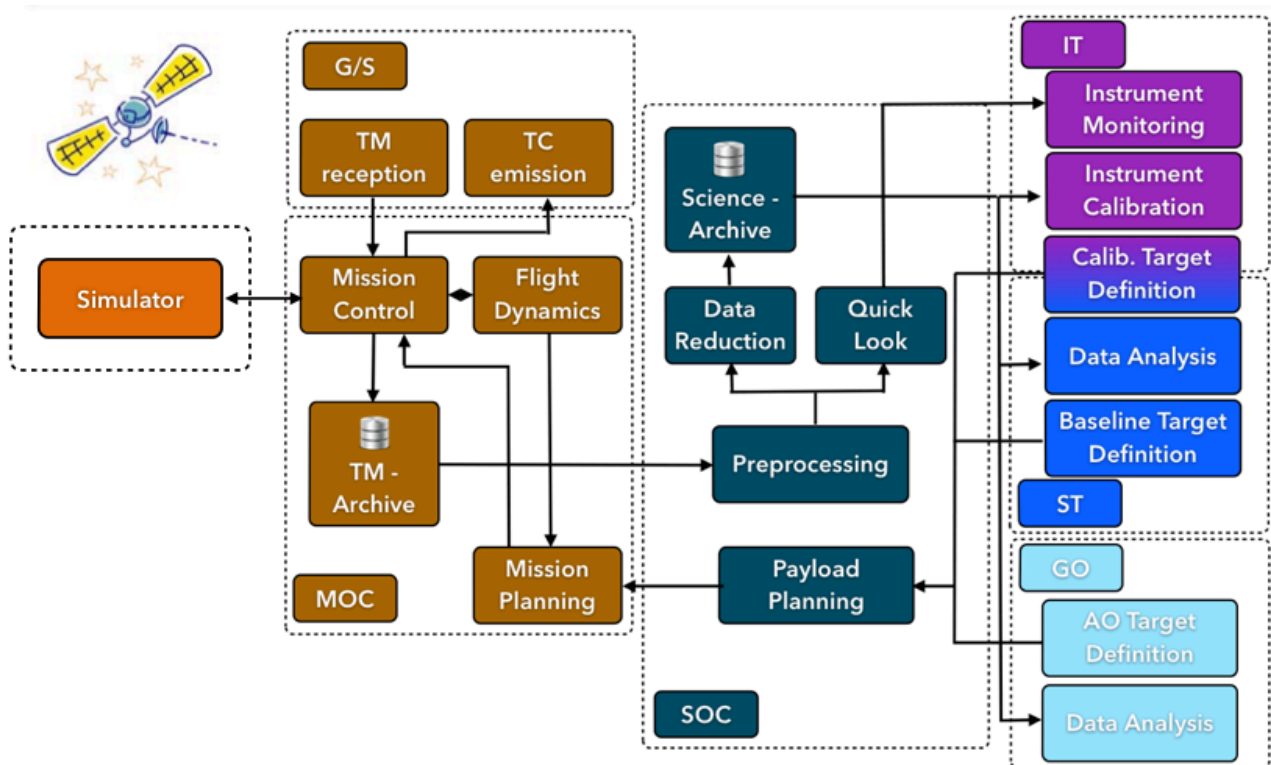


Figure 52 | Overview of the operations concept.

6.2.1 Staffing and operations automation

Following the low-cost approach of the CHEOPS mission, the MOC will only be staffed during normal office hours. The nominal on-ground data processing activities will be executed in an automated manner. Mission Planning will require human intervention. Additional human resources will be available for the commissioning period as well as for contingency situations during nominal operations.

6.2.2 Mission planning

The duration of the planning period as well as the frequency of possible re-planning exercises will be adapted to the low-cost approach. A short-term planning period of two to four weeks is currently discussed.

Except for contingencies, the capability for fast reaction to on-board or physical events in the sky is not foreseen.

6.2.3 Health and safety critical monitoring

At the MOC the platform and instrument housekeeping data will be monitored for health and safety critical events on-board the satellite. In case of an event the spacecraft provider and/or the Science Operations Centre will be informed to initiate the contingency handling.

6.2.4 Auxiliary data

Auxiliary data like orbit and attitude information or time correlation between on-board time and UTC will be made available by the MOC to the SOC. The level of processing at the MOC depends on the final selection of the spacecraft. In case a GPS sensor is available on-board the spacecraft the on-ground processing can be kept to a minimum.

6.2.5 Subsystem provision, integration and validation

Many of the subsystems operated by the MOC will be provided by industry and will be integrated by the Satellite Applications Catapult. For example, the Mission Control System is to be delivered by the eventually selected spacecraft provider. This reduces the development effort and facilitates the integration and validation of the space to ground interface(s). This impacts positively on mission cost and schedule.

6.3 Science operations and data handling/archiving

The Science Operations aspects of the CHEOPS mission are described in the following sub-sections.

6.3.1 Staffing and operations automation

Similar to the Mission Operations at the MOC, the Science Operations will be done to a very large extent in an automated way. Two nominal activities being the exception: payload planning and data quality checks before the science data is archived and made available to the CHEOPS Science Team or the Guest Observers.

6.3.2 Science target definition

Targets for CHEOPS scientific observations can be defined in two ways:

- core science programme;
- open-time science programmes.

6.3.2.1 Core science programme

Targets in the scope of the core science program are defined by the CHEOPS Science Team. 80% of the available science observation time will be dedicated to the core science program. CHEOPS is conceived as a follow-up mission of already detected exoplanets. Hence, the list of science targets is known well in advance of the actual execution of the observation sequence(s). Many targets will be known before the launch of the CHEOPS satellite. Additional targets will be added as new exoplanets of interest are detected by other ground-based or space-borne instruments, like the Next Generation Transit Survey or NASA's *TESS* mission. *TESS* was recently accepted with a launch date very close to the one of CHEOPS. NGTS is to be installed and commissioned in 2013 at ESO's Paranal observation site in Chile.

6.3.2.2 Open-time science programmes

The remaining 20% of the available CHEOPS science observation time will be dedicated to targets proposed by guest observers. ESA will issue regular announcements of opportunity to the general community for this open-time science program. A Time Allocation Committee will rank the proposals and provide them as a prioritised target list to the SOC. This target list will be merged with the one for the core science program to

generate the payload schedule. Tools to assist the proposal process will be available along with an Instrument Observer Manual.

6.3.3 Payload planning

The prioritised target lists from the core science programme and the open-time science programmes are used together with the instrument, spacecraft and mission constraints to produce the instrument schedule. This schedule together with the required instrument settings is transferred to the MOC where telecommands are created and uploaded to the spacecraft. As an alternative to the traditional planning approach which requires a feedback loop between the mission planners at the MOC and the SOC, the consortium is evaluating a more integrated approach where all constraints are applied at the same time to reduce the human effort related to the mission planning.

6.3.4 Data processing

Once the telemetry has been received and checked for health and safety critical events at the MOC, the science and housekeeping data will be transferred to the SOC. Here the data will be pre-processed to extract the raw science images and auxiliary data from the information encoded in the telemetry and auxiliary data streams.

6.3.4.1 Quick Look

Directly after the preprocessing, the automated Quick Look will be triggered to perform the initial Instrument Monitoring and Quality Checks. In case of non-nominal instrument behaviour, the operator at the SOC will receive an alert with the relevant information. At the beginning of the next business day, the operator will perform the required follow-up and, if needed, inform the Instrument Team of the event. The Instrument Team will then perform a deeper analysis of the problem and propose a solution. Possible solutions are updates of calibrations files or, if required, updates of the instrument on-board software. A new set of calibration files or an image of the new on-board software will be provided to the SOC where the updates will be copied to the archive. On-board software will be forwarded to the MOC for upload at a time agreed with the SOC and Instrument Team.

6.3.4.2 Data Reduction

Once all data products for a given observation programme have been preprocessed at the SOC, the Data Reduction pipeline will be executed to apply the automatic calibration and corrections to the raw images and to extract the light curves for the specific targets. After the successful completion of this step, a manual inspection of the data products and their quality will be done at the SOC.

6.3.5 Data archiving and distribution

Upon the successful manual inspection of the data products at the SOC all raw and derived data for a given observation will be archived. High-level data products like images and light curves will be available in the form of FITS files. Low-level information contained in the telemetry or auxiliary data streams will be available in the native format. At the time of data ingestion the data rights will be applied so that CHEOPS Science Team members and Guest Observers have access limited to their data only. The Instrument Team will have access to all data for Instrument Monitoring and troubleshooting purposes. The Science Team or the Guest Observers will then be informed about the availability of their data in the archive. Following this notification and after a proprietary period of one year all data will become publicly available via the CHEOPS Science Archive.

Archive mirror

Regularly, the data in the archive will be synchronised with the archive mirror site. The location of this mirror site is TBD. In case the primary archive is unavailable, the archive mirror will be switched online until the primary site is again available. Data ingestion will only be done to the primary archive.

6.3.6 Data analysis

The analysis of the light curves to extract the attributes of the transit and the exoplanet is outside the scope of the Data Reduction performed at the SOC. Based on the detailed scientific analysis of their data, the Science Team members will provide feedback on the data quality and as such on the completion status of their observations to the SOC. This will allow the flagging of the corresponding observations as completed, to be extended or even repeated. A similar process for the data of the open-time science program is currently being discussed.

6.3.7 In-flight calibrations

In addition to the automatic calibrations (for example at the beginning of an observation sequence), dedicated monitoring and characterisation observations will be defined between the Science and Instrument Team. These observations will be merged with those of the core and open-time science programmes. Detailed Calibration Requirements and the corresponding Calibration Plan are currently in preparation by the Consortium.

6.3.8 Instrument monitoring

On a regular basis, the Instrument Team will monitor the science and housekeeping data and high-level data products, to derive optimal sets of calibrations and data corrections. These will be made available to the SOC to be included in the Data Processing in Quick Look and the Data Reduction. The monitoring will be done partly remotely, using the tools for data visualization available at the SOC. For deeper analyses data might have to be transferred from the SOC to the Instrument Team site.

6.4 Data Products

The CHEOPS data products are defined in three levels as follows:

- L0 data result from the unpacking of data packets received at the MOC from the ground station. They contain the science data and meta-data, as well as the housekeeping and auxiliary data. The housekeeping data (e.g., platform and instrument assembly status) are used at the level of the MOC for spacecraft monitoring. All the L0 data are sent to the SOC, where they are directly archived and used as inputs for the data preprocessing.
- L0.5 data result from the preprocessing of L0 data at the SOC. These are the raw 2D images and their associated meta-data. They are archived and used as inputs for the data reduction. These data are used as input to the quick look (in view of producing the payload monitoring).
- L1 data result from the data reduction of L0.5 data at the SOC. The data reduction produces calibrated science, error, and data quality 2D images as well as the science and engineering meta-data. L1 data are archived, science-ready, intermediate 2D products of the data reduction, which are further processed to produce the L2 data.
- L2 data are the final product of the data reduction, obtained by performing a photometric extraction on the L1 data. They consist of 1D photometric time series (light curves) and associated auxiliary and meta- data. These are the CHEOPS final science products, which are expected to be used as input to the science analysis by scientists in the CHEOPS Science Team and the general community (who could anyway access all data levels). These data will be used for the light curve quality monitoring allowing a precise assessment of the instrument photometric precision.

7 Management

CHEOPS is a Small mission in the ESA Science Programme to be implemented in partnership with Switzerland, and with a number of Member States delivering significant contributions. These Member States are Austria, Belgium, France, Germany, Hungary, Italy, Portugal, Sweden, and UK, and will cooperate under a Swiss led CHEOPS Mission Consortium (CMC). The CMC is led by a principal investigator (PI). The PI of the project is Prof. Willy Benz, Physikalisches Institut, Universität Bern.

The management approach applied to the CHEOPS mission is based on the agreements among the parties described in the Multilateral Agreement (MLA) and follows on the fundamental organisational principles defined in the Science Management Plan (SMP).

7.1 Project management

ESA will be in charge of the overall mission architecture with the support of the CMC. As such, ESA will manage the overall CHEOPS spacecraft development. In particular, ESA will provide, within the remit of the MLA:

- The design, implementation and management of the CHEOPS Platform that will accommodate the Instrument assembly system (CIS).
- The CCD procurement for the CIS.
- The satellite integration and tests, including the Instrument assembly integration on the Platform.
- Satellite qualification, acceptance and testing.
- The procurement of the mission control system, the spacecraft simulator and the flight dynamics system.
- The launch vehicle procurement and launch operations.
- In-orbit commissioning.

During the development and commissioning phases, an ESA-appointed Project Manager will be responsible for implementing and managing the ESA's activities listed above. The ESA Project Manager will be the routine interface to the CMC Project Manager.

Within the remit of the MLA, the CMC will provide the following mission elements:

- Development, procurement, integration, qualification, verification and calibration of the Instrument assembly. This will also include:
 - Definition and maintenance of the Instrument assembly specification and verification of compliance with the science requirements.
 - Contribution and support to the definition (and maintenance) of the interfaces between Instrument assembly and platform.
 - Ensuring an adequate level of test and calibration of the instrument, both on ground and in orbit.
- Supporting as required system level integration and verification activities.
- Supporting as required instrument operations in orbit.
- The System Level AIV services and facilities to the spacecraft contractor as defined in the related System AIV Interface Control Document.
- Monitoring and evaluation of the overall science performance.
- The CHEOPS ground segment, including:
 - The Ground station(s).
 - The Mission Operations Centre (MOC)

- The Science Operations Centre (SOC)
- Mission and science operations following completion of the in-orbit commissioning phase.

During the development and commissioning phases, the PI will appoint a CMC Project Manager, who will be responsible for managing and implementing the CMC provided elements listed above. The CMC Project Manager will be the routine interface to the ESA Project Manager.

After in-orbit commissioning phase, the PI will appoint a Mission Manager, who will assume responsibility for operations of the S/C, its payload, and the Ground Segment.

7.1.1 Organisational structure

7.1.1.1 Overview

Figure 53 summarises the CHEOPS Project organisation, showing the ESA and the CMC respective management structures in charge of the provision of the mission elements as described in the previous section. The project partnership is reflected in the joint Project Office and the Joint Management Team (JMT).

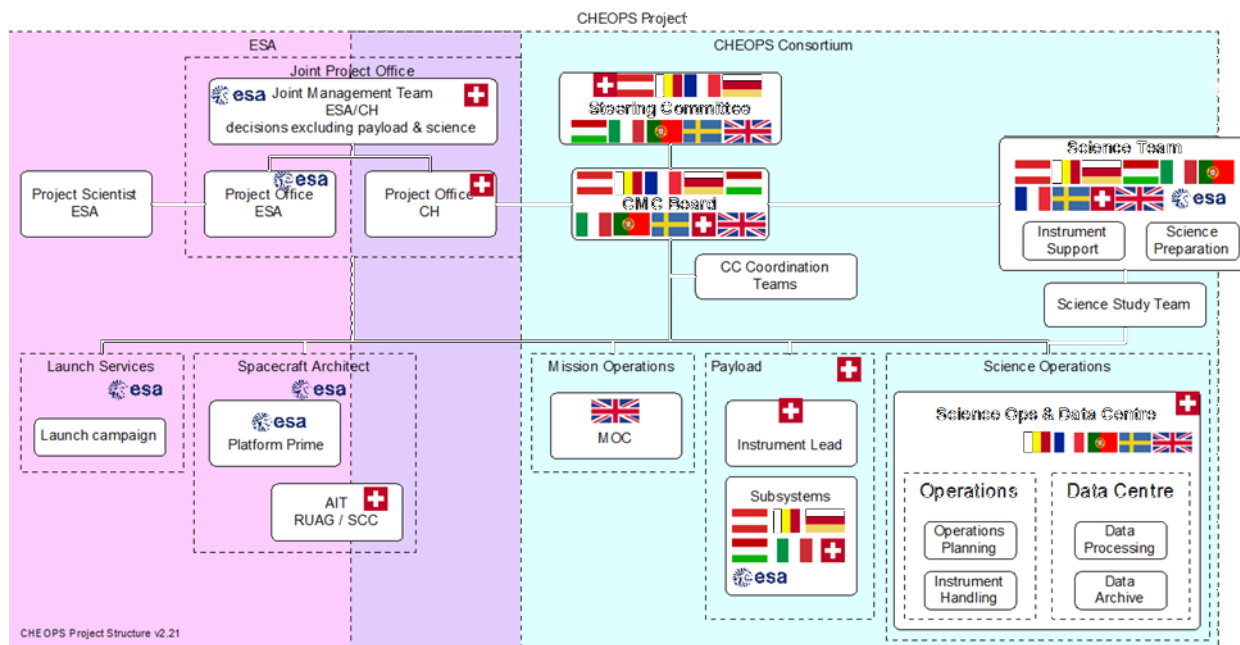


Figure 53 | Summary Organogram of the CHEOPS project.

7.1.1.2 Joint Management Team

A joint ESA-CMC management team has been constituted to coordinate, monitor and discuss issues with major programmatic and financial implications, like design options, work distribution and reinforcement, schedule execution, and launcher. This team is a consultative body, and will consist of the PI, a representative of the Swiss Space Office, the Head of the Future Missions Office, the ESA Project Manager, the CMC Project Manager, the ESA PS, and a representative of the CMC Project Science Office.

7.1.1.3 Joint Project Office

The Joint ESA/Swiss Project Management Office will be run by the ESA Project Manager interfacing to the CMC Project Manager. The ESA Project Office will coordinate all ESA activities. The CMC Project Manager will coordinate all consortium activities and interface to the top level ESA activities.

7.1.1.4 *Steering Committee*

A Multi-Lateral Agreement (MLA) will be established between ESA, Switzerland and the CMC funding agencies to formalise the commitments and deliverables of all parties. The CHEOPS Steering Committee is charged with resolving problems of programmatic or budgetary nature in relation with the contributions from the Member States.

7.1.2 CHEOPS Mission Consortium Board

The CHEOPS Mission Consortium Board (CMC Board) is the top-level decision-making entity of the CMC. All consortium activities will be monitored by the CMC Board, which will serve as interface between the consortium on one hand, and the national agencies and institutes involved in the consortium on the other hand. The CMC Board addresses problems concerning the procurement of elements of the mission, either payload, ground segment or science preparation activities, before they eventually reach the JMT or Steering Committee levels.

The CMC is chaired by the PI, and consists of two members for each CMC country. The composition of the Board will be such that all mission relevant areas of expertise, both scientific and technical, are present. Two members of the ESA CHEOPS Team will have standing invitations as observers to the CMC Board meetings.

The CMC Board creates and disbands Working Groups for study of particular topics. Each Working Group will contain a member of the Board, if possible.

The CMC Board also appoints the CHEOPS Consortium Coordination Team (CCCT), which is working for the day-to-day coordination of the technical activities. The Consortium Coordination Team is composed of the CMC project managers and the sub-system project managers.

7.2 Schedule

Table 19 summarises the major milestones of the project.

Table 19 | CHEOPS Mission Milestones and Phases.

Project element	Milestone
Spacecraft & Mission level milestones	Phase 1 Kick-off - end June 2013
	PRR data package delivery – end November 2013
	SRR data package delivery – end February 2014
	Mission adoption by SPC – Feb 2014 (SPC approval of Phase 2)
	Phase 2 Contractor selection – March 2014 (end of Phase 1)
	Bridging Phase – April-June 2014 (part of Phase 2)
	PDR – July 2014
	CDR – June 2015
	Delivery of the platform for system level AIT – September 2016
	Delivery of operation systems to the MOC & training: - First delivery: March 2016 - Final delivery: October 2016
	End of system level AIT (spacecraft AR) – March 2017
	FAR ^(*) – April 2017 (not including system level contingency - to be agreed at SRR).
	LRR and Launch – October/December 2017 (including contingency)

Instrument	PRR – June 2013
	SRR – September 2013
	PDR – March 2014
	STM testing completed – December 2014
	OptoMechanical CDR – October 2014
	CDR – March 2015
	EM delivery – March 2015
	QR ^(*) – September 2016
	Delivery of the instrument for system level AIV – Sep 2016
Ground Segment	GS Requirements Review – October 2013 (before system PRR)
	GS Design review – October 2014 (before system CDR)
	Integration of mission control system and simulator - March 2016
	GS Implementation Review – December 2016
	GS Readiness Review – September 2017
	Operational Readiness Review – Before LRR

^(*) Actual review approach with respect to final Qualification, Acceptance and Flight readiness shall be defined at the end of phase A/B1, based on schedule optimization and verification approach arguments.

7.3 Science Management

The responsibility for the scientific outcome of the mission and for maximising its scientific return rests on the CMC. The CMC will exploit the scientific results of the mission and assure their diffusion as widely as possible.

For this purpose, the PI will set up a Project Science Office, led by the Mission Scientist. The CMC Project Science Office will coordinate the scientific aspects of the Instrument assembly and operations provision, and, in coordination with the ESA Project Scientists (PS), provide documentation and technical support for the open time AO.

The ESA PS will closely collaborate with the PI and the CMC Project Science Office, to ensure that the maximum scientific return is achieved within programmatic constraints, during all mission phases. The ESA PS will be act as ESA’s interface with the CMC, the ESA Project Manager and the general community for all scientific matters. He/she will also represent the interests of the general community and organise the activities related to their participation in the mission.

7.3.1 CHEOPS Science Team

A CHEOPS Science Team (CST) will be constituted in the CMC, which will advise the PI on scientific matters, in particular:

- science requirements;
- the core observing programme that will fulfil the core scientific objectives;
- observation and calibration strategies;
- processing and analysis of the data;
- definition of data products;
- quality of the data products to be released to the general community;
- scientific exploitation of the data;
- publication rules inside the CMC;
- public outreach, communication, and education activities.

Other tasks of the CST will be:

- Monitor the mission’s development and operations in order to ensure the achievement of the scientific objectives.
- Support the activities of the ESA PS (e.g., by providing input to ESA reviews, production of documentation, public outreach and communication).

The CST will consist of:

- CMC scientists appointed by the PI. Some of them will be ex-officio members with key positions in the project.
- Scientists appointed by ESA following an AO.

The PI will appoint the CST chair. The ESA PS will closely follow the CST activities.

To ensure a commensurate involvement of scientists from ESA Member States in the CHEOPS mission, five CST members, corresponding to a fraction of 20% of the non-ex-officio CST members, will be appointed by ESA through an AO.

The ESA-appointed scientists in the CST will be full members of the CST with the same rights and responsibilities as the CMC appointed members.

The AO for membership in the CST will be open to scientists in the ESA Member States. Scientists whose institutional affiliation would allow access to the CHEOPS core science proprietary data through other channels are not eligible for the participation in the AO.

7.3.2 Guest observers

Twenty per cent of the observing time will be open to guest observers to conduct scientific investigations. Proposals will be requested yearly through an open ESA AO to the general scientific community. An AO will be issued six months before launch. Proposals will not be allowed to include targets that are in the core science programme target list defined and announced by the CMC prior to each AO. Proposals will be selected on scientific merit by a CHEOPS Time Allocation Committee (TAC) appointed by ESA in consultation with the PI. In order to allow important new targets to be included in the open time programme at any time during the mission, up to 25% of the open time will be allocated to a discretionary programme. The discretionary programme will be overseen by ESA, in consultation with the chair of the TAC and the PI.

7.3.3 Data rights

The members of the CST will have access to all data of the core science programme as soon as they are available.

The data from a particular target of the core observing programme and the open time programme will have associated a 1-year proprietary period, after which the L0 to L2 data will be publicly available through the CHEOPS science archive. The 1-year proprietary time will begin just after the last measurement on that particular target has been received, and the planetary transit observation declared complete by the CST after the corresponding quality-check. In order to ensure a timely publication of scientific results, the proprietary time will not exceed 1.5 years counting from the first measurement of the corresponding target. This is in the context that most planetary transits will need few measurements (from 1 to ~3) before the required precision has been reached. Since the vast majority of targets will have short period planets, the time to complete the required set of measurements will generally be of a few months.

During the proprietary time, the open time observers will have access to data products of the same type and quality as the CMC. This will also apply to the general community once the proprietary period has expired.

8 Communication and outreach

ESA and the CMC will be jointly responsible for planning and coordinating public outreach, communication, and education activities related to the mission.

Perhaps nothing excites the scientific imagination of the public more than research which attempts to help address the question: are we alone in the Universe? The study of extrasolar planets is also unmatched in its ability to attract young people to study math, science, and engineering of all types. Communication and outreach activities will seek to capitalise on these two potentials through a vigorous programme associated with the CHEOPS mission concept, focusing on a dynamic public outreach program accessible to the widest possible audience. The CMC will make strong attempts to measure the success of the communication efforts as an on-going tool to improve strategies.

As a central piece of the outreach programme, the CMC proposes to develop an exhibit on exoplanets and space travel based on CHEOPS in collaboration with the Verkehrshaus in Lucerne, a museum which attracts more than 500,000 visitors per year. Members of the CMC have collaborated in the past with this museum (<http://www.verkehrshaus.ch/de/planetarium/>). The focus will be on exoplanet discoveries, the possibilities for life, as well as programmatic components of the mission itself, using these aspects to educate the public about basic science (e.g., thermal considerations of the instrument as a means to convey energy conservation). The CMC will examine the possibility to make the exhibit available for museums all over Europe from 2015 through the duration of the programme. Funds to support the development of the exhibit will come from specific Institute contributions, corporate donations, as well as Outreach Funds available through partner countries (such as the Outreach Program of the Swiss Society of Astronomy and Astrophysics). The CMC also plan to create Citizen Science modules for students and the general public on-line, similar to the “Planet Hunters” project utilising the Kepler data (<http://www.planethunters.org/>). Taking advantage of unique celestial events, such as the transits of Mercury in 2016 and 2019, the CMC will organise a series of public events in partner countries and other ESA member states. Finally, the CMC will coordinate a Speakers Bureau from among the CHEOPS Science Team to support public events throughout Europe on exoplanet (transit) science with a focus on the CHEOPS mission.

9 References

- Adams, E. R., Seager, S., & Elkins-Tanton, L. 2008, *ApJ*, 673, 1160
- Adibekyan, V. Zh., et al. 2012, *A&A*, 543, A89
- Agol, E., et al. 2005, *MNRAS*, 359, 567
- Alibert, Y. 2013, *A&A*, in press (arXiv:1311.3039)
- Alibert, Y., et al. 2013, *A&A*, 558, A109
- Bakos, G., et al. 2010, *ApJ*, 710, 1724
- Batalha, N. et al. 2013, *ApJS*, 204, 24
- Batygin, K., & Stevenson, D. J. 2013, *ApJL*, 769, L9
- Bean, J. L., Miller-Ricci Kempton, E., & Homeier, D. 2010, *Nature*, 468, 669
- Ben-Jaffel, L. 2007, *ApJL*, 671, L61
- Ben-Jaffel, L., & Sona Hosseini, S. 2010, *ApJ*, 709, 1284
- Benneke, B., & Seager, S. 2012, *ApJ*, 753, 100
- Berta, Z., et al. 2012, *ApJ*, 747, 35
- Bond, J. C., O'Brien, D. P., & Lauer, D. S. et al. 2010, *ApJ*, 715, 1050
- Bonfils, X., et al. 2013, *A&A*, 549, 109
- Bonfils, X., et al. 2012, *A&A*, 546, 27
- Borucki, W., et al., 2009, *Nature*, 325, 709
- Borucki, W., et al., 2011, *ApJ*, 736, 19
- Bourrier, V., et al., 2013, *A&A*, 551, A63
- Bourrier, V., & Lecavelier des Etangs, A., 2013, *A&A*, 557, A124
- Boyajian, T., et al. 2013, *ApJ*, 771, 40
- Butler, R. P., et al. 2004, *ApJ*, 617, 580
- Charbonneau, D., et al. 2000, *ApJL*, 529, L45
- Charbonneau, D., et al. 2002, *ApJ*, 568, 377
- Charbonneau, D., et al. 2009, *Nature*, 462, 891
- Chatterjee S., et al. 2008, *ApJ*, 686, 580.
- Chiang, E., & Laughlin, G. 2013, *MNRAS*, 431, 3444
- Claire, M. W. et al. 2012, *ApJ*, 757, 95
- Cooper, C. S., & Showman, A. P. 2005, *ApJL*, 629, L45
- Cowan, N. B., & Agol, E. 2008, *ApJL*, 678, L129
- Cowan, N. B., & Agol, E. 2011, *ApJ*, 726, 82
- Cowan, N. B., et al. 2012, *ApJ*, 747, 82
- Crossfield, I. J. M. 2012, *A&A*, 545, A97
- Cumming, A. et al. 2004, *MNRAS*, 354, 1165
- Davis, T. A., & Wheatley, P. J. 2009, *MNRAS*, 396, 1012

- de Mooij, E. J. W., et al. 2012, *A&A*, 538, A46
- Deeg, H.-J., et al. 2009, *A&A*, 506, 343
- Deming, D., et al. 2009, *PASP*, 121, 952
- Deming, D., et al. 2013, *ApJ*, 774, 95
- Demory, B.-O., et al. 2011, *ApJL*, 735, L12
- Demory, B.-O., et al. 2012, *ApJL*, 751, L28
- Demory, B.-O., et al. 2013, *ApJ*, 768, 154
- Doyle, L. R., & Deeg, H.-J. 2004, *IAUS*, 213, 80
- Dragomir, D., et al. 2013, *ApJL*, 772, L2
- Écuillon, A., et al. 2006, *A&A*, 445, 633
- Ehrenreich, D., & Désert, J.-M. 2011, *A&A*
- Ehrenreich, D., Lecavelier des Etangs, A., & Delfosse, X. 2011, *A&A*, 529, 80
- Ehrenreich, D., et al. 2006, *ApJ*, 651, 535
- Ehrenreich, D., et al. 2012, *A&A*, 547, A18
- Elkins-Tanton, L. T., & Seager, S. 2008, *ApJ*, 685, 1237
- Erkaev, N. V., et al., 2007, *A&A*, 472, 329
- Erkaev, N. V., et al., 2013, *Astrobiology*, submitted (arXiv:1212.4982)
- Evans, T. M., et al., 2013, *ApJL*, 772, 16
- Fabrycky, D. C., et al. 2012, *ApJ*, 750, 114
- Faigler, S., et al. 2013, *ApJ*, 771, 26
- Fang, J., & Margot, J.-L. 2012, *ApJ*, 761, 92
- Fernandes, J. M., Vaz, A. I. F., & Vicente, L. N. 2011, *A&A*, 532, 20
- Fortier, A., et al. 2013, *A&A*, 549, 44
- Fortney, J. J., Marley, M. S., & Barnes, J. W. 2007, *ApJ*, 659, 1661
- Fortney, J. J., et al. 2008, *ApJ*, 678, 1419
- Fraine, J., et al. 2013, *ApJ*, 765, 127
- France, K., et al. 2012, *ApJL*, 750, L32
- France, K., et al. 2013, *ApJ*, 763, 149
- Fressin, F., et al. 2011, *ApJS*, 197, 5
- Gilliland, R. L., et al. 2011, *ApJS*, 197, 6
- Gillon, M., et al. 2012, *A&A*, 539, 28
- Gillon, M., et al. 2007, *A&A*, 472, L13
- Gillon, M., et al. 2007b, *A&A*, 471, L51
- Grasset, O., Schneider, J., & Sotin, C. 2009, *ApJ*, 693, 722
- Grillmair, C. J. et al. 2007, *ApJL*, 658, 115
- Güdel, M. 2004, *A&ARv*, 12, 71
- Guillot, T., et al. 2006, *A&A*, 453, L21
- Hébrard, G., et al. 2008, *A&A*, 488, 763

- Heng, K., & Demory, B.-O. 2013, *ApJ*, 777, 100
- Heng, K., Menou, K., & Phillipps, P. J. 2011, *MNRAS*, 413, 2380
- Heng, K., et al. 2012, *MNRAS*, 420, 20
- Holman, M. J., & Murray, N. W. 2005, *Science*, 307, 1288
- Holmström, M., et al. 2008, *Nature*, 451, 970
- Juric, M., & Tremaine, S. 2008, *ApJ*, 686, 603
- Kalas, P., et al. 2008, *Science*, 322, 1345
- Kipping, D. M. 2009a, *MNRAS*, 392, 181
- Kipping, D. M. 2009b, *MNRAS*, 396, 1797
- Kipping, D. M. et al. 2010, *MNRAS*, 407, 301
- Kipping, D. M. et al. 2012, *ApJ*, 750, 115
- Kipping, D. M. et al. 2013, *ApJ*, 770, 101
- Kipping, D. M., Spiegel, D., & Sasselov, D. D. 2013, *MNRAS*, 434, 1883
- Kjeldsen, H., & Bedding, T. R. 1995, *A&A*, 293, 87
- Knutson, H.A., et al. 2007, *Nature*, 447, 183
- Knutson, H.A., et al. 2009, *ApJ*, 690, 822
- Knutson, H.A., et al. 2011, *ApJ*, 735, 27
- Kuchner, M. 2003, *ApJL*, 596, 105
- Lagrange, A.-M., et al. 2009, *A&A*, 493, L21
- Lammer, H. 2013, *Springer Briefs in Astronomy*, Springer Publishing House, Heidelberg, New York
- Lammer, H., et al. 2009, *A&A*, 506, 399
- Lammer, H., et al. 2011, *Astron. Space Sci.*, 335, 39
- Lammer, H., et al. 2013, *MNRAS*, 430, 1247
- Lecavelier des Etangs, A. 2007, *A&A*, 461, 1185
- Lecavelier des Etangs, A., et al. 2012, *A&A*, 543, L4
- Léger, A., et al. 2004, *Icarus*, 169, 499
- Léger, A., et al. 2009, *A&A*, 506, 287
- Leitzinger, M. et al. 2011, *Planet. Space Sci.*, 59, 1472
- Lin, D. N. C., Bodenheimer, P., & Richardson, D. C. 1996, *Nature*, 380, 606
- Linsky, J. L., et al. 2010, *ApJ*, 717, 1291
- Linsky, J. L., et al. 2013, *ApJ*, 766, 69
- Lissauer, J. J., et al. 2011, *Nature*, 470, 53
- Lissauer, J. J., et al. 2013, *ApJ*, 770, 131
- Liu, C., et al. 2012, *MNRAS*, 426, 2463
- Lovis, C., et al. 2011, *A&A*, 528, 112
- Madhusudhan, N., & Seager, S. 2009, *ApJ*, 707, 24
- Marois, C., et al. 2008, *Science*, 322, 1348
- Mayor, M., & Queloz, D. 1995, *Nature*, 378, 355

- Mayor, M., et al. 2011, A&A, submitted (arXiv:1109.2497)
- McArthur, B. E., et al. 2004, ApJL, 614, 81
- Molenda-Zakowicz, J., et al. 2013, MNRAS, 434, 1422
- Mordasini, C., et al. 2012, A&A, 547, A112
- Murray-Clay, R. A., et al. 2009, ApJ, 693, 23
- Nascimbeni, V., et al. 2013, A&A, 559, 32
- Nesvorny, D. 2012, Science, 336, 1133
- Neves, V., et al. 2012, A&A, 538, 25
- Neves, V., et al. 2013, A&A, 551, 36
- Önehag, A. et al. 2012, A&A, 542, 33
- Penz, T., et al. 2008, A&A, 477, 309
- Pepe, F., et al. 2013, Nature, 503, 377
- Pont, F., et al. 2013, MNRAS, 432, 2917
- Queloz, D., et al. 2000, A&A, 359, L13
- Ribas, I., et al. 2005, ApJ, 622, 680
- Sanchis-Ojeda, R., et al. 2011, ApJ, 733, 127
- Santos, N. C., et al. 2004, A&A 426, L19
- Sanz-Forcada, J., et al. 2011, A&A, 532, A6
- Scuflaire, R., et al. 2008, Ap&SS, 316, 83
- Seager, S., & Mallén-Ornelas, G. 2003, ApJ, 585, 1038
- Seager, S., Deming, D., & Valenti, J. A. 2009, in *Astrophysics in the Next Decade*, Springer Netherlands, 123
- Sekiya, M., et al., 1980, Earth Planet. Sci. Lett., 50, 197
- Showman, A. P., & Guillot, T. 2002, A&A, 385, 166
- Showman, A. P., et al. 2009, ApJ, 699, 564
- Shustov, B., et al., 2009, Astrophys. Space Sci., 320, 187
- Simon, A. E., et al. 2007, A&A 470, 727
- Simon, A. E., et al. 2009, EM&P 105, 385
- Simon, A. E., et al. 2010, MNRAS 406, 2038
- Simon, A. E., et al. 2012, MNRAS 419, 164
- Snellen, I.A.G., de Mooij, E.J.W., & Albrecht, S. 2009, Nature, 459, 543
- Soderblom 2010, ARA&A, 48, 581
- Sousa, S., et al. 2008, A&A, 487, 373
- Southworth, D. 2008, MNRAS, 386, 1644
- Sotin, C., Grasset, O., & Mocquet, A. 2007, Icarus, 191, 337
- Szabó, Gy. M., et al. 2006, A&A 450, 395
- Szabó, Gy. M., et al. 2013, A&A 553, 17
- Telleschi, A., et al. 2005, ApJ, 622, 653

-
- Torres, G., et al. 2010, *A&ARv*, 18, 67
- Torres, G., et al. 2012, *ApJ*, 757, 161
- Triaud, A. H. M. J. 2011, *A&A*, 534, L6
- Tsantaki, M., et al. 2013, *A&A*, 555, 150
- Udry, S., & Santos, N. C. 2007, *ARA&A*, 45, 397
- Valencia, D., Sasselov, D. D., & O'Connell, R. J. 2007, *ApJ*, 656, 545
- Valencia, D., Ikoma, M., & Guillot, T. 2010, *A&A*, 516, 20
- Ventura, P., D'Antona, F., & Mazzitelli, I. 2008, *Ap&SS*, 316, 93
- Veras, D., Ford, E. B., & Payne, M. J. 2011, *ApJ*, 727, 74
- Vidal-Madjar, A., et al., 2003, *Nature*, 422, 143
- Vidal-Madjar, A., et al., 2004, *ApJL*, 604, L69
- Ward, W. R. 1997, *Icarus*, 126, 261
- Watson, A. J., Donahue, T. M., & Walker, J. C. G. 1981, *Icarus*, 48, 150
- Weidner, C., & Horne, K. 2010, *A&A*, 521, 76
- Welsh, W. F., et al. 2010, *ApJL*, 713, 145
- Winn, J. N., et al. 2011, *ApJL*, 737, 18
- White, T. R., et al. 2011, *ApJ*, 743, 161
- Wood, B. E., et al. 2005, *ApJS*, 159, 118
- Yelle, R., 2004, *Icarus*, 170, 323
- Zechmeister, M., & Kürster, M. 2009, *A&A*, 496, 577
- Zsom, A., et al. 2013, *ApJ*, 778, 109

10 List of Acronyms

ADC	Analogue-to-Digital Converter	EEE	Electrical, Electronic, Electromechanical
AIMO	Advanced Inverted Mode Operation	EFM	Electric and Functional Model
AIT	Assembly, Integration and Testing	ELT	Extremely Large Telescope
AIV	Assembly, Integration and Verification	EM	Electrical Model
AO	Announcement of Opportunity	EMC	Electromagnetic Compatibility
AOCS	Attitude and Orbit Control System	ESA	European Space Agency
APE	Absolute Pointing Error	ESO	European Southern Observatory
APS	Application Software	ESOC	European Space Operations Centre
AR	Acceptance Review	ESPRESSO	Echelle SPectrograph for Rocky Exoplanet- and Stable Spectroscopic Observations
BCA	Baffle and Cover Assembly	ESTEC	European Space and Technology Centre
BEE	Back End Electronics	ETH	Eidgenössische Technische Hochschule
BEO	Back End Optics	EUV	Extreme Ultraviolet
CASA	Construcciones Aeronáuticas S.A.	FAR	Flight Acceptance Review
CAUP	Centro de Astrofísica da Universidade do Porto	FEE	Front-End Electronics
CCCT	CHEOPS Consortium Coordination Team	FF	Flat Field
CCD	Charged Couple Device	FITS	Flexible Image Transport System
CCDSD	Consultative Committee for Space Data Systems	FM	Flight Model
CDR	Critical Design Review	FOV	Field Of View
CFRP	Carbon-Fiber-Reinforced Polymer	FPA	Focal Plane Assembly
CHARA	Center for High Angular Resolution Astronomy	FPGA	Field-Programmable Gate Array
CHEOPS	CHAracterising ExOPlanet Satellite	FPM	Focal Plane Module
CIS	CHEOPS Instrument Assembly	FT	Fault Tolerant
CLES	Code Liégeois d'Évolution Stellaire	FUV	Far Ultraviolet
CMC	CHEOPS Mission Consortium	GLS	Generalized Lomb-Scargle
CNES	Centre National d'Études Spatiales	GPS	Global Positioning System
CoRoT	COncvection ROTation and planetary Transits	GS	Ground Segment
COS	Cosmic Origins Spectrograph	GTO	Geostationary Transfer Orbit
CSL	Centre Spatial de Liège	HARPS	High Accuracy Radial velocity Planet Searcher
CST	CHEOPS Science Team	HAT	Hungarian Automated Telescope
CTE	Coefficient of Thermal Expansion	HST	Hubble Space Telescope
DC	Digital Converter	INAF	Istituto Nazionale di Astrofisica
DLR	Deutsches Zentrum für Luft- und Raumfahrt	IRFM	Infrared Flux Method
DPU	Data Processing Unit	ITT	Invitation To Tender
ECSS	European Cooperation for Space Standardization	IWF	Institut für Weltraumforschung
EDAC	Error Detection and Correction	JAXA	Japan Aerospace Exploration Agency
		JMT	Joint Management Team

JUICE	Jupiter ICy moons Explorer	PWM	Pulse Width Modulation
JWST	James Webb Space Telescope	QE	Quantum Efficiency
KELT	Kilodegree Extremely Little Telescope	QES	Qatar Exoplanet Survey
KON	Konkoly Observatory	QR	Qualification Review
LAM	Laboratoire d'Astrophysique de Marseille	RAL	Rutherford Appleton Laboratory
LGA	Low Gain Antenna	ROSAT	ROentgen SATellite
LOS	Line Of Sight	RSSZ	RUAG Space Zürich
LRR	Launch Readiness Review	RV	Radial Velocity
LSP	Launch Service Programme	SAA	South Atlantic Anomaly
LTAN	Local Time of Ascending Node	SCU	Sensor Electronics Controller Unit
LV	Launch Vehicle	SDRAM	Synchronous Dynamic Random Access Memory
MASCARA	Multi-site All-sky CAmERA	SEM	Sensor Electronics Module
MCMC	Markov Chain MonteCarlo	SEOSAT	Satélite Español de Observación de la Tierra
MIRI	Mid Infrared Instrument	SMP	Science Management Plan
MLA	Multilateral Agreement	SOC	Science Operations Centre
MOC	Mission Operations Centre	SOPHIE	Spectrographe pour l'Observation des Phénomènes des Intérieurs stellaires et des Exoplanètes
MOST	Microvariability and Oscillations of STars telescope	SPC	Science Programme Committee
MPPT	Maximum Power Point Tracker	SRE	Science and Robotic Exploration Directorate
MROI	Magdalena Ridge Observatory Interferometer	SRR	System Requirements Review
NASA	National Aeronautics and Space Administration	SSO	Sun-Synchronous Orbit
NGTS	Next-Generation Transit Survey	SSTL	Surrey Satellite Technology Ltd
NIRISS	Near-InfraRed Imager and Slitless Spectrograph	STM	Structural Model
NIRSpec	Near Infrared Spectrograph	TAC	Time Allocation Committee
NUV	Near Ultraviolet	TBC	To Be Confirmed
OTA	Optical Telescope Assembly	TBD	To Be Defined
PBS	Primary Boot Software	TC	Telecommand
PCB	Printed Circuit Board	TESS	Transiting Exoplanet Survey Satellite
PCU	Power Conditioning Unit	TID	Total Integrated Dose
PDR	Preliminary Design Review	TM	Telemetry
PEPT	Positive Expulsion Propellant Tank	TTV	Transit Time Variation
PFM	Proto Flight Model	UBE	University of Bern
PI	Principal Investigator	UGE	University of Geneva
PRNU	Pixel-to-pixel Response Non-Uniformity	UTC	Universal Time Coordinated
PROM	Programmable Read-Only Memory	UV	Ultraviolet
PRR	Preliminary Requirements Review	VLT	Very Large Telescope
PS	Project Scientist	VLTI	Very Large Telescope Interferometer
PSF	Point Spread Function	WASP	Wide Angle Search for Planets
PST	Point Source Transmittance	WSO	World Space Observatory
PSU	Power Supply Unit	XMM	X-ray Multi-Mirror Mission
		XUV	Extreme Ultraviolet